

# PREDICTION OF FILM COOLING

BY  
AMER AHMAD AMER

1109

Submitted in partial fulfillment of the requirements for the degree of Master of  
Science in Mechanical Engineering.

Faculty of Graduate Studies

University of Jordan

11  
1109

Amman

March , 1990

The Examining Committee considers this thesis satisfactory and acceptable for the award of the Degree of Master of Science in Mechanical Engineering.

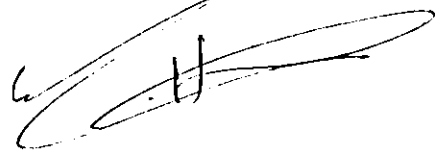
Dr. Bassam A Jubran  
Mechanical Engineering Department  
University of Jordan

Chairman of Committee



Dr. Mohammad A Hamdan  
Mechanical Engineering Department  
University of Jordan

Member of Committee



Dr. Mohammad A Al-Sa'ad  
Mechanical Engineering Department  
University of Jordan

Member of Committee



# ACKNOWLEDGEMENTS

It is of my pleasure to express my gratitude to all people who helped me in completing the present work. Special thanks are indebted to my supervisors Dr. B Jubran and Dr. M Hamdan; whom without their support, encouragement, sound guidance, and advice, my work could have been infinitely more difficult. Also I highly appreciate the great assistance conducted through computer center staff at the Faculty of Engineering and Technology, especially Miss. R Shouhada.

I would like also to present my special thanks to Dr. M Malin, of CHAM ltd for his great help in turbulence modelling during my visit to England in Nov.1989, as well as the helpful suggestions given by Dr. T Abu-Arab of Jordan University of Science and Technology during my work.

Finally, not to forget, the support and great care given to me by all my family members throughout my research.

# ABSTRACT

The present investigation is a theoretical one involving the prediction of film cooling from two rows of holes. Predictions of film cooling effectiveness and the velocity field from two rows of holes inclined in the streamwise direction are presented using different two-equation-models of turbulence;  $k - \omega$  model of Spalding (1971) was used together with a modified version of Ilegbusi and Spalding (1983), as well as the standard  $k - \epsilon$  model accompanied with its non-isotropic version of Bergeles (1976).

PHOENICS package of CHAM Ltd was used to carry out the present investigation. Only isotropic version of  $k - \epsilon$  model was built-in the package, the non-isotropic effect was introduced by the author. Also, the author formulated the  $k - \omega$  model as well as the modified version of it into PHOENICS through the GROUND file making use of the accessible subroutines supplemented with the package.

Comparisons between the predicted results using the previously mentioned models and previous experimental results indicate that the ability of a turbulence model to predict the experimental results depends very much on the blowing rate as well as on the distance downstream from the injection holes. Finally conclusions and recommendations are presented, thoroughly expressed and discussed.

# NOMENCLATURE

<sup>1</sup>  $C_1, C_2, C_3, C_4, C_5$  : further constants or functions of the  $k - \omega$  model.

$C_c$  : concentration of the foreign gas in the injected gas.

$C_{iw}$  : concentration of the foreign gas at an impermeable wall.

$C_m$  : concentration of the foreign gas in the main stream.

$c_p$  : specific heat at a constant pressure.

$C_\mu$  : coefficient in the turbulence model.

$D$  : diameter of injection hole.

$e_{ij}$  : rate of strain tensor.

$E$  : constant in the law of the wall.

$G$  : rate of generation of turbulence energy per unit volume.

$h$  : static enthalpy.

$h'$  : enthalpy fluctuation.

$I$  : momentum ratio.

$k$  : turbulent energy.

$\ell$  : length scale of turbulent motion.

$M$  : blowing rate.

$P$  : pitch distance between holes.

$R$  : Reynolds shear stress.

$Re$  : Reynolds number.

$S$  : source term of turbulent quantities.

---

<sup>1</sup>This list is confined mainly to frequently-used symbols.

$U_c$  : resultant coolant velocity.

$U_m, U_\infty$  : main stream velocity.

$U_\tau$  : friction velocity.

$u, u_1$  : spanwise velocity fluctuation.

$v, u_2$  : normal to the test surface velocity fluctuation.

$w, u_3$  : streamwise velocity fluctuation.

$X$  : distance measured in the lateral direction.

$Y$  : distance normal to the test surface.

$Z$  : distance measured from the centerline of first row of holes in the stream wise direction.

## Greek symbols

$\delta$  : boundary layer thickness.

$\delta_{ij}$  : Kronecker delta.

$\epsilon$  : dissipation rate of  $k$ .

$\eta$  : local film cooling effectiveness.

$\bar{\eta}$  : average film cooling effectiveness.

$\mu$  : laminar kinematic viscosity.

$\rho$  : density of the fluid.

$\nu$  : kinematic molecular viscosity.

$\nu_t$  : eddy ( or turbulent )viscosity.

$\omega$  : time-average vorticity.

$\Gamma$  : effective exchange coefficient.

$\sigma$  : Prandtl-Schmidt number  $\equiv \Gamma/\mu$ .

$\kappa$  : Von Karman's constant.

## Subscripts

$ad$  : adiabatic.

$c$  : coolant.

$f$  : reference.

$m$  : main stream.

$t$  : turbulent.

$i$  : represents the direction in tensor form and takes the value of 1, 2 or 3.

# Contents

ACKNOWLEDGEMENTS . . . . .	v
ABSTRACT . . . . .	vii
NOMENCLATURE . . . . .	xii
<b>1 Introduction</b>	<b>1</b>
1.1 INTRODUCTION . . . . .	1
1.2 GAS TURBINE BLADE COOLING . . . . .	2
1.2.1 Convection Cooling . . . . .	3
1.2.2 Film Cooling . . . . .	3
1.2.3 Transpiration Cooling . . . . .	3
1.2.4 Comparison of Cooling Techniques . . . . .	4
1.3 OUTLINE OF THEORETICAL PROGRAM . . . . .	4
1.4 LAYOUT OF THE THESIS . . . . .	5
<b>2 Literature Survey</b>	<b>7</b>
2.1 INTRODUCTION . . . . .	7
2.2 EXPERIMENTAL STUDIES . . . . .	8
2.3 THEORETICAL STUDIES . . . . .	9
2.3.1 Analytical Studies . . . . .	9
2.3.2 Numerical Studies . . . . .	10
<b>3 Mathematical Interpretation and Simulation</b>	<b>15</b>
3.1 INTRODUCTION . . . . .	15



3.2	THE PARTIAL DIFFERENTIAL EQUATIONS . . . . .	16
3.3	ASSUMPTIONS MADE . . . . .	17
3.4	PHOENICS IMPLEMENTATION . . . . .	18
3.4.1	Structure of PHOENICS . . . . .	18
3.4.2	Differential Equations . . . . .	19
3.4.3	Solution Procedures Employed . . . . .	21
3.5	NUMERICAL SOLUTION OF EQUATIONS . . . . .	23
<b>4</b>	<b>Turbulence Modelling</b>	<b>25</b>
4.1	BACKGROUND . . . . .	25
4.1.1	Equations of Motion . . . . .	26
4.1.2	Classification of Turbulence Models . . . . .	27
4.1.3	Near-wall Approaches . . . . .	30
4.2	$k - \omega$ MODEL . . . . .	31
4.2.1	Empirical Constants and Functions . . . . .	33
4.2.2	Modified Version of $k - \omega$ Model . . . . .	35
4.3	$k - \epsilon$ MODEL . . . . .	36
4.3.1	Modified Version $k - \epsilon$ Model . . . . .	37
4.4	WALL BOUNDARY CONDITIONS . . . . .	37
<b>5</b>	<b>Discussion of Results</b>	<b>41</b>
5.1	PRELIMINARY TESTS . . . . .	41
5.1.1	Effect of Injectant Velocity Profile . . . . .	41
5.1.2	Grid Dependence Effect . . . . .	41
5.2	FILM COOLING EFFECTIVENESS RESULTS . . . . .	42
5.2.1	Comparison of Different Turbulence Models . . . . .	44
5.3	VELOCITY PROFILES RESULTS . . . . .	46
5.3.1	Comparison of Different Turbulence Models . . . . .	48

5.4	TURBULENT KINETIC ENERGY RESULTS . . . . .	50
<b>6</b>	<b>Conclusions and Recommendations</b>	<b>53</b>
6.1	CONCLUSIONS . . . . .	53
6.2	RECOMMENDATIONS . . . . .	55
	REFERENCES . . . . .	63
	APPENDIX I . . . . .	92
	APPENDIX II . . . . .	95

# Chapter 1

## Introduction

### 1.1 INTRODUCTION

In the last four decades since World War II, great progress has been made in the performance and the thermal efficiency of all types of gas turbines; in particular in the aero-engine because of higher thrust to weight ratio by the military, and the reduced fuel consumption desired by the civil aircraft operation.

The gas turbine industry has continuously sought means of achieving a higher engine thermodynamic efficiency by increasing the turbine inlet temperature. This requires reliable and efficient cooling schemes that provide minimum cycle penalty for use of that coolant. Traditional schemes use compressor air, that is bypassed to the cooling system, although phase-change cooling is currently being considered as an alternative. Air-cooling a surface is basically carried out in two ways: the first method is to internally cool the back side of a surface: and the second method couples the first with a film cooling process, whereby the coolant is dumped through the surface to alter the external convection process.

Recently, the attention of some researchers has been directed to discrete hole film cooling leading to a single row and multiple rows cooling. In this method cooling air is injected into the main stream in order to establish a protecting film on the

blade surface. Because of design configurations, injection through slots is usually not possible and the cooling air has to be introduced through the previously mentioned discrete holes, Jubran (1984).

## 1.2 GAS TURBINE BLADE COOLING

In a typical gas turbine air is taken in by a compressor, by which the pressure is raised through several stages within the compressor, each consisting of a row of rotating blades and a row of stator blades. Then air enters the combustion chambers, undergoes a combustion process, producing a flow of hot and high pressure gas to be used to drive the engine by means of a turbine. Like the compressor the turbine consists of alternate rows of static blades (known as "nozzle guide vanes") and rotating turbine blades. The engine provides a propulsive force because of the momentum supplied to the jet of gas which emerges at the rear.

Since the blades are subjected to an extremely hot gas flow and the flow temperature should be as high as possible in order to obtain a higher thermal efficiency, then cooling techniques must be used to cool the surface of the blade. The air coolant in practice is taken from the flow through the engine immediately after the compressor, before the combustion chamber. The designer is faced with a compromise between loss of mass flow and hence decreased thrust as opposed to improved cooling with its attendant decrease in blade metal temperature. This would give an improved fatigue life and allow higher turbine entry temperature which is responsible for producing an engine with greater efficiency.

The following three techniques have been used or proposed for the gas turbine blade cooling.

### **1.2.1 Convection Cooling**

In this method which is the least complicated one; the heat picked up by the blades from the hot gases is conducted through the blade wall to cooling air that is flowing through the internal passages in the blade. In general, fins are used on the inside (coolant side) of the wall to increase the surface area exposed to the cooling air flow and to stir up the cold air inside boundary fig.(1.1a).

A variation of the convection cooling is the impingement cooling; where jets of cooling air are directed against the inner surface of the blade wall to transfer heat in a more efficient way than can be done with normal convection cooling fig.(1.1b).

### **1.2.2 Film Cooling**

Film cooling is a technique which prevents the hot gases from reaching a wall to decrease the wall temperature by locally introducing a cold gas, usually air into the boundary layer of the hot gas stream, through a single or multiple openings.

The manner in which the coolant emerges from the surface of the blade depends on the geometry of the injection holes through which it flows and the pressure which is available to drive it fig.(1.1c).

### **1.2.3 Transpiration Cooling**

The most efficient use of cooling air can be attained by passing air through a porous wall to establish a complete and continuous blanket of cool air on the outer surface of the blade, the air that transpires through the porous wall picks up heat very effectively from the wall by convection. The uniform film established on the outer wall results in an even greater reduction of gas to wall heat transfer coefficient than was accomplished in film cooling fig.(1.1d).

## 1.2.4 Comparison of Cooling Techniques

Convection cooling is currently being used in operational gas turbine engines with some augmentation from film cooling in critical regions. Nowadays the trend is to improve film cooling techniques and apply transpiration cooling in the future.

It must be pointed out that where convection cooling can provide adequate protection, this technique have several advantages over the other two methods. The holes or slots in the blade required for film cooling or transpiration cooling provide weaker structures than solid walls of a convection cooled surface. Also these openings are susceptible to vibration and fatigue failure. Foreign objects may block the small openings, these foreign objects may be due to oxidation or due to dirty cooling air, and finally the fabrication techniques are more difficult for film cooling and transpiration cooled blade than the fabrication for convection cooled blade.

## 1.3 OUTLINE OF THEORETICAL PROGRAM

The theoretical program involves several steps; first, an investigation through several turbulence models was carried out, followed by the testing of the embodied standard isotropic  $k - \epsilon$  model for the prediction of film cooling over two rows of holes, then the non-isotropic effect of  $k - \epsilon$  model, based on the work of Bergeles (1976) and Rodi (1972), was tested and compared with the standard  $k - \epsilon$  model. Second, the  $k - \omega$  model was introduced into PHOENICS together with its modified version , based on the work of Ilegbusi and Spalding (1985), and tested against predictions of  $k - \epsilon$  model. Third, several tests were carried out to investigate the effect of using various coolant velocity profiles over the injection holes on the prediction of film cooling.

Finally the predicted results were compared with the experimental results for film cooling from two rows of holes injected at  $30^\circ$  to the main stream, Jubran (1984).

## 1.4 LAYOUT OF THE THESIS

The thesis is divided into six chapters, of which this introduction is the first. Chapter 2 is a literature survey of the work done on prediction of film cooling with stress on numerical studies.

Chapter 3 describes mathematical interpretation and simulation of film cooling; in this chapter the assumptions made are clarified together with the justification for adopting PHOENICS for simulating such a problem. Chapter 4 briefly describes several turbulence models with more emphasize on two-equation models. Special care was taken in exploring both  $k - \omega$  model and  $k - \epsilon$  model.

Chapter 5 discusses the predicted results when compared with experimental ones. Finally chapter 6 reports the concluding remarks gained from the present investigation, followed by recommendations for future work.

# Chapter 2

## Literature Survey

### 2.1 INTRODUCTION

Film cooling is a technique used to protect a solid surface from high temperature main stream by releasing a coolant on the surface to be protected. The coolant, usually air, is injected through internal passages of the blade into the boundary layer of hot gas stream as shown in Fig(2. 1). This technique is a complex one, and many parameters affect the performance of film cooling process. In order to explore these effects many researchers have carried out both experimental and theoretical studies.

Theoretical studies lies in two groups; the first involves analytical modelling of film cooling process as well as finding the correct parameter for correlating experimental data in order to develop empirical relations capable of predicting film cooling effectiveness.

These empirical relations have many restrictions and *can not* be applied away from the specified range and conditions upon which it was formulated. Examples of these are those of Brown (1967), Ramsey et.al. (1970), Saluja (1977), and Jubran (1984). The second group of models are those based on the solution of continuity, momentum, and energy equations, as originated by Patankar and Spalding (1972).



Since this research is intended to predict film cooling process using different turbulence models, more attention will be paid to theoretical studies in the form of solving momentum, and energy equations rather than empirical relations.

## 2.2 EXPERIMENTAL STUDIES

The experimental studies conducted on film cooling have been based upon two techniques;

- the mass transfer technique; in which concentration of injected gas at the surface of the blade is measured and non-dimensionlised by the wall effectiveness ( $\eta$ ) given by:

$$\eta = \frac{C_{iw} - C_m}{C_c - C_m} \quad (2.1)$$

where;

$C_m$  is the concentration of foreign gas in the main stream.

$C_c$  is the concentration of foreign gas in the injected gas.

$C_{iw}$  is the concentration of foreign gas at an impermeable wall.

- the heat transfer technique, followed by research workers of Minnesota University, in which the adiabatic wall temperature ( $T_{aw}$ ) has been measured and non-dimensionlised by using the film cooling effectiveness ( $\eta$ ) given by:

$$\eta = \frac{T_m - T_{aw}}{T_m - T_c} \quad (2.2)$$

where;

$T_m$  is the temperature of foreign gas in the main stream.

$T_c$  is the temperature of foreign gas in the injected gas.

Many experimental studies have been carried out to study both *operational factors* such as: blowing rate, density ratio, main stream intensity and turbulence scale, main stream pressure gradient and Mach number, boundary layer and injectant fluid velocity, and *geometrical factors* related to the geometry of the hole as well as arrangement of holes, angle of injection and the shape of the blade.

Good account of literature regarding the experimental investigations conducted on film cooling is given by Jubran (1984).

## 2.3 THEORETICAL STUDIES

### 2.3.1 Analytical Studies

Analytical studies are based on a simple model which can be used to correlate data from experiments. Examples are those of Brown (1967) and Ramsey et al.(1970). Brown (1967) developed a heat balance model for two-dimensional film cooling, where he considered the boundary layer over a flat plate which has an injection slot at some position upstream. Ramsey et.al. (1970) developed a model, for predicting three-dimensional film cooling, making use of a heat source technique. In their model; the injection of the coolant was simulated by the presence of a heat sink of strength equal to the net enthalpy of the injection at the point of injection on the film cooled surfaces.

**385793**

Almost all workers developed correlations for film cooling effectiveness ( $\eta$ ) nearly of the same form, Jubran (1984). More details may be found in Jubran (1984) and Goldstein (1971).

### 2.3.2 Numerical Studies

As the flow field is strongly three-dimensional in the vicinity of the injection holes, basically a three-dimensional calculation procedure is necessary. Patankar and Spalding (1972) developed a numerical solution for solving the three-dimensional boundary layer heat transfer problem for parabolic flows. For injection through discrete tangential slots, Patankar, Rastogi and Whitelaw (1973) also presented a three-dimensional calculation procedure. Patankar, Basu and Alpay (1977) described a finite-difference solution for the three-dimensional flow field generated by a round turbulent jet deflected by a main stream normal to the jet axis and analysed the injection at high blowing rates from a single hole. Khan et.al. (1982) predicted the injection through a row of holes. Bergeles, Gosman and Launder (1976,1980,1981) analysed the three-dimensional discrete hole cooling process, but their calculation procedure was based upon a partially parabolic one and hence not capable of handling regions with recirculation and reverse flow, their prediction was for laminar as well as for turbulent flows, with single-row and multi-row cooling.

Demuren (1983) presented detailed computations of the steady flow of a row of turbulent jets issuing normally into a nearly uniform cross flow; using three-dimensional finite-difference numerical procedures; the QUICK scheme which employs a higher-order-accurate difference approximation for the convection terms proved to produce better results than the more widely employed hybrid (central/upwind) scheme. Demuren and Rodi (1983) and Demuren, Rodi and Schönung (1985) presented detailed computational studies of film cooling by a row of holes, the partial differential equations were solved with the three-dimensional locally-elliptic method of Rodi and Srivasta (1980) which is an extension of the partial-parabolic procedure of Pratap and Spalding (1976) allowing for an elliptic treatment of local regions

with reverse flow, and hence saving computer storage over a fully-elliptic method. Demuren, Rodi and Schönung (1985) also analysed the influence of the injection angle, the relative spacing and the blowing rate on the cooling effectiveness with their three-dimensional calculation method, which is applicable to high blowing rates.

A different approach was adopted by several authors in which faster prediction methods were employed; these prediction methods are suitably extended two-dimensional boundary layer procedures. These procedures are faster, and more suitable for parametric studies than three-dimensional calculation methods. Few attempts have been made to extend boundary layer codes for the prediction of film cooling. Herring (1975) proposed a prediction method for the behaviour of a turbulent boundary layer with heat transfer under the influence of transpiration with discrete jets. He treated the boundary layer as a laterally averaged flow and introduced the effects of non-uniformity in the form of additional source terms to the equations of motion. Herring obtained the non-uniformity interaction terms by an integral method, where he assumed locally uniform flow axisymmetry of the jets and negligible interaction between the jets and the wall, his prediction method showed agreement with his own experimental data but for low blowing rates ( $M < 1.0$ ).

Crawford, Kays and Moffat (1976) extended their boundary layer program STAN5 by an injection model, derived from a one-dimensional momentum and energy balance. The derived model can not predict flows with high blowing rates where the fluid velocity above the injected cooling jet can be higher than in the free stream due to the blockage effects of the injected jet. The authors modelled the lateral mixing by augmentation of the mixing length in their turbulence model. Miller and Crawford (1984) extended the work of Crawford et.al.(1976) and applied basically the same model, calculating also the film cooling effectiveness, but for each cool-

ing configuration they had to adjust the two constants in their film cooling model. They compared their predictions with experimental results; for blowing rates less than 1.0, injection angles less than  $45^\circ$ , and relative spacings larger than 2.0. For these configurations they obtained good agreement.

Schönung and Rodi (1987) described a new film cooling model incorporated into a two-dimensional boundary layer procedure. The governing mean flow equations together with the turbulence model are presented, by same authors, with modifications to account for the elliptic nature of the flow after the injection (*injection model*) and for the three-dimensionality of the flow (*dispersion model*). They presented their results for flows over flat plates as well as over model gas turbine blades.

$k - \epsilon$  model is the most commonly used turbulence model for prediction of film cooling. Extensions were considered to account for acceleration, Stoll and Straub (1987), and Jubran (1989), they investigated both experimental and theoretical heat transfer and cooling film stability in a convergent-divergent nozzles where a parabolic finite difference boundary layer code was employed. The  $k - \epsilon$  model was refined by Bergeles, Gosman and Launder (1978); where they proposed the non-isotropic version of  $k - \epsilon$  model in order to account for the anisotropy of the eddy viscosity and diffusivity, examples of the later are Demuren, Rodi and Schönung (1985), and Jubran (1984), the latter author applied PHOENICS package developed by CHAM for his prediction.

It is to be mentioned that there is no reason, however, to suppose that, if an equal amount of attention was given to it, another two-equation model would not perform as well, or even better than the  $k - \epsilon$  model, Markatos (1986).

Although  $k - \epsilon$  model has become more popular because of the practical advan-

tage that the  $\epsilon$ -equation requires no extra terms near the walls and also because  $\epsilon$  it self appears in the  $k$ -equation and the  $\epsilon$ -equation requires no secondary source terms,  $k - \epsilon$  model superiority is very dubious. Because it may be that some of the 'constants' should not be constants in two-equation models other than the  $k - \epsilon$  model, and perhaps also the true behaviour of turbulence requires that the gradients of more than one turbulence property drive diffusional effects. Also the above mentioned superiority does not ensure that the  $k - \epsilon$  model will predict various entities much better than other turbulence models for all types of flows.

In general, Two-equation models need considerable adjustment of the empirical input; especially when flows with recirculation are considered. This adjustment is usually accepted by engineers. Till now, no one could put a definitive answer to which of the available two equation models is the best ?.

Reviews of the turbulence models, proposed by earlier workers, can be found in several publications like those of Launder and Spalding (1971); Rodi and Spalding (1970);and Daly and Harlow (1970).

General description, about all turbulence models, will be given in chapter 4.

# Chapter 3

## Mathematical Interpretation and Simulation

### 3.1 INTRODUCTION

In this chapter the mathematical basis upon which the film cooling problem is dependent, together with the computer simulation ( *PHOENICS* computer code version 1.4 of October 1987, developed by *CHAM* ) are briefly explored.

The first step is to present the physical laws representing the problem and put them into mathematical form suitable to the computer code, or the computer code itself can be modified to suit the problem considered. The package which was adopted has several features that justify its selection among other computer codes for; these features are:

1. *PHOENICS* is a computer code which simulates fluid-flow, heat transfer, chemical-reaction and related phenomena.
2. *PHOENICS* simulations can be conducted on various scales. For example, the attention may be confined to one bank of tubes within an industrial heat exchanger; or the fine details of the flow within a single tube may be simulated.
3. *PHOENICS* solves the conservation equations of mass, momentum, and energy; which are the same equations used for the film cooling problem in ques-

tion.

4. *PHOENICS* contains built-in representations of viscous and convection terms. The package is flexible and provides means where the user can add, modify or change with limitations.
5. Finally, *PHOENICS* provides, as well as all the information needed by the design engineer, a comprehensive insight which aids imagination and promotes understanding.

### 3.2 THE PARTIAL DIFFERENTIAL EQUATIONS

The partial differential equations representing the film cooling problem are presented mathematically in tensor form notations as follows:-

Mass continuity.

$$\frac{D\rho}{Dt} + \rho \frac{\partial U_j}{\partial x_j} = 0 \quad (3.1)$$

Momentum.

$$\rho \frac{DU_j}{Dt} = -\frac{\partial P}{\partial x_i} + \frac{\partial}{\partial x_j}(\mu e_{ij}) \quad (3.2)$$

Energy.

$$\rho \frac{Dh}{Dt} = \frac{\partial}{\partial x_j} \left( K \frac{\partial T}{\partial x_j} \right) + \frac{\partial}{\partial x_j} (\mu U_i e_{ij}) \quad (3.3)$$

Where:

$U_i$  is the instantaneous velocity.

$e_{ij}$  is the rate of strain tensor.

$$e_{ij} = \frac{\partial U_i}{\partial x_j} + \frac{\partial U_j}{\partial x_i} - 2/3 \frac{\partial U_k}{\partial x_k} \delta_{ij}$$

$h$  is the total specific energy given by;

$$h = h_{ref} + \int_{T_{ref}}^T c_p dT + 1/2(u_j u_j)$$

$c_p$  is the specific heat of fluid under constant pressure.

$\delta_{ij}$  is the Kronecker delta.



$\frac{D}{Dt}$  is the total derivative given by:

$$\frac{D}{Dt} = \frac{\partial}{\partial t} + U_j \frac{\partial}{\partial x_j} = \frac{\partial}{\partial t} + U_1 \frac{\partial}{\partial x} + U_2 \frac{\partial}{\partial y} + U_3 \frac{\partial}{\partial z}$$

The previous equations may appear simple, but their solution is very complex due to nonlinear convection term and due to the fact that the problem is a turbulent one.

### 3.3 ASSUMPTIONS MADE

The following assumptions are adopted to simplify the equations and reduce the computer time needed for solving:

- (a) Steady state : this assumption is justified by the time scale being greater than that of the turbulent flow for practical problems.
- (b) Boundary layer assumptions: this assumption is justifiable for low blowing rates where the jets are attached to the surface and the flow has a predominant direction as well as at distances far away from the injection holes. The recirculation zone near to the injection holes implies that the parabolic procedure, in which the disturbance has no effect upstream, can not be applied; instead an elliptic procedure, where influences are exerted in both positive and negative directions for all existent space dimensions, is to be applied.
- (c) Incompressible flow: this assumption is justified by the fact that zero pressure gradient prevails along the flat plate together with very low Mach number.

## 3.4 PHOENICS IMPLEMENTATION

The main objective of this research is to predict both film cooling effectiveness ( $\eta$ ) and velocity profiles for the film cooling utilizing a package of special features simulating heat-flow as well as fluid-flow. PHOENICS is already installed on the VAX-8700 computer system in the University of Jordan. Such simulation will be no better than the model provided by the user, since the accuracy and realism of results will be heavily dependent on the assumptions made by the user as well as the computer time consumed during execution.

### 3.4.1 Structure of PHOENICS

PHOENICS solves discretised versions of the partial differential equations governing the balance of mass, momentum, energy, and of scalar quantities such as chemical-species concentration or turbulence energy, and indeed of any entity which can be expressed in terms of; time-dependence, diffusion, convection, and source terms, Spalding (1987).

Input data switches are available to determine the flow being single- two-phase or multi-phase, steady or transient, and to determine whether the flow is one-dimensional, two-dimensional, or three-dimensional. There is no restriction to the nature of the process, number of solved-for variables, fineness of the computational grid, the time offered by user for program execution, or the complexity of the described phenomena.

The architecture of PHOENICS is modular; the user is free to use the built-in features of fluid properties and initial boundary conditions as well as discretisation formulae and method of solution in the package or to attach his own coding at the

designated connection points in the open-source subroutines provided.

PHOENICS is a four-part program written in a highly portable version of Fortran based on ANSI FORTRAN 66 but with character handling features of ANSI FORTRAN 77. The main equation solver EARTH, the input-data setting pre-processor "Satellite", the graphics post-processor PHOTON, and finally the self-instruction part GUIDE as shown in fig (3-1). The input file library supplied with PHOENICS is supplemented with hundreds of case studies; which may be used as it is for a relevant problem with minor modifications or may be used as a starting point for a different problem. A special feature of PHOENICS is the "PHOENICS Input Language" PIL supplied for easier and compact communication between PHOENICS and user.

### 3.4.2 Differential Equations

The laws of conservation of mass, chemical species, momentum energy and other fluid properties for which PHOENICS solves, can all be expressed in the form , Rosten and Spalding (1987),

$$\underbrace{\frac{\partial}{\partial t} (r_i \rho_i \phi_i)}_{\text{transient}} + \text{div} \left( \underbrace{r_i \rho_i \vec{v}_i \phi_i}_{\text{convection}} - \underbrace{r_i \Gamma_{\phi_i} \text{grad } \phi_i}_{\text{diffusion}} \right) = \underbrace{r_i S_{\phi_i}}_{\text{source}} \quad (3.4)$$

where:

$t$ : stands for time;

$r_i$ : stands for volume fraction of phase  $i$ ;

$\rho_i$ : stands for density of phase  $i$ ;

$\phi_i$ : stands for any conserved property of phase  $i$ , such as enthalpy, momentum per unit mass, mass fraction a chemical species, turbulence energy, etc.;

$\vec{v}_i$ : stands for velocity vector of phase  $i$ ;

$\Gamma_{\phi_i}$ : stands for exchange coefficient of entity  $\phi$  in phase  $i$ ;

and,

$S_{\phi_i}$ : stands for the source rate of  $\phi_i$ .

When time averaged values of various quantities in question, as is commonly the case when turbulent flows are to be simulated, special expressions may have to be introduced for  $\Gamma$  and  $S$ , accounting for the corrections between velocity, density,  $\phi$ 's, and other quantities of the flow and of the fluid. The responsibility for selecting the special expressions for among those which could be attached, rests with the user. PHOENICS mainly works out the quantitative consequences, Rosten and Spalding (1987).

It is presumed that the time on which the averaging is made is long compared to the time scale of turbulent motion.

PHOENICS employs *finite – volume* (also called *finite – domain*) formulation of equations which are derived by integration of differential equations over control volumes of finite size (called *cells* or *sub – domains*) which, taken together, wholly fill the domain under study, after which interpolating schemes are used to approximate the resulting volume, area and time averages where a wide variety of interpolation assumption may be selected by the user or even invented and attached through the access facilities provided. Whatever the users option, the result is a set of finite volume equations FVE's having the form,

$$a_P \phi_P = a_N \phi_N + a_S \phi_S + a_E \phi_E + a_W \phi_W + a_H \phi_H + a_L \phi_L + b \quad (3.5)$$

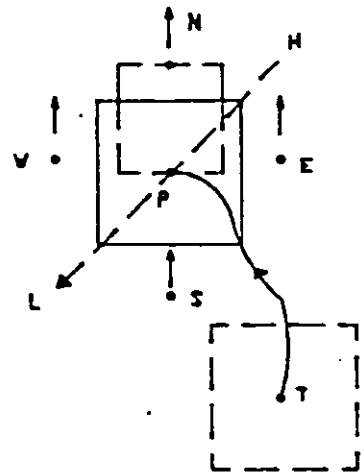
where,

$a_P, a_N, \dots$  are coefficients;

$b$  is a representation of the source appropriate to  $\phi$  for the cell.

Subscripts have the following meanings (according to the diagram).

- P: typical point (i.e. node) within cell;
- N: north-neighbour node, in positive-y direction,
- S: south-neighbour node, in negative-y direction,
- E: east-neighbour node, in positive-x direction,
- W: west-neighbour node, in negative-x direction,
- H: high-neighbour node, in positive-z direction,
- L: low-neighbour node, in negative-z direction, and,
- T: grid node at earlier time.



The PHOENICS FVE's differ from 'finite-difference' equations in:

- origin(no Taylor-series are used);
- values of coefficients (as a consequence).

And also differ from 'finite-element' equations in:

- origin(neither variational principle nor Galerkin weighting is used);
- number of nodes referred to (8 in PHOENICS, for three-dimensional transient problems; usually more in 'finite-element' problems).

PHOENICS solves the set of FVE's in an iterative manner since they are non-linear, by reason of the a's, and b's being themselves dependent on the  $\phi$ 's.

### 3.4.3 Solution Procedures Employed

The sets of linear equations described in the previous section have to be solved, i.e. the values of  $\phi_P$  have to be obtained for all points. Several built-in procedures

are attached to PHOENICS such as;

1. Procedures for solving sets of linear equations which entails;
  - (a) Jacobi point-by-point,
  - (b) Slab-wise simultaneous,
  - (c) Three-dimensional simultaneous,
  - (d) Hybrid methods,
  - (e) The partial elimination algorithm.
  
2. Solution of linked hydrodynamic equations.

PHOENICS embodies a variant of the SIMPLE ( Semi-Implicit Method for Pressure Linked Equations ) algorithm, having the following essential ideas;

- the pressure field is guessed;
- the corresponding velocity fields are computed;
- the resulting errors in the continuity equation are computed; and
- these errors are used as quantitative indicators of corrections which should be made to the pressures, and of the corresponding velocity corrections.

SIMPLE provides good velocity fields (satisfying continuity at least) but poor pressure fields and requires much under-relaxation of pressures and/or velocities if convergence is to be procured especially for fine grids. SIMPLER

(standing for SIMPLE Revised) is a suitable cure for such problems but involves additional computational work while SIMPLEST (standing for SIMPLE Shortened) used by PHOENICS provides the supreme cure.

3. InterPhase Slip Algorithm (IPSA). A more elaborate algorithm used in the .NOT.ONEPHS mode, i.e. when two sets of velocity components have to be obtained, and also the volume fractions of phases.

Additional information on mathematical procedures used by PHOENICS may be conducted through Spalding (1987).

### 3.5 NUMERICAL SOLUTION OF EQUATIONS

The mathematical equations of continuity, momentum, energy and equations governing the conservation of turbulent quantities are solved simultaneously by the previously mentioned numerical procedure embodied in PHOENICS.

All these are carried over  $x - y$  plane and marched downstream to the next plane in the  $z$  direction. However since the problem is elliptic in nature due to recirculation involved; the procedure used here involves iteration at each  $x - y$  plane for pressure field for the whole domain until the solution is converged.

The research aims at testing two equation models for the problem in question, Prediction of Film Cooling, two models were tested; the  $k - \epsilon$  model of Harlow and Nakayama (1968) and the  $k - \omega$  model of Spalding (1969) together with a modified version of the  $k - \omega$  model of Ilegbusi and Spalding (1983).

Since PHOENICS package was employed the details of numerical procedure as

well as derivations of finite difference equations are not given, on the other hand more details are present in references [14,27,30,31,47,48,49,50,51].



# Chapter 4

## Turbulence Modelling

### 4.1 BACKGROUND

Turbulence is the most common and the most complicated kind of fluid motion. Although it is difficult to give a precise definition of turbulence; one can list its features. Turbulent flows are unsteady, highly irregular, diffusive (which causes rapid mixing and increased rates of momentum, heat and mass transfer), dissipative (the kinetic energy of the turbulence is converted into heat via work done against viscous stresses), three-dimensional and at large Reynolds numbers, and finally such flows are rotational and with high levels of fluctuating vorticity.

In spite of all recent advances in computer technology, the solution of time-dependent three-dimensional Navier-Stokes equations which are believed to be able to describe turbulent flows is complicated. This is due to the fact that the storage capacity and speed of present-day computers is still insufficient to allow a solution for any practically relevant turbulent flow. The reason is that the turbulent motion contains elements which are much smaller than the extent of the flow domain, typically of the order of  $10^{-3}$  times smaller. Hence, it is of practical importance to describe turbulent motion in terms of time-averaged quantities rather than instantaneous.

Substitution of apparent mean (Reynolds) stresses for the actual transfer of momentum by the velocity fluctuations increase the number of unknowns above the number of equations. The problem is then to supply the information missing from the time averaged equations by formulating a model to describe some or all of the six independent Reynolds stresses,  $-\rho\overline{u_i u_j}$ .

The exact Reynolds stresses transport equations can be derived from the time-dependent Navier-Stokes equations expressing the conservation of each momentum. In turbulence modelling one uses a finite number of Reynolds stress transport equations with the supply of missing information from experimental results. The time-averaged scalar transport equation contains the turbulent heat or mass flux,  $-\rho\overline{u_i \phi}$ , where  $\phi$  is the fluctuating scalar quantity. One has to model this term to solve the scalar transport equation, Nallasamy (1987).

#### 4.1.1 Equations of Motion

The time-averaged continuity and momentum equations are:

$$\frac{\partial \overline{u_i}}{\partial x_j} = 0 \quad (4.1)$$

$$\frac{\partial \overline{u_i}}{\partial t} + \overline{u_j} \frac{\partial \overline{u_i}}{\partial x_j} = -\frac{1}{\rho} \frac{\partial \overline{P}}{\partial x_i} + \frac{\mu}{\rho} \nabla^2 u_i - \frac{\partial R_{ij}}{\partial x_j} \quad (4.2)$$

Where  $R_{ij} = \overline{u_i u_j}$ , the Reynolds stress. In order to establish a turbulence model it is necessary to evaluate  $R_{ij}$  in terms of  $\overline{u_i}$ , constants evolved will be determined through experimental data.

### 4.1.2 Classification of Turbulence Models

Turbulence models are classified according to the number of differential equations solved in addition to the mean flow equations as follows:-

- (I) Zero equation models.
- (II) One equation models.
- (III) two equation models.
- (IV) Stress equation models.

The two equation models;  $k-\omega$  together with  $k-\epsilon$ , are to be more high-lightened than other models since they are to be employed for this specific problem (Prediction of film cooling).

- (I) Zero equation models.

Zero equation models are mostly based on the eddy viscosity concept. The Prandtl's mixing length hypothesis (1925), still one of the most widely used models, relates the turbulent transport terms to the local gradient of mean flow quantities. For example, for thin shear layers,

$$-\overline{u'v'} = \nu_t \frac{\partial U}{\partial y} \quad \text{where} \quad \nu_t \text{ is the eddy viscosity.}$$

The hypothesis calculates the distribution of eddy viscosity by relating it to the mean velocity gradient:

$$\nu_t = C_\mu \ell_m^2 \left| \frac{\partial U}{\partial y} \right| \quad (4.3)$$

This model is basically suitable only for simple shear-layer-dominated flows or when turbulence modelling is not important because the flow is pressure driven. It is easy to implement in Navier-Stokes computer codes, and computationally economical. On the other hand this model is unsuitable for complex flows because it is very difficult to estimate the distribution of the mixing length.

The mixing length model implies that the turbulence is in local equilibrium, so that the model can not account for the transport effects of turbulence.

(II) One equation models.

This model requires the solution of one equation for the turbulent kinetic energy,  $k$ , being derived from the Navier-Stokes equations. Eddy viscosity  $\nu_t$  is modelled by the so-called Kolmogorov-Prandtl expression  $\nu_t = C_\mu k^{1/2} \ell$  where  $\ell$  is the flow dependent length scale which is difficult to be determined for complex flows with separation, streamline curvature or rotation. This model is not widely used since it performs only marginally better than the Zero equation models.

(III) two equation models.

This is the most commonly used type of models in the present day engineering calculation. In this model a second differential equation is provided to evaluate the length scale so as not to be determined as a function of the position throughout the flow, this differential equation or the so-called *transport equation* is derived from the Navier-Stokes equations. In general, one looks at  $Z$  which is a quantity of  $k$  &  $\ell$  where  $Z = k^\alpha \ell^\beta$ , Nallasamy (1987), where  $\alpha$  and  $\beta$  are exponents, thus;

$$\rho \frac{DZ}{Dt} = \frac{\partial}{\partial y} \left( \frac{\mu_t}{\sigma_z} \frac{\partial Z}{\partial y} \right) + Z \left[ C_1 \frac{\mu_t}{k} \left( \frac{\partial U}{\partial y} \right)^2 - C_2 \rho^2 \frac{k}{\mu_t} \right] + S_z \quad (4.4)$$

where:

$\sigma_z$  is Prandtl number for the diffusion of  $Z$ ,

$S_z$  is a secondary source term,

$C_1, C_2$  are constants.

Several suggestions were adopted by different authors, for  $Z$ , as follows:

- Kolmogorov (1942)  $Z = k^{1/2}/\ell \equiv \omega^{1/2}$
- Harlow and Nakayama (1968)  $Z = k^{3/2}/\ell \equiv \epsilon$
- Rotta (1951)  $Z = k\ell$
- Spalding (1969)  $Z = k/\ell^2 \equiv \omega$
- Saffman (1970)  $Z = k/\ell^2 \equiv \omega$
- Zeierman and Wolfstein (1986)  $Z = \ell/k^{1/2}$

Three different kinds of two equation models were experimented by Imperial College group lead by D B Spalding, Nallasamy (1987):  $k - k\ell$ ;  $k - \omega$  and  $k - \epsilon$ . Here  $\ell$  is a length representing the macroscale of turbulence being defined as  $\ell = C_D k^{3/2}/\epsilon$ , where  $C_D$  is a constant.

$\omega$  is a quantity having the dimension of  $(time)^{-2}$  and represents the time average square of the vorticity fluctuations, and is defined by

$$\omega = \epsilon^2 / (C_D k)^2 \quad (4.5)$$

where;

$$\epsilon = \nu \frac{\overline{\partial u_j \partial u_i}}{\partial x_k \partial x_k} \quad (4.6)$$

Spalding (1971), obtained the following relations:

$$\frac{dk\ell}{k\ell} = 5/2 \frac{dk}{k} - \frac{d\epsilon}{\epsilon} \quad (4.7)$$

$$\frac{d\omega}{\omega} = -2 \frac{dk}{k} + 2 \frac{d\epsilon}{\epsilon} \quad (4.8)$$

The three models are closely related to one another though they differ in the forms of diffusion and near wall terms employed.

#### (IV) Stress equation models.

These models are classified as;

1. Reynold-stress-Transport models: these are models involving transport equations for all components of the Reynold-stress tensor; and in general, a transport equation is required for the length scale.

A full stress model can provide a more realistic and rigorous approach to account for complex strain fields associated with curvature, rotation and other effects.

However, for three-dimensional flows it may be prohibitively expensive from a computational standpoint.

2. Algebraic Stress models: these are models intermediate to two-equation eddy-viscosity models and stress transport models. The stress-transport equations are simplified to provide algebraic expressions for the turbulent stresses which are solved together with transport equations for the turbulent kinetic energy and a length scale.

Algebraic stress models have been used successfully to account for the effect of the body forces( buoyancy,swirl,rotation), but are unsuitable for flows too far removed from equilibrium. These models are rather complex and difficult to implement for general three-dimensional elliptic flows.

#### 4.1.3 Near-wall Approaches

The wall no-slip condition ensures that over some region of the wall layer, viscous effects on the transport processes must be large. The representation of the processes within a mathematical model raises two problems.

First, the model of turbulence for this region must address the problem of appro-

priately viscous effects into the system of equations employed. Secondly, a very fine computational mesh is required to resolve the rapid variation of flow variables which occurs within this region.

Two methods are adopted for the solution of such problem:

#### Wall-Function Method

In this method viscous sub-layer is bridged by employing wall functions; providing the near-wall boundary conditions for the momentum and turbulence transport equations. These wall functions are empirical formulae connecting the wall conditions to the dependent variables at the near-wall grid node. This grid node is presumed to lie in fully-turbulent fluid.

The advantages of this approach are that it escapes the need to extend the computations right to the wall, and it avoids the need to account for viscous effects in the turbulence model.

#### Low-Reynolds-Number Method

This method implies using a very fine-grid analysis in which computations are extended through the viscosity-affected sub-layer close enough to the wall to allow laminar-flow boundary conditions to be applied.

For more details on this method, the reader is advised to refer to Nallasamy (1987).

## 4.2 $k - \omega$ MODEL

We suppose that, for the steady-state situations to which attention will be here confined, the distributions of  $k$  and  $\omega$  will obey the differential equations, Spalding (1971):

$$G.grad k - div(\Gamma_k grad k) = S_k \quad (4.9)$$

$$G.grad \omega - div(\Gamma_\omega grad \omega) = S_\omega \quad (4.10)$$

where;  $G$  is the time-mean mass-velocity vector,  $\Gamma_k$  and  $\Gamma_\omega$  are scalar quantities playing the parts in the "effective exchange coefficients". And  $S_k$  and  $S_\omega$  represent source rates per unit volume. Of course, the  $\Gamma_{grad}$  terms represent simplifications of the real turbulent-exchange process which may not accord with experimental findings; nevertheless it is reasonable to suppose that the movements of large eddies convey fluctuation energy and vorticity fluctuations from regions of large fluctuations into neighbouring regions where the fluctuations are smaller.

$S_k$  is made up of two terms; a positive one,  $G$ , which is a consequence of the interaction of the turbulent stresses with the gradient of the time-mean motion; and a negative one,  $D$ , due to the action of laminar viscosity in damping out the fluctuating velocity gradients, where these terms are represented as,

$$G = \mu_t \left( \frac{\partial u_j}{\partial x_k} + \frac{\partial u_k}{\partial x_j} \right) \frac{\partial u_j}{\partial x_j} \quad (4.11)$$

$$D = C_D \rho k \omega^{1/2} \quad (4.12)$$

$C_D$  is a constant ( $\approx 0.09$ ) for high Reynolds-number turbulence, Spalding (1971).

And the length scale may be deduced from the following equation,

$$\ell = (k/\omega)^{1/2} \quad (4.13)$$

The source of  $\omega$ ;  $S_\omega$  is also made up of positive and negative terms. Specifically, it is presumed that:

$$S_\omega = C_1 \mu_t (\text{grad } \Omega)^2 + C_3 \frac{\omega}{k} G - C_2 \rho \omega (\omega)^{1/2} \quad (4.14)$$

where  $C_1, C_2$ , and  $C_3$  are either constants or functions of locally-determinate arguments, and  $\Omega$  is the magnitude of the local time-mean-vorticity vector.

effective exchange coefficients  $\Gamma_k$  and  $\Gamma_\omega$  are deduced from the following relation:



$$\sigma_k = \mu_t / \Gamma_k, \quad \sigma_\omega = \mu_t / \Gamma_\omega, \quad (4.15)$$

where  $\sigma_k$  and  $\sigma_\omega$  are called Prandtl-Schmidt numbers and lie in the neighbourhood of unity.

### 4.2.1 Empirical Constants and Functions

#### The value of $C_D$ .

The value of  $C_D$  is derived under the assumption of equal generation and dissipation terms; this assumption is justified by the large Reynolds number in the neighbourhood of a wall implying that these are the only significant terms in  $k$ -equation thus;

$$\mu_t \left( \frac{\partial u}{\partial y} \right)^2 = C_D \rho k \omega^{\frac{1}{2}} \quad (4.16)$$

since  $\tau_t = \mu_t \frac{\partial u}{\partial y}$ ;  $\omega$  degenerates to;

$$\omega = \frac{1}{C_D} \left( \frac{\partial u}{\partial y} \right)^2 \quad (4.17)$$

and  $\omega$  degenerates to;

$$k = \frac{1}{C_D^{\frac{1}{2}}} \frac{\tau_t}{\rho} \quad (4.18)$$

Now experimental data in boundary layers of various kinds have shown that  $\tau_t / (\rho k)$  takes a value of 0.3; thus giving  $C_D$  a value of 0.09.

#### The value of $C_2$ .

When homogeneous turbulence decays downstream of a grid then, according to Spalding (1971);

$$\rho u \frac{dk}{dx} = -C_D \rho k \omega^{\frac{1}{2}}, \quad (4.19)$$

and:

$$\rho u \frac{d\omega}{dx} = -C_2 \rho \omega \omega^{\frac{1}{2}}. \quad (4.20)$$

thus we conclude that  $k^{C_2} \omega^{-C_D} = \text{const.}$ ; and since the length scale  $\ell$  is equal to  $\left(\frac{k}{\omega}\right)^{1/2}$ , then,

$$\frac{\ell}{k} \frac{dk}{d\ell} = \frac{2C_D}{C_D - C_2} \quad (4.21)$$

again according to experimental data  $\frac{\ell}{k} \frac{dk}{d\ell}$  is of the order of -2; this gives  $C_2$  a value of 0.18 which is twice  $C_D$ .

#### Relation between employed constants.

Since  $\mu_t = \kappa y \sqrt{\tau \rho}$  in a uniform shear layer adjacent to the wall; then

$$\omega = \frac{1}{C_D \kappa^2} \frac{\tau / \rho}{y^2} \quad (4.22)$$

$$\left(\frac{\partial u}{\partial y}\right)^2 = \frac{1}{\kappa^2} \frac{\tau / \rho}{y^2} \quad (4.23)$$

$$\left(\frac{\partial^2 u}{\partial y^2}\right)^2 = \frac{1}{\kappa^2} \frac{\tau / \rho}{y^4} \quad (4.24)$$

$$G = D = \frac{\rho (\tau / \rho)^{3/2}}{\kappa y}. \quad (4.25)$$

Now with some mathematical manipulations the following relation may be obtained;

$$\left(\frac{4}{\sigma_\omega} + C_1 C_D\right) \kappa^2 + C_3 C_D^{1/2} - \frac{C_2}{C_D^{1/2}} = 0 \quad (4.26)$$

The last equation implies that there is no freedom to determine each of the constants  $\sigma_\omega$ ,  $C_1$  and  $C_3$  independently; if the model is to accord with the well-established data for the law of wall, Spalding (1971).

## 4.2.2 Modified Version of $k-\omega$ Model

The objectionable feature of the earlier version of  $k-\omega$  model was its inclusion of the term  $(\frac{k}{\omega})/y^2$  which becomes significant for small  $y$ . It was recognised that the gradient of the length scale would serve equal well to characterize the effect of the wall in causing strong eddy-size variations.

The difference between the original  $k-\omega$  model and the modified version is the source term of the vorticity fluctuation. The modified source term is, Illegbusi and Spalding (1985);

$$\underbrace{S_\omega}_{\text{modified}} = \underbrace{S_\omega}_{\text{old}} - C_4 \rho \omega^{3/2} \left( \left| \text{grad} \left( \frac{k}{\omega} \right)^{1/2} \right| \right)^{C_b} \quad (4.27)$$

where;

$$\underbrace{S_\omega}_{\text{old}} = S_\omega \text{ appearing in eq. (4.14)}$$

The values of auxiliary constants

All constants are compatible with those established by earlier work, and have been adopted for this modified version without change. Of the two remaining constants,  $C_b$  was guessed to equal 2.0, implying that the new term is proportional to the square of the gradient of the turbulence length scale and therefore independent of its sign. The constant  $C_4$  can be derived through the relation, Spalding (1971):

$$\left( \frac{4}{\sigma_\omega} + C_1 C_D - C_\mu C_4 \right) \kappa^2 - C_2 C_\mu C_D^{-1/2} + C_3 C_D^{1/2} C_\mu^{-1/2} = 0 \quad (4.28)$$

From this relation,  $C_4$  is deduced to equal 2.97; and it is this value which was employed in the computations considered Illegbusi and Spalding (1985).

### 4.3 $k$ - $\epsilon$ MODEL

Now, considering the  $k$ - $\epsilon$  model, one solves two differential equations ,Launder and Spalding (1974); one for the turbulent kinetic energy and the other one is for its dissipation rate.

(a)  $k$ -equation

$$\frac{Dk}{Dt} = \frac{1}{\rho} \frac{\partial}{\partial x_k} \left[ \frac{\mu_t}{\sigma_k} \frac{\partial k}{\partial x_k} \right] + \frac{\mu_t}{\rho} \left( \frac{\partial U_i}{\partial x_k} + \frac{\partial U_k}{\partial x_i} \right) \frac{\partial U_i}{\partial x_k} - \epsilon \quad (4.29)$$

(b)  $\epsilon$ -equation

$$\frac{D\epsilon}{Dt} = \frac{1}{\rho} \frac{\partial}{\partial x_k} \left[ \frac{\mu_t}{\sigma_\epsilon} \frac{\partial \epsilon}{\partial x_k} \right] + \frac{C_1}{\rho} \mu_t \frac{\epsilon}{k} \left( \frac{\partial U_i}{\partial x_k} + \frac{\partial U_k}{\partial x_i} \right) \frac{\partial U_i}{\partial x_k} - C_2 \frac{\epsilon^2}{k} \quad (4.30)$$

where:

$$\mu_t = C_\mu \rho k^2 / \epsilon \text{ and,}$$

$$C_\mu = 0.09 , C_1 = 1.44 , C_2 = 1.92 , \sigma_k = 1.0 , \sigma_\epsilon = 1.3 \quad \text{Launder and Spalding (1974).}$$

These constants were adopted according to the recommendations of Launder et.al.(1972), after extensive examination of free turbulent flows. The above mentioned constants have been found, by the same authors, to be appropriate to plane jets and mixing layers and need to be modified for curvature, low Reynolds number, near wall effect, etc.

$k$ - $\epsilon$  model is widely used due to the fact that the use of an equation for the dissipation of turbulence energy,  $\epsilon$  , which can be related to a length scale by  $\epsilon = k^{3/2} / \ell$ . This latter form has a number of advantages; it is a quantity which appears directly in the equation for  $k$ , and so calculating it removes the need for any assumption about this term. It is also simply an algebraic function of the fluctuating veloc-

ity gradients and an exact equation may therefore be readily constructed from the Navier-Stokes equations.

The  $k$ - $\epsilon$  model is the only two-equation model which permits  $\sigma_\epsilon$  to have a reasonable value which will fit the experimental data for the spread of the various entities at locations far from walls, without modification of any constants.

### 4.3.1 Modified Version $k$ - $\epsilon$ Model

The standard  $k$ - $\epsilon$  model is based on the assumption that the eddy viscosity is the same for all Reynolds stresses (isotropic eddy viscosity). This assumption is too crude in certain flow situations; for example it does not produce the turbulence-driven secondary motions in square ducts which have been observed in experiments. On the other hand, simple thin shear layers flow situations are not influenced by this assumption because only the shear stress  $\overline{uv}$  is important in such flows. The standard version of  $k$ - $\epsilon$  model was refined by the introduction of a so-called algebraic stress model, where the individual stresses  $\overline{u_i u_j}$  are directly related to the mean-velocity gradients, Rodi (1980).

## 4.4 WALL BOUNDARY CONDITIONS

The simplest set of wall functions are those appropriate to a near-wall layer in local equilibrium, and may be written as follows, Rodi(1982) <sup>1</sup>.

$$\frac{U_p}{U_\tau} = \frac{1}{\kappa} \ln \left( E \frac{U_\tau y_p}{\nu} \right) \quad (4.31)$$

---

<sup>1</sup>Concepts to be discussed in this section are those having direct relation to present research only.

$$k_p = \frac{U_\tau^2}{\sqrt{C_\mu C_D}} \quad (4.32)$$

$$\epsilon_p = \frac{U_\tau^3}{\kappa y_p} \quad (4.33)$$

which enables the energy  $k_p$  to be deduced from  $U_\tau$ ; and

$$\omega_p = \kappa^{-2} C_D^{-1/2} k_p / y_p^2 \quad (4.34)$$

In these relations; the resultant velocity parallel to the wall,  $U_p$ , the kinetic energy  $k_p$  and dissipation rate  $\epsilon_p$  at the point  $y_p$  are related to the resultant friction velocity  $U_\tau$ , where p is first computational point near the wall and is to be located in the fully turbulent log-low region.  $k_p$  and  $\epsilon_p$  and  $\omega_p$  are computed by assuming that the generation and dissipation of energy are equal in the near wall layer where the shear stress is uniform and the length scale is proportional to the distance from the wall.

The heat transfer counterpart was that developed by Launder et.al.(1975). For both momentum and heat the diffusive transport properties are proportional to that of the normal stresses in respective direction. Bergeles (1976) suggested <sup>2</sup> that in order to explain the near-wall temperature profiles, the fluctuating energy function  $\Gamma$  in the lateral direction must be greater than that in the normal to the surface direction (i.e.  $\Gamma_x > \Gamma_y$ ) where  $\Gamma_i = 0.31 \frac{k}{\epsilon} \overline{u_i^2}$ . He also suggested the following relation:

$$\frac{\Gamma_x}{\Gamma_y} = \frac{\mu_{tx}}{\mu_{ty}} = 1 + C_m \left(1 - \frac{y}{\delta}\right) \quad \text{for } y < \delta \quad (4.35)$$

i.e. assuming non-isotropic viscosity, and

$$\frac{\Gamma_x}{\Gamma_y} = \frac{\mu_{tx}}{\mu_{ty}} = 1 \quad \text{for } y > \delta \quad (4.36)$$

---

<sup>2</sup>this suggestion was related to  $k - \epsilon$  turbulence model.

i.e. assuming isotropic viscosity.

The constant  $C_m$  for the present investigation was found to be 3.5 and  $\overline{u_y^2}$  was assumed to be  $k/3$ , which leads to the following expressions for the effective turbulent viscosity and diffusivity respectively:

$$\mu_{ty} = C_\mu k^2 / \epsilon \quad (4.37)$$

$$\Gamma_y = C_\tau k^2 / \epsilon \quad (4.38)$$

where  $C_\mu$  and  $C_\tau$  are 0.09 and 0.1, respectively.  $C_\mu$  was deduced, from the function model  $C_\mu = f(\overline{E/\epsilon})$  of Rodi (1972)<sup>3</sup> which represents the variation of  $C_\mu$  with  $(\overline{E/\epsilon})$  the ratio of production to dissipation, under the assumption of equilibrium i.e.  $(\overline{E/\epsilon}) = 1$ .

---

<sup>3</sup>the function model is shown in fig.(4-1)

# Chapter 5

## Discussion of Results

### 5.1 PRELIMINARY TESTS

#### 5.1.1 Effect of Injectant Velocity Profile

The following three profiles were employed for the injectant over the holes;

$$\frac{U}{U_c} = \left(\frac{Y}{D}\right)^{1/7} \quad (5.1)$$

$$\frac{U}{U_c} = \frac{3X}{4D} \quad (5.2)$$

$$\frac{U}{U_c} = 1 - \left(\frac{Y}{D}\right)^2 \quad (5.3)$$

Fig.(5.1a) and fig.(5.1b) show the predicted velocity profiles at the center line of the first row of holes, ( $X/D=0.0$ ). It is evident that the effect is visible only at  $0.3 < Y/D < 0.8$ , and a linear injection profile tends to increase the velocity by about 15% from that due to a power law or parabolic injection on the flow field immediately behind the injection holes as far as  $Z/D < 2.5$ . The effect of a parabolic velocity profile is negligible compared with the power law profile. On the other hand, power law profile was employed, for its universality, in the present work.

#### 5.1.2 Grid Dependence Effect

The grid used over the test section; shown in fig.(5.2) is selected in such a way to insure convergence and to reduce the residuals for almost all variables. The grid



was developed in such a way that near the wall, the grid is very fine and expands in the direction of increasing  $Y$  to account for the excessive changes in properties near the wall.

The grid specification in the  $Z$ -direction has 3 large cells at the leading edge to ensure fully developed flow over the test section. However, over the hole region the grid is made small to account for the severe changes in that region. Far away from the hole region, the grid is enlarged all over the remaining  $Z$ -extent, where the flow exhibits boundary layer flow profile (parabolic profile).

Finally, this distribution is efficient enough for the computer time to be economical, where if a uniform and fine grid were employed over the whole domain; the computer time will be very long compared with the prescribed non-uniform grid.

## 5.2 FILM COOLING EFFECTIVENESS RESULTS

The local film cooling effectiveness predictions were taken for six blowing rates namely ( $M=0.1,0.2,0.35,0.508,0.7,1.0$ ) at several lateral positions. The local film cooling effectiveness predictions were used to find the lateral averaged film cooling effectiveness by integrating the area under the graph of film cooling effectiveness in the lateral direction, i.e.

$$\bar{\eta} = \frac{1}{P/2D} \int_0^{P/2D} \eta d(X/D) \quad (5.4)$$

where:

$P$  is the pitch distance between holes,

$D$  is the diameter of the injection hole,

$X$  is the distance measured laterally across the surface.

The predicted results of local film cooling effectiveness ( $\eta$ ) for the six previously mentioned blowing rates, at the center line of the first row of holes ( $X/D=0.0$ ) are shown in figs(5-3a,5-3b). At low blowing rates ( $M=0.1,0.2,0.35$ ); the maximum film cooling effectiveness occurs in the vicinity of the hole, and as downstream distance is increased,  $\eta$  starts to decrease due to the dilution of the jet. At higher blowing rates, i.e. ( $M=0.508,0.70,1.0$ ),  $\eta$  nearly exhibits the same behaviour as that of low blowing rates in the sense that it tends to decrease with the increase in the stream-wise distance.

A reduction in the film cooling effectiveness is observed with higher blowing rates compared with those of lower blowing rates at the vicinity of the holes; this is due to the fact that the jet tends to lift off the surface. Increasing the blowing rate will increase the film cooling effectiveness to some extent after which the high momentum possessed by the coolant will lift the jet off the surface and hence the mainstream flow is introduced underneath the jet reducing the film cooling effectiveness.

At the center line of the second row of holes ( $X/D=1.5$ ), the film cooling effectiveness decreased to a minimum then started to increase till  $Z/D=11.3$  which is the edge of the second row of holes, where  $\eta$  started to decrease with further increase in the streamwise direction ( $Z/D$ ), fig.(5-3c).

Similar trends to those at the center line of the first row of holes at  $X/D=0.0$  for both low and high blowing rates are shown in figs(5-3c,5-3d), with further increase in blowing rate; the jet starts to lift off the surface. This lift off is confirmed by the reduction in  $\eta$  in the vicinity of the holes.

The general trends obtained from the predicted results of film cooling effectiveness are identical to the experimental trends reported by Jubran (1989), Schönung and Rodi (1987), and Goldstein et.al. (1968).

### 5.2.1 Comparison of Different Turbulence Models

Three blowing rates were selected for the purpose of comparison of different turbulence models for the prediction of film cooling effectiveness with experimental results of Jubran (1989), namely  $M=0.2, 0.508$  and  $1.0$ . Jubran (1989) carried out his experimental investigation in a low-speed recirculatory wind tunnel with a uniform free stream at a controlled velocity up to  $15$  m/s and temperature up to  $60^\circ\text{C}$ . Cold air was injected through the base of the working section. Temperature measurements were made on the base of the working section downstream of the cold air injection tubes in the streamwise and lateral directions. The injection configurations investigated were two symmetric staggered rows of holes of constant hole diameter (equal to  $19.4$  mm) spaced  $10$  hole diameters in the streamwise direction, the pitch to diameter ratio was  $3$ , and the angle of injection was  $30$  deg. to the streamwise direction and  $90$  deg. to the lateral direction. A detailed description of the experimental work is reported in Jubran and Brown (1985).

Various turbulence models were employed for the prediction of film cooling effectiveness; these models are: isotropic  $k - \epsilon$  model, non isotropic  $k - \epsilon$  model,  $k - \omega$  model, and a modified version of  $k - \omega$  model.

At the center line of the first row of holes ( $X/D=0.0$ ) all turbulence models tend to well predict film cooling effectiveness for  $Z/D < 5$  at  $M=0.2$ , however, as  $Z/D$  is increased; all turbulence models tend to over predict  $\eta$  with the non isotropic

$k - \epsilon$  model giving the best prediction, fig.(5-4a). Fig.(5-4b) shows the predicted results for a lateral position  $X/D=0.9$ . The predicted results indicate that all models over predict  $\eta$ , which may be contributed to the fact that all turbulence models considered tend to spread the jet of coolant much more than that occurring in reality.

At  $X/D=1.5$ , fig.(5-4c), again all turbulence models tend to over predict  $\eta$  for almost all positions in the streamwise direction with the isotropic  $k - \epsilon$  model producing least mixing of all other models for  $Z/D < 10.0$  and hence higher predicted values of film cooling effectiveness are achieved. Both versions of  $k - \omega$  model seem to predict the reversing flow occurring at the edge of the second row of holes ( $X/D=11.3$ ) much better than both versions of  $k - \epsilon$  model.

As the blowing rate ( $M$ ) is increased to  $M=0.508$ , at  $X/D=0.0$ , fig.(5-5a), all turbulence models employed tend to under predict film cooling effectiveness in the vicinity of the hole. This may be explained by the fact that if the secondary flow (coolant) has high momentum; the jet tends to lift off and a pair of vortices are formed, which introduce the mainstream fluid underneath the jet as a result. This phenomenon is sometimes called pumping effect. Hence the film cooling effectiveness is reduced by isolating the secondary jet from the wall. With further increase in the streamwise direction ( $Z/D$ ); all models tend to over predict  $\eta$  with the isotropic  $k - \epsilon$  model giving the best prediction. Moving laterally to  $X/D=0.9$ , fig.(5-5b), both versions of  $k - \epsilon$  model tend to well predict  $\eta$  for all positions in the  $Z/D$  direction, while both versions of  $k - \omega$  model tend to under predict  $\eta$  everywhere. The modified version of  $k - \omega$  model produces the highest mixing for  $Z/D < 10.0$  and hence gives poor prediction of film cooling effectiveness.

For a higher blowing rate of  $M=1.0$ , it can be concluded that for all lateral po-

sitions ( $X/D=0.0$ ,  $X/D=0.9$  and  $X/D=1.5$ ), figs(5-6a,5-6b,5-6c); both versions of  $k - \epsilon$  model tend to over predict local film cooling effectiveness, while the modified version of  $k - \omega$  model tends to under predict  $\eta$ .  $k - \omega$  model seems to give the best predictions for  $\eta$  at this high blowing rate.

The over prediction of  $\eta$  attained when  $k - \epsilon$  models are used, and the under prediction of  $\eta$  attained when  $k - \omega$  models are used may be explained by the fact that both versions of  $k - \epsilon$  model tend to spread the jet over the surface and hence increase the effectiveness, while both versions of  $k - \omega$  model tend to dilute the jet and hence reduce film cooling effectiveness.

The average film cooling effectiveness ( $\bar{\eta}$ ) graphs against  $Z/D$  are shown in figs(5-7). For all blowing rates;  $\bar{\eta}$  decreases with distance downstream up to  $Z/D=20.0$ , after which it becomes uniform for further increase in the streamwise direction, this is an indication that the jet is well merged by  $Z/D=20.0$ .

Both versions of  $k - \epsilon$  model tend to produce similar predictions of  $\bar{\eta}$ , also both versions of  $k - \omega$  give identical predictions for  $\bar{\eta}$ . In general, this may be explained by the fact that  $k - \omega$  model introduces more mixing than  $k - \epsilon$  model and hence reduces the average film cooling effectiveness. Due to the lack of experimental results for these particular predicted results of  $\bar{\eta}$ , no comparison with experimental results is presented.

### 5.3 VELOCITY PROFILES RESULTS

Before analysing the results of velocity profiles predictions it is helpful to describe the behaviour of the jet in cross flow. When a jet enters a cross flow its shape tends

to change due to the non-uniform pressure field created by the flow around it. A pair of vortices are created behind the jet as a result, these vortices gain momentum from the jet and move along the path of the jet increasing or decreasing their strength depending on the momentum ratio  $I$ , where

$$I = \frac{\rho_c U_c^2}{\rho_m U_m^2},$$

which affects the degree of viscous action by its control over the velocity profiles downstream of the injection.

Predictions for the velocity profiles were carried out for the six previously mentioned blowing rates; namely  $M=0.1, 0.2, 0.35, 0.508, 0.7$ , and  $1.0$ .

For low blowing rates, i.e.  $M=0.1, 0.2, 0.35$  and at the center line of the first row of holes ( $X/D=0.0$ ), the effect of injection is small and the profiles are approaching those of two dimensional boundary layer flow ones in the vicinity of the hole ( $Z/D=2.3$ ), fig.(5-8a). At  $Z/D=10.0$ , fig.(5-8b), a velocity deficit is observed, especially for  $M=0.35$ , due to the splashing of the coolant from the second row of holes.

Predictions of velocity profiles at the center line of the second row of holes ( $X/D=1.5$ ) are shown for several streamwise positions. At  $Z/D=1.3$ , fig.(5-8c) shows that velocity profiles are similar to those of two dimensional boundary layer flow, however, at  $M=0.35$  the jet starts to lift off decelerating the flow very close to the wall.

With further increase in the streamwise distance to  $Z/D=12.3$  and  $Z/D=14.9$ , figs(5-8d,5-8e) show that the velocity gradient downstream increased on that upstream, hence mixing is increased, this is confirmed by the faster rate of decay of

film cooling effectiveness at the downstream row than that at the upstream row of holes.

For higher blowing rates, i.e.  $M=0.508, 0.7, 1.0$ , and at  $X/D=0.0$ ; fig.(5-9a) shows that the velocity profiles are identical with those of two dimensional boundary layer flow for  $Z/D=2.3$ , while increasing  $Z/D$  distance to 10.0, fig.(5-9b) represents the recirculation in the vicinity of the wall. At  $X/D=1.5$ , fig.(5-9c) shows that there is a region of nearly constant velocity in the vicinity of  $Y/D=0.4$ , which is an indication that the jet has lifted off. Downstream at  $Z/D=12.3$ , the profiles start to recover to the two dimensional boundary layer flow, fig.(5-9d). At  $Z/D=14.9$ , fig.(5-9e), the mixing is higher than that at the center line of the first row of holes.

Finally, it should be mentioned, that all velocity profiles for high blowing rates are identical, however, the mixing and lift off of the jet become more severe with increasing the blowing rate.

### 5.3.1 Comparison of Different Turbulence Models

Velocity profiles employing the previously mentioned models are compared with the experimental results of Jubran (1989). At a low blowing rate of  $M=0.2$ , and at the center line of the first row of holes, both versions of  $k - \epsilon$  model tend to well predict velocity profiles in the vicinity of the hole, fig.(5-9a), while both versions of  $k - \omega$  model tend to under predict velocity profiles. With further increase in the streamwise direction to  $Z/D=10.0$ , both versions of  $k - \epsilon$  model tend to over predict velocity, while both versions of  $k - \omega$  model have the tendency to under predict velocity, fig.(5-9b). This is explained by the fact that  $k - \epsilon$  model tend to spread the jet more than the  $k - \omega$  models with increase in  $Z/D$  distance.

At the center line of the second row of holes ( $X/D=1.5$ ), figs(5-9c,5-9d,5-9e) show that both  $k - \omega$  model and its modified version tend to decelerate the flow under predicting the velocity for all streamwise locations considered. At  $Z/D=1.3$ , fig.(5-9c) shows that velocity is under predicted by  $k - \epsilon$  models for  $Y/D < 0.5$ , and is over predicted for  $Y/D > 0.5$ . Figs(5-9d,5-9e) show that  $k - \epsilon$  models tend to accelerate the flow for increasing  $Z/D$  distance, attaining the two dimensional boundary layer flow profile.

At a higher blowing rate of  $M=0.508$  and  $X/D=0.0$ , fig.(5-10a) shows that all models tend to over predict velocity for  $Y/D < 0.4$ ;  $k - \epsilon$  models tend to over predict velocity for all locations normal to the surface. Only  $k - \omega$  model was able to nearly predict the lift off of the jet, which is expressed by the nearly constant velocity for  $Y/D < 0.4$ . As  $Z/D$  distance is increased to 10.0; all turbulence models tend to decelerate the flow in the vicinity of the wall ( $Y/D < 0.5$ ), for higher positions normal to the surface;  $k - \epsilon$  models tend to over predict velocity, while  $k - \omega$  models tend to produce under predictions of velocity. Again  $k - \omega$  model gave best of all predictions for this position.

At the center line of the second row of holes ( $X/D=1.5$ ); all models tend to decelerate the flow at  $Z/D=1.3$ , fig.(5-10c), with  $k - \omega$  model giving the best prediction for velocity.  $k - \epsilon$  models tend to accelerate the flow with increasing the mainstream distance ( $Z/D$ ) to 12.3, fig.(5-10d) and  $Z/D=14.9$ , fig.(5-10e), and also they,  $k - \epsilon$  models, tend to recover the two dimensional boundary layer flow profile for further increase in  $Z/D$ .

At a higher blowing rate of  $M=1.0$ , and at  $X/D=0.0$ ,  $k - \epsilon$  models tend to well



predict velocities for  $Y/D < 0.3$  . While the modified version of  $k - \omega$  model tends to under predict velocity; the  $k - \omega$  model tends to give average values of experimental ones, fig.(5-11a), where it over predicts for  $Y/D < 0.5$  and under predicts for  $Y/D > 0.5$  . Moving downstream up to  $Z/D=10.0$ ; all models, but the  $k - \omega$  model, tend to under predict velocity and reflect a recirculation region in the vicinity of the wall. On the other hand,  $k - \omega$  model gives quite accurate predictions for velocity.

At  $X/D=1.5$ , all models considered have the tendency to decelerate the flow and could not represent the lift off of the jet as the  $k - \omega$  model, for  $Z/D=1.3$ , as shown in fig.(5-11c). The flow is accelerated by the  $k - \epsilon$  models when  $Z/D$  distance is increased to 12.3, fig.(5-11d), and further to  $Z/D=14.9$ , fig.(5-11e). The modified version of  $k - \omega$  model tends to under predict velocity always for this particular lateral position of  $X/D=1.5$  . The  $k - \omega$  model seems to give acceptable predictions of velocity profiles at  $X/D=1.5$  .

## 5.4 TURBULENT KINETIC ENERGY RESULTS

The predicted turbulent kinetic energy results for various distances in the stream-wise direction are shown in figs(5-13a to 5-13f). The mentioned figures show that the maximum turbulent kinetic energy ( $k$ ) is occurring very close to the hole and very close to the wall. Increasing the distance normal to the wall as well as increasing the distance downstream the holes tend to reduce the values of  $k$ .

The predicted results of  $k$ , for all values of blowing rates, indicate that as the blowing rate increases the value of turbulent kinetic energy is increased, as one might expect, this also can be seen in the previously mentioned figures.

For a more detailed explanation; it can be said that for a blowing rate of  $M=0.1$  and at  $X/D=0.0$ , fig.(5-13a), the high recirculation and turbulent kinetic energy in the vicinity of the hole was only at  $Z/D < 2.3$ , after which the effect of recirculation becomes very small due to the low blowing rate which signifies low momentum ratio. Now, increasing the blowing rate up to 0.35, fig.(5-13b), the recirculation continues to affect the film cooling effectiveness in all streamwise locations, due to the high momentum of jet. Finally, increasing  $M$  up to 0.7 a lift off of the jet is observed by the reduction of film cooling effectiveness over that of 0.35 blowing rate, and the higher values of  $k$ ,fig.(5-13c). High turbulence possessed by  $Z/D=10.0$  may be due to both the effect of the spread of the jet of the second row of holes, and the high momentum of the jet.

At  $X/D=1.5$ , fig.(5-13d) shows that for a low blowing rate of  $M=0.1$ ; turbulent kinetic energy increases with increasing  $Z/D$  till it attains its peak at about  $Z/D=12.3$ , then decays with further increase in the main stream direction. This increase in  $k$  is in the vicinity of the hole in the downstream row of holes, is a measure of the high circulation and hence mixing at that region.

At a higher blowing rate of  $M=0.35$ , tips of  $k$  occur for almost all locations as shown in fig.(5-13e), this will indicate a reverse flow and affects  $\eta$  profile for  $Z/D < 7.0$ , the reverse flow is responsible for more mixing and hence a reduction in the film cooling effectiveness with further increase in  $Z/D$  distance.

At a higher blowing rate of  $M=0.7$ , fig.(5-13f), the jet has lifted off and the main-stream flow is introduced underneath the jet close to the surface. At  $Z/D=10.0$  very high turbulent kinetic energy is restricted to small distances from the surface indicating high recirculation and hence much more mixing than that at  $M=0.35$ .

# Chapter 6

## Conclusions and Recommendations

### 6.1 CONCLUSIONS

This section tends to assess the important points which have emerged from the present investigation. They may be listed as follows:

1. It can be concluded that the  $k - \omega$  model tends to predict film cooling effectiveness better than the standard isotropic  $k - \epsilon$  model or the non isotropic  $k - \epsilon$  model or even the modified version of  $k - \omega$  model, at high blowing rates.
2. The non isotropic  $k - \epsilon$  model seems to have better predictions of  $\eta$  over the isotropic  $k - \epsilon$  model, especially for low blowing rates where it helps in the spreading of the jet much more than the standard  $k - \epsilon$  model.
3. Isotropic  $k - \epsilon$  model produces the best predictions for  $\eta$  at the center line of the first row of holes ( $X/D=0.0$ ).
4. The non isotropic version of  $k - \epsilon$  model predicts  $\eta$  much better than other models considered in this investigation for  $X/D=0.9$ .
5. At the center line of the second row of holes ( $X/D=1.5$ ), for blowing rate  $M \geq 0.508$  both versions of  $k - \epsilon$  model tend to well predict the film cooling

- effectiveness ( $\eta$ ) downstream the second row of holes at  $Z/D > 10.0$ . On the other hand, these models tend to over predict  $\eta$  for  $Z/D < 10.0$  for low blowing rates.
6. The prediction of the average film cooling effectiveness,  $\bar{\eta}$ , for all blowing rates using both versions of  $k - \epsilon$  model are very much identical but give higher values than those obtained by the two versions of  $k - \omega$  model. The two versions of  $k - \omega$  model produce identical predictions  $\bar{\eta}$ .
  7. The ability of any turbulence model to predict the film cooling effectiveness satisfactorily is very much dependent on the blowing rate in question as well as the distance from the injection holes. This is to say that no specific model can be generalized for all blowing rates at all locations. Therefore, it seems, that the main cause for quite poor predictions in certain cases is due to the assumption of equilibrium flow and only accounting for two components of Reynolds shear stresses.
  8. Both versions of  $k - \epsilon$  model tend to accelerate the flow for all blowing rates and locations investigated. At low blowing rates the prediction of the velocity profiles at the center line of the first row of holes is very satisfactory, especially in the vicinity of the holes. Furthermore, at high blowing rates the prediction is less satisfactory for almost all locations downstream the first row and the second row of holes.
  9. Both versions of  $k - \omega$  model tend to poorly predict the velocity profiles for almost all blowing rates and locations downstream the first row and second row of holes.
  10.  $k - \epsilon$  model ensures less iterations for all variables and hence smaller residuals for the same computer time provided for a  $k - \omega$  model. This is due to the

difficulties in evaluating the turbulent quantity  $\omega$  over the  $\epsilon$  quantity, especially for a problem with high recirculation and reverse flow.

11. Achieving convergence for  $\omega$  is not as quick as the  $\epsilon$  quantity, where  $\omega$  keeps penetrating with increasing iterations before it reaches a steady state value.

## 6.2 RECOMMENDATIONS

The literature survey in chapter 2 together with the present investigation suggest that there are few areas which need further investigation; some of these areas are mentioned in this section as follows:

1. In deriving the turbulence modelling closure; only the shear stresses  $\overline{u_1 u_2}$  and  $\overline{u_1 u_3}$  were taken into account, this is not valid at high blowing rates, so the third component  $\overline{u_3 u_2}$  must be taken into account as well.
2. The prediction in this particular investigation was for the experimental case of film cooling over a flat plate, i.e. the real case of a gas turbine blade was not predicted. It is highly recommended to predict the actual case using the built-in feature, of the body fitted coordinates, of PHOENICS and hence investigate the effect of curvature over a real turbine blade.
3. Another turbulence model, belonging to the two-equation-models of turbulence class, may be tested for the same problem; which is the  $k - k\ell$  model. In this model a transport equation for  $k\ell$  is solved together with the  $k$  equation.
4. Source terms related to turbulent quantities, should be considered for other direction than the normal to the surface direction; like the spanwise direction which may affect the spread of the jet.

5. The equilibrium assumption of production and dissipation terms and hence constant  $C_\mu$  may not always be valid especially for high blowing rates over the region of holes so the function model of Rodi (1972) described in chapter 4 may be employed for  $C_\mu$ ; i.e.  $C_\mu = 0.09$  is only correct for a flow in equilibrium, which is not the case for high blowing rates. This assumption is worth investigation.
6. To investigate the effect of density of coolant on film cooling of a gas turbine blades.
7. It is worth noting that not much attention has been given to the modelling of the turbulent heat flux  $-\overline{\rho h' u_i}$  and this would require further investigation.

# REFERENCES

- [1] G Bergeles, Three-dimensional discrete hole cooling process- An experimental and theoretical study. Ph D thesis, Mech. Eng. Dept., Imperial College, 1976.
- [2] G Bergeles, A D Gosman and B E Launder, The prediction of three-dimensional discrete hole cooling process: Part I Laminar flow, ASME J. of Heat Transfer, Vol.98, No.3, p.379, 1976.
- [3] G Bergeles, A D Gosman and B E Launder, The prediction of three-dimensional discrete hole cooling process: Part II Turbulent flow, ASME J. of Heat Transfer, Vol.103, p.141, 1981.
- [4] G Bergeles, A D Gosman and B E Launder, Double-row discrete hole cooling: An experimental and numerical study, J. Engg. for power, Vol.102, p.498, 1980.
- [5] A Brown, Theoretical and experimental investigation into film cooling. JSME 1967 Semi-international symposium, Tokyo, 1967.
- [6] M E Crawford, W M Kays and R J Moffat, Heat transfer to a full coverage film cooled surface with 30° slant hole injection, NASA Contractor Report NASA CR-2786, 1976.

- [7] B J Daly and F H Harlow, Transport theory of turbulence, Los Alamos Laboratory Report No. LA-DC-11304, 1970.
- [8] A O Demuren, Numerical calculations of steady three-dimensional turbulent jets in cross flow, *Comp. Meth. Appl. Mech. Engg.*, Vol.37, pp.309-328, 1983.
- [9] A O Demuren, W Rodi, Three-dimensional calculation of film cooling by a row of jets, *Proceedings of the Fifth GAMM-Conference on Numerical Methods in Fluid Mechanics, Rome*, pp.49-56, Oct.5-7, 1983.
- [10] A O Demuren, W Rodi and B Schönung, Systematic study of film cooling with three-dimensional calculation procedure. ASME paper 85-IGT-2, 1985.
- [11] R J Goldstein, Film cooling-*Advances in heat transfer* (T F Irvin and J P Hartnelt, eds) vol.7, pp.321-379, 1971.
- [12] R J Goldstein, G Shavit and T S Chen, Film cooling effectiveness with injection through a porous section, *J of heat transfer*, pp.353-361, Aug.1965.
- [13] R J Goldstein, E R G Eckert and J W Ramsey, Film cooling with injection through holes: Adiabatic wall temperatures downstream of a circular hole, *Transactions of ASME; J of Engg. for power*, pp.384-395, Oct.1968.
- [14] F H Harlow and A A Amsden, Numerical calculation of multi-phase fluid flow. *J Comp Phys* , Vol.17, 1975, pp.19-52.



- [15] H J Herring, A method of predicting the behaviour of a turbulent boundary layer with discrete transpiration jets, *Journal of Engg. for Power*, Vol.97, p.214, 1975.
- [16] J O Ilegbusi and D B Spalding, An improved version of the  $k-\omega$  model of turbulence. *Jr of Heat Transfer*, Vol.107, pp.63-69, 1985.
- [17] B A Jubran, Film cooling from two rows of holes inclined in the streamwise and spanwise directions. PhD Thesis, University of Wales, Institute of Science and Technology, Cardiff, England 1984.
- [18] B A Jubran, Correlation and prediction of film cooling from two rows of holes. *ASME paper*, Vol.111, pp.502-509, 1989.
- [19] Z A Khan, J J McGuirk and J H Whitelaw, A row of jets in cross flow, *AGARD CP 308*, 1982.
- [20] B E Launder and D B Spalding, The numerical computation of turbulent flows. *Computer methods in applied mechanics and engineering* 3, pp.269-289, 1974.
- [21] B E Launder and D B Spalding, *Lectures in mathematical models of turbulence*. Academic press, 1972.
- [22] B E Launder and D B Spalding, Turbulence models and their application to the prediction of internal flows. Paper 1 of *Inst. Mech. Engg. Symposium on Internal flows*, University of Salford, England, 20-22 April 1971.

- [23] B E Launder, A Morse, W Rodi and D B Spalding, The prediction of free shear flows-A comparison of the six turbulence models. Proceedings of NASA conference on free shear flows, Langley (1972), (Also Imperial College, Mechanical Engineering Department report TM/TN/A/19.
- [24] N C Markatos, The mathematical modelling of turbulent flows. Appl. Math. Modelling, Vol.10, pp.190-220, 1986.
- [25] K L Miller and M E Crawford, Numerical simulation of single, double and multiple row film cooling effectiveness and heat transfer, ASME 84-GT-112, 1984.
- [26] M Nallasamy, Turbulence models and their applications to the prediction of internal flows: A review. Computers & Fluids Vol.15, No.2, pp.151-194, 1987.
- [27] S V Patankar and D B Spalding, A calculation procedure for heat, mass and momentum transfer in three-dimensional parabolic flows, IJHMT, Vol.15, pp.1787-1806, Pergamon Press, 1972.
- [28] S V Patankar, A K Rastogi and J H Whitelaw, The effectiveness of three-dimensional film cooling slots-II Predictions, Int. J. Heat and Mass Transfer, Vol.16, pp.1665-1681, 1973.
- [29] S V Patankar, D K Basu and S A Alpay, Prediction of three-dimensional velocity field of a deflected jet, ASME J. Fluids Engg., Vol.15, pp.758-762, 1977.
- [30] S V Patankar, Numerical heat transfer and fluid flow, Hemisphere 1980.

- [31] S V Patankar, A calculation procedure for two-dimensional elliptic problems, Numerical Heat Transfer, Vol.4, pp.409-426,1981.
- [32] V S Pratap and D B Spalding, Fluid flow and heat transfer in three-dimensional duct flows, Int. J. Heat and Mass Transfer, Vol.19, 1976.
- [33] J W Ramsey, R J Goldstein and E R G Eckert, 4<sup>th</sup> international heat transfer conference. Paper No.FC85, vol.111, Elsevier publishing co., Amsterdam, 1970.
- [34] W Rodi, Turbulence models and their application in hydraulics-A state of art paper. IHAR, Delft, The Netherlands, 1980.
- [35] W Rodi, Turbulence models and their application in hydraulics. presented by the IAHR-section on fundamentals of division II: Experimental and MAtheMatical Fluid Dynamics, 1980.
- [36] W Rodi, The prediction of free turbulent boundary layers by use of two-equation model of turbulence. Ph D thesis, University of London, 1972.
- [37] W Rodi and D B Spalding, A two-parameter model of turbulence and its application to free jets, Wärme und Stoffübertragung, Vol.3, pp.85-95, 1970.
- [38] W Rodi and S K Srivasta, A locally elliptic calculation procedure for three-dimensional flows and its application to a jet in cross flow, Comp. Meth. Appl. Mech. Engg., Vol.23, pp.67-83, 1980.

- [39] H I Rosten and D B Spalding, PHOENICS-84 Reference handbook. CHAM TR/100 (PHOENICS Beginners Guide), CHAM ltd, London, 1987.
- [40] H I Rosten and D B Spalding, PHOENICS-84 Reference handbook. CHAM TR/140 (PHOTON User Guide), CHAM ltd, London, 1987.
- [41] H I Rosten and D B Spalding, PHOENICS-84 Reference handbook. CHAM TR/200 (PHOENICS Reference Manual), CHAM ltd, London, 1987.
- [42] H I Rosten and D B Spalding, PHOENICS-84 Reference handbook. CHAM TR/300 (PHOENICS Instruction Course), CHAM ltd, London, 1987.
- [43] C L Saluja, Film cooling from rows of discrete holes, Ph D thesis, University of Wales Institute of Science and Technology, Cardiff, 1977.
- [44] H Schlichting, Boundary layer theory (7<sup>th</sup> ed). Mc Graw Hill, 1979.
- [45] B Schönung and W Rodi, Prediction of film cooling by a row of holes with a two dimensional boundary layer procedure. ASME paper 87-GT-122,1987.
- [46] D B Spalding, The PHOENICS computer code. CFD/87/3, CFDU, Imperial College, London, 1987.

- [47] D B Spalding, Mathematical modelling of fluid-mechanics, heat-transfer and chemical-reaction processes, A lecture course, CFDU report HTS/80/1.
- [48] D B Spalding, The calculation of free convection phenomena in gas-liquid mixtures, ICHMT Seminar, Dubrovnik 1976, in 'Turbulent Buoyant Convection', Eds N Afgan and D B Spalding, Hemisphere, Washington, 1977, pp.569-586, CFDU report HTS/76/11.
- [49] D B Spalding, Numerical computation of multiphase flows, A course of 12 lectures, with GENMIX2P listing and 5 appendices. Imperial College CFDU report HTS/81/8.
- [50] D B Spalding, Numerical computation of multiphase fluid flow and heat transfer, contribution to 'Recent advances in numerical methods in fluids, Eds C Taylor and K Morgan, pp.139-167.
- [51] D B Spalding, New developments and computed results, CFDU report HTS/81/2.
- [52] D B Spalding, The  $k - \omega$  model of turbulence. TM/TN/A/16, Imperial College, London, 1971.
- [53] J Stoll and J Straub, Film cooling and heat transfer in nozzles. ASME paper 87-GT-117, 1987.

# APPENDIX I

## Listing of computer program.

This appendix lists the Q1 and GROUND codes written for the problem of film cooling in conjunction with PHOENICS package. The  $k - \omega$  turbulence model of Spalding (1971), is explored as an example since it is not feasible to list all the files for all turbulence models employed.

The list of the previously mentioned codes contain comment cards which help understanding the different fortran statements, together with PHOENICS Input Language (PIL) commands as well.

The PHOENICS package signifies  $Z$ -direction as the main stream flow direction, and  $X$ -direction as the spanwise or lateral direction, while  $Y$ -direction is the direction normal to the test surface.

It should be mentioned that it is neither possible to describe each command in the Q1 file nor the GROUND file in details. On the other hand, reader is advised to refer to Rosten and Spalding (1987), for any detailed explanation.

## Q1 LISTING

A listing of the data file Q1 is shown after the following brief explanation about this file. In this section, the noteworthy features of each data group are presented.

- Data Group 1: Run Title.

This data group is used to specify the run title together with some reals to be used in the Q1 file and the GROUND file to be described latter in this appendix.

- Data Group 2: Flow Type.

Both cartesian grid and elliptic nature of the flow are selected by default, i.e. (CARTES=T, and PARAB=F respectively). Also the flow is steady by the default setting (STEADY=T), because the flow is independent of time.

- Data Group 3: X-Grid Specification.

The X-direction is the spanwise direction for the film cooling simulation and consists of 24 non-uniform cells in that direction.

- Data Group 4: Y-Grid Specification.

The Y-direction consists of 15 cells in that direction, which are not uniform, however, it is made very small in the vicinity of the wall.

- Data Group 5: Z-Grid Specification.

The Z-direction is the streamwise direction for the film cooling simulation and

consists of 30 non-uniform cells in that direction. Very close to the holes the cells are made very small and as the distance increased downstream the cells get bigger and bigger.

- Data Group 7: Variables Stored, Solved and Named.

The variables identified for the solution are: pressure correction, the three velocity components, the two turbulence quantities  $k$  and  $\omega$ , and the enthalpy in the form of temperature.

- Data Group 9: Properties of the Medium.

In this group the density, and viscosity of air are described, together with the initial fields, for the solved for variables, of the problem considered.

- Data Group 13: Boundary Conditions.

This data group describes 21 regions (PATCHs) over the whole domain. The first patch (INLET) reflects the inlet boundary conditions at  $Z=1$  in the (X-Y) plane; which extends from the first to the last  $Y$  inclusive at the inlet.

The second patch (OUTLET) describes the outlet boundary conditions in the (X-Y) plane at  $Z=30$ ; i.e. it is located very far from the holes to describe the free stream boundary conditions.

The WALL patch describes the wall boundary conditions, obeying the Blasius distribution <sup>1</sup>.

---

<sup>1</sup>For more details; reader is advised to refer to PHOENICS manuals, Rosten and Spalding (1987).



Finally the remaining 18 patches describe the holes over the test section. Each 6 represent a hole at a specified location. COVAL is a command used to describe the values at the prescribed PATCHs, and GRND indicates that the value is to be calculated in the GROUND subroutine.

- Data Group 15: Termination of Iteration.

In this data group the number of sweeps (outer iterations) is set to a number , usually achieved by several trials to insure a steady solution, after which values will not change significantly with increasing the number of sweeps.

Finally, the other PIL commands appearing at end of the Q1 file are for relaxation and printout control.

GROUP 1. Run title and other preliminaries

TALK=F;RUN( 1, 1);VDU=TTY

TEXT(Pred. of film cooling k-w)

REAL(CMUM,CDM,CMUCDM,CMUCD,CD,CMU,CD25,CD5,VFSQIN)  
REAL(C1W,C2W,C3W,C2WP)  
C1W=3.5;C2W=0.17;C3W=1.12;C2WP=17.31  
CD=0.09;CMU=1.0;CMUCD=0.09;CD25=0.548;CD5=0.3  
CMUM=1.0;CDM=0.09;CMUCDM=CMUM\*CDM  
VFSQIN=(0.0418/(CMUCDM\*0.09))\*\*2  
RG(1)=CMUCD;RG(2)=CD;RG(3)=CMU;RG(4)=CD25;RG(5)=C1W  
RG(6)=C2W;RG(7)=C3W;RG(8)=C2WP;RG(9)=CD5

GROUP 2. Transience; time-step specification

GROUP 3. X-direction grid specification

NX=24  
XFRAC(1)=-2.  
XFRAC(2)=0.0097  
XFRAC(3)=2.  
XFRAC(4)=0.00485  
XFRAC(5)=1.  
XFRAC(6)=0.002  
XFRAC(7)=1.  
XFRAC(8)=0.00285  
XFRAC(9)=1.  
XFRAC(10)=0.00485  
XFRAC(11)=3.  
XFRAC(12)=0.00257  
XFRAC(13)=1.  
XFRAC(14)=0.00198  
XFRAC(15)=2.  
XFRAC(16)=0.00485  
XFRAC(17)=1.  
XFRAC(18)=0.002  
XFRAC(19)=1.  
XFRAC(20)=0.00285  
XFRAC(21)=7.  
XFRAC(22)=0.00485  
XFRAC(23)=2.  
XFRAC(24)=0.0097

GROUP 4. Y-direction grid specification

NY=15  
YFRAC(1)=-5.0  
YFRAC(2)=0.001  
YFRAC(3)=5.  
YFRAC(4)=0.003  
YFRAC(5)=5.  
YFRAC(6)=0.0255

GROUP 5. Z-direction grid specification

NZ=30  
ZFRAC(1)=-3.

ZFRAC(2)=0.177  
ZFRAC(3)=6.  
ZFRAC(4)=0.00647  
ZFRAC(5)=1.  
ZFRAC(6)=0.00582  
ZFRAC(7)=2.  
ZFRAC(8)=0.0194  
ZFRAC(9)=2.  
ZFRAC(10)=0.05644  
ZFRAC(11)=6.  
ZFRAC(12)=0.00647  
ZFRAC(13)=1.  
ZFRAC(14)=0.00582  
ZFRAC(15)=1.  
ZFRAC(16)=0.0194  
ZFRAC(17)=1.  
ZFRAC(18)=0.0388  
ZFRAC(19)=1.  
ZFRAC(20)=0.01164  
ZFRAC(21)=6.0  
ZFRAC(22)=0.19432

GROUP 6. Body-fitted coordinates or grid distortion

GROUP 7. Variables stored, solved & named

NAME(14)=TEMP  
NAME(50)=VFSQ  
SOLUTN(P1,Y,Y,Y,N,N,N)  
SOLUTN(U1,Y,Y,N,N,N,N)  
SOLUTN(V1,Y,Y,N,N,N,N)  
SOLUTN(W1,Y,Y,N,N,N,N)  
SOLUTN(VFSQ,Y,Y,N,N,N,N)  
SOLUTN(TEMP,Y,Y,N,N,N,Y)  
SOLUTN(KE,Y,Y,N,N,N,N)  
STORE(ETA,EBAR,XOD,YOD,ZOD)  
STORE(ENUT,EL1,EP)

GROUP 8. Terms (in differential equations) & devices

TERMS(TEMP,N,P,P,P,P,P)  
TERMS(P1,N,P,P,P,P,P)  
TERMS(KE,N,Y,Y,Y,Y,N)  
TERMS(VFSQ,N,Y,Y,Y,Y,N)

GROUP 9. Properties of the medium (or media)

PRT(TEMP)=0.86  
PRNDTL(TEMP)=0.71  
PRT(KE)=1.0;PRT(VFSQ)=1.0  
RHO1=1.0733  
ENUL=1.863E-5  
ENUT=GRND;EL1=GRND

GROUP 10. Inter-phase-transfer processes and properties

GROUP 11. Initialization of variable or porosity fields

INITIAL FIELDS  
FIINIT(ETA)=0.0

```

FIINIT(VFSQ)=VFSQIN
FIINIT(P1)=0.0
FIINIT(W1)=10.0
FIINIT(KE)=0.09
FIINIT(TEMP)=328.0

```

GROUP 12. Convection and diffusion adjustments

GROUP 13. Boundary conditions and special sources

```

      AT Z=1 (inlet)
PATCH(INLET,LOW,1,NX,1,NY,1,1,1,1)
COVAL(INLET,P1,FIXFLU,10.733)
COVAL(INLET,W1,ONLYMS,1.0E1)
COVAL(INLET,KE,ONLYMS,0.09)
COVAL(INLET,VFSQ,ONLYMS,VFSQIN)
COVAL(INLET,TEMP,ONLYMS,328.0)
      AT Z=NZ (outlet)
PATCH(FREE,NORTH,1,NX,1,NY,NZ,NZ,1,1)
COVAL(FREE,P1,1.E5,0.0)
COVAL(FREE,W1,ONLYMS,1.E1)
COVAL(FREE,KE,ONLYMS,0.018)
COVAL(FREE,VFSQ,ONLYMS,3.165E11)
COVAL(FREE,TEMP,ONLYMS,328.0)
      WALL FUNCT
PATCH(WFUN,SWALL,1,NX,1,1,1,NZ,1,1)
COVAL(WFUN,U1,GRND2,0.0)
COVAL(WFUN,W1,GRND2,0.0)
COVAL(WFUN,V1,GRND2,0.0)
COVAL(WFUN,KE,GRND2,GRND2)
COVAL(WFUN,VFSQ,GRND2,GRND2)
COVAL(WFUN,TEMP,GRND2,SAME)

```

```

      BCONDS OVER THE HOLES
PATCH(A1,SOUTH,5,5,1,1,4,4,1,1)
COVAL(A1,P1,FIXFLU,GRND)
COVAL(A1,V1,FIXVAL,GRND)
COVAL(A1,W1,FIXVAL,GRND)
COVAL(A1,KE,FIXVAL,GRND)
COVAL(A1,VFSQ,FIXVAL,GRND)
COVAL(A1,TEMP,FIXVAL,298.0)

```

```

PATCH(A2,SOUTH,4,6,1,1,5,5,1,1)
COVAL(A2,P1,FIXFLU,GRND)
COVAL(A2,V1,FIXVAL,GRND)
COVAL(A2,W1,FIXVAL,GRND)
COVAL(A2,KE,FIXVAL,GRND)
COVAL(A2,VFSQ,FIXVAL,GRND)
COVAL(A2,TEMP,FIXVAL,298.0)

```

```

PATCH(A3,SOUTH,3,7,1,1,6,6,1,1)
COVAL(A3,P1,FIXFLU,GRND)
COVAL(A3,V1,FIXVAL,GRND)
COVAL(A3,W1,FIXVAL,GRND)
COVAL(A3,KE,FIXVAL,GRND)
COVAL(A3,VFSQ,FIXVAL,GRND)
COVAL(A3,TEMP,FIXVAL,298.0)

```

```

PATCH(A4,SOUTH,4,6,1,1,7,7,1,1)
COVAL(A4,P1,FIXFLU,GRND)

```

COVAL(A4,V1, FIXVAL, GRND)  
COVAL(A4,W1, FIXVAL, GRND)  
COVAL(A4,KE, FIXVAL, GRND)  
COVAL(A4,VFSQ, FIXVAL, GRND)  
COVAL(A4,TEMP, FIXVAL, 298.0)

PATCH(A5,SOUTH,5,5,1,1,8,8,1,1)  
COVAL(A5,P1, FIXFLU, GRND)  
COVAL(A5,V1, FIXVAL, GRND)  
COVAL(A5,W1, FIXVAL, GRND)  
COVAL(A5,KE, FIXVAL, GRND)  
COVAL(A5,VFSQ, FIXVAL, GRND)  
COVAL(A5,TEMP, FIXVAL, 298.0)

PATCH(A6,SOUTH,5,5,1,1,9,9,1,1)  
COVAL(A6,P1, FIXFLU, GRND)  
COVAL(A6,V1, FIXVAL, GRND)  
COVAL(A6,W1, FIXVAL, GRND)  
COVAL(A6,KE, FIXVAL, GRND)  
COVAL(A6,VFSQ, FIXVAL, GRND)  
COVAL(A6,TEMP, FIXVAL, 298.0)

PATCH(B1,SOUTH,20,20,1,1,4,4,1,1)  
COVAL(B1,P1, FIXFLU, GRND)  
COVAL(B1,V1, FIXVAL, GRND)  
COVAL(B1,W1, FIXVAL, GRND)  
COVAL(B1,KE, FIXVAL, GRND)  
COVAL(B1,VFSQ, FIXVAL, GRND)  
COVAL(B1,TEMP, FIXVAL, 298.0)

PATCH(B2,SOUTH,20,21,1,1,5,5,1,1)  
COVAL(B2,P1, FIXFLU, GRND)  
COVAL(B2,V1, FIXVAL, GRND)  
COVAL(B2,W1, FIXVAL, GRND)  
COVAL(B2,KE, FIXVAL, GRND)  
COVAL(B2,VFSQ, FIXVAL, GRND)  
COVAL(B2,TEMP, FIXVAL, 298.0)

PATCH(B3,SOUTH,19,22,1,1,6,6,1,1)  
COVAL(B3,P1, FIXFLU, GRND)  
COVAL(B3,V1, FIXVAL, GRND)  
COVAL(B3,W1, FIXVAL, GRND)  
COVAL(B3,KE, FIXVAL, GRND)  
COVAL(B3,VFSQ, FIXVAL, GRND)  
COVAL(B3,TEMP, FIXVAL, 298.0)

PATCH(B4,SOUTH,20,21,1,1,7,7,1,1)  
COVAL(B4,P1, FIXFLU, GRND)  
COVAL(B4,V1, FIXVAL, GRND)  
COVAL(B4,W1, FIXVAL, GRND)  
COVAL(B4,KE, FIXVAL, GRND)  
COVAL(B4,VFSQ, FIXVAL, GRND)  
COVAL(B4,TEMP, FIXVAL, 298.0)

PATCH(B5,SOUTH,20,20,1,1,8,8,1,1)  
COVAL(B5,P1, FIXFLU, GRND)  
COVAL(B5,V1, FIXVAL, GRND)  
COVAL(B5,W1, FIXVAL, GRND)  
COVAL(B5,KE, FIXVAL, GRND)  
COVAL(B5,VFSQ, FIXVAL, GRND)

```

COVAL(B5,TEMP,FIXVAL,298.0)

PATCH(B6,SOUTH,20,20,1,1,9,9,1,1)
COVAL(B6,P1,FIXFLU,GRND)
COVAL(B6,V1,FIXVAL,GRND)
COVAL(B6,W1,FIXVAL,GRND)
COVAL(B6,KE,FIXVAL,GRND)
COVAL(B6,VFSQ,FIXVAL,GRND)
COVAL(B6,TEMP,FIXVAL,298.0)

PATCH(C1,SOUTH,14,14,1,1,15,15,1,1)
COVAL(C1,P1,FIXFLU,GRND)
COVAL(C1,V1,FIXVAL,GRND)
COVAL(C1,W1,FIXVAL,GRND)
COVAL(C1,KE,FIXVAL,GRND)
COVAL(C1,VFSQ,FIXVAL,GRND)
COVAL(C1,TEMP,FIXVAL,298.0)

PATCH(C2,SOUTH,13,15,1,1,16,16,1,1)
COVAL(C2,P1,FIXFLU,GRND)
COVAL(C2,V1,FIXVAL,GRND)
COVAL(C2,W1,FIXVAL,GRND)
COVAL(C2,KE,FIXVAL,GRND)
COVAL(C2,VFSQ,FIXVAL,GRND)
COVAL(C2,TEMP,FIXVAL,298.0)

PATCH(C3,SOUTH,12,16,1,1,17,17,1,1)
COVAL(C3,P1,FIXFLU,GRND)
COVAL(C3,V1,FIXVAL,GRND)
COVAL(C3,W1,FIXVAL,GRND)
COVAL(C3,KE,FIXVAL,GRND)
COVAL(C3,VFSQ,FIXVAL,GRND)
COVAL(C3,TEMP,FIXVAL,298.0)

PATCH(C4,SOUTH,13,15,1,1,18,18,1,1)
COVAL(C4,P1,FIXFLU,GRND)
COVAL(C4,V1,FIXVAL,GRND)
COVAL(C4,W1,FIXVAL,GRND)
COVAL(C4,KE,FIXVAL,GRND)
COVAL(C4,VFSQ,FIXVAL,GRND)
COVAL(C4,TEMP,FIXVAL,298.0)

PATCH(C5,SOUTH,14,14,1,1,19,19,1,1)
COVAL(C5,P1,FIXFLU,GRND)
COVAL(C5,V1,FIXVAL,GRND)
COVAL(C5,W1,FIXVAL,GRND)
COVAL(C5,KE,FIXVAL,GRND)
COVAL(C5,VFSQ,FIXVAL,GRND)
COVAL(C5,TEMP,FIXVAL,298.0)

PATCH(C6,SOUTH,14,14,1,1,20,20,1,1)
COVAL(C6,P1,FIXFLU,GRND)
COVAL(C6,V1,FIXVAL,GRND)
COVAL(C6,W1,FIXVAL,GRND)
COVAL(C6,KE,FIXVAL,GRND)
COVAL(C6,VFSQ,FIXVAL,GRND)
COVAL(C6,TEMP,FIXVAL,298.0)

```

Special sources related to k-w model

```
PATCH(KWSOR1,PHASEM,1,NX,1,NY,1,NZ,1,1)
COVAL(KWSOR1,KE,GRND,GRND1)
COVAL(KWSOR1,VFSQ,GRND,GRND1)
PATCH(KWSOR2,PHASEM,1,NX,1,NY,1,NZ,1,1)
COVAL(KWSOR2,VFSQ,FIXFLU,GRND1)
```

GROUP 14. Downstream pressure for PARAB=.TRUE.

GROUP 15. Termination of sweeps

```
LSWEEP=120
LSWEEP=80
```

GROUP 16. Termination of iterations

```
LITER(TEMP)=40
LITER(VFSQ)=100
```

GROUP 17. Under-relaxation devices

```
RELAX(P1,LINRLX,0.1)
RELAX(U1,FALSDT,0.01)
RELAX(V1,FALSDT,0.1)
RELAX(W1,FALSDT,0.01)
RELAX(KE,FALSDT,0.1)
RELAX(EP,FALSDT,0.01)
RELAX(TEMP,FALSDT,0.1)
RELAX(VFSQ,FALSDT,0.3)
```

GROUP 18. Limits on variables or increments to them

```
VARMAX(VFSQ)=1.E20
VARMAX(TEMP)=328.0
VARMIN(TEMP)=300.0
```

GROUP 19. Data communicated by satellite to GROUND

```
USEGRX=T
GENK=T
```

GROUP 20. Preliminary print-out

```
NPRINT=LSWEEP
```

GROUP 21. Print-out of variables

```
OUTPUT(P1,N,N,N,Y,N,N)
OUTPUT(U1,N,N,N,Y,N,N)
OUTPUT(V1,N,N,N,Y,N,N)
OUTPUT(W1,N,N,N,Y,Y,Y)
OUTPUT(KE,N,N,N,Y,Y,Y)
OUTPUT(VFSQ,N,N,N,Y,Y,Y)
OUTPUT(TEMP,N,N,N,Y,Y,Y)
```

```
OUTPUT(EP,N,N,N,Y,Y,Y)
OUTPUT(ETA,Y,N,N,N,N,N)
OUTPUT(EBAR,N,N,N,N,N,N)
OUTPUT(ENUT,N,N,N,N,N,N)
OUTPUT(EL1,N,N,N,N,N,N)
OUTPUT(XOD,N,N,N,N,N,N)
```

```
OUTPUT(YOD,N,N,N,N,N,N)
OUTPUT(ZOD,N,N,N,N,N,N)
```

GROUP 22. Spot-value print-out

GROUP 23. Field print-out and plot control

PLOTS

```
PATCH(F1,PROFIL,5,5,1,1,4,NZ,1,1)
PLOT(F1,ETA,0.0,0.0)
PATCH(F2,PROFIL,14,14,1,1,4,NZ,1,1)
PLOT(F2,ETA,0.0,0.0)
PATCH(F3,PROFIL,20,20,1,1,4,NZ,1,1)
PLOT(F3,ETA,0.0,0.0)
PATCH(F4,PROFIL,21,21,1,1,4,NZ,1,1)
PLOT(F4,ETA,0.0,0.0)
```

W1-output

```
YZPR=T;NXPRIN=9;IXPRF=5;IXPRL=14;NZPRIN=1
IZPRF=10;IZPRL=11;NYPRIN=1;IYPRF=1;IYPRL=15
YZPR=T;NXPRIN=9;IXPRF=5;IXPRL=14;NZPRIN=4
IZPRF=17;IZPRL=21;NYPRIN=1;IYPRF=1;IYPRL=15
YZPR=T;NXPRIN=9;IXPRF=5;IXPRL=14;NZPRIN=1
IZPRF=24;IZPRL=24;NYPRIN=1;IYPRF=1;IYPRL=15
```

ETA-output

```
XZPR=T;NXPRIN=1;IXPRF=1;IXPRL=NX;NZPRIN=1;IZPRF=1
IZPRL=NZ;NYPRIN=1;IYPRF=1;IYPRL=1
```

EBAR-output

```
YZPR=T;NXPRIN=1;IXPRF=1;IXPRL=1;NZPRIN=1;IZPRF=1
IZPRL=NZ;NYPRIN=1;IYPRF=1;IYPRL=1
```

ECHO=F

GROUP 24. Dumps for restarts

```
AUTOPS=T;RESTRT(ALL)
      RESTRT(ALL)
STOP
```



## GROUND LISTING

The listing of GROUND file, which is a fortran subroutine, is shown after the following description.

Firstly, the F-array is modified to 400000 instead of the 50000 built in value. Then several dimension statements and data statements are added to the beginning of the GROUND file.

Here is a brief description on the data groups which are compatible with those of Q1 file:

- GROUP 1

Special arrays for storing values are called in this data group. These arrays are necessary for mathematical manipulation carried out through this subroutine.

- GROUP 9

Since  $EL1=GRND$ , and  $ENUT=GRND$  in Q1 file, then it is essential to describe the calculation of such variables in GROUND subroutine. The method is implemented in this group in the related section for each variable.

- GROUP 13

In this group the source terms for all solved for variables at the hole position is calculated. Also source terms related to turbulent quantities  $k$  and  $\omega$  are evaluated in this data group.

- GROUP 19

In this data group at the start of iteration section average value of film cooling effectiveness (laterally averaged using Trapezoidal rule) is calculated. Also the local film cooling effectiveness is calculated in this section.

Finally, a special subroutine was supplemented by the author at the end of the GROUND subroutine for the aid of calculating vorticity term. Also several functions needed for special calculations throughout GROUND file are defined and added to this subroutine.

```

C FILE NAME GROUND.FTN-----22 April 87
C THIS IS THE MAIN PROGRAM OF EARTH
C
C (C) COPYRIGHT 1984, LAST REVISION 1987.
C CONCENTRATION HEAT AND MOMENTUM LTD. ALL RIGHTS RESERVED.
C This subroutine and the remainder of the PHOENICS code are
C proprietary software owned by Concentration Heat and Momentum
C Limited, 40 High Street, Wimbledon, London SW19 5AU, England.
C
C
C PROGRAM MAIN
C
C 1 The following two COMMON's, which appear identically in the
C satellite MAIN program, allow up to 50 dependent variables to
C be solved for (or their storage spaces to be occupied by
C other variables, such as density). If a larger number is
C required, the 50's should be replaced, in the next 8 lines,
C by the required larger number; and the 200 in COMMON/F01/
C should be replaced by 4 times the required number. Numbers
C less than 50 are not permitted.
C
COMMON/LGE4/L4(50)
1/LDB1/L5(50)/IDA1/I1(50)/IDA2/I2(50)/IDA3/I3(50)/IDA4/I4(50)
1/IDA5/I5(50)/IDA6/I6(50)/GI1/I7(50)/GI2/I8(50)/HDA1/IH1(50)
1/GH1/IH2(50)/RDA1/R1(50)/RDA2/R2(50)/RDA3/R3(50)/RDA4/R4(50)
1/RDA5/R5(50)/RDA6/R6(50)/RDA7/R7(50)/RDA8/R8(50)/RDA9/R9(50)
1/RDA10/R10(50)/RDA11/R11(50)
1/GR1/R12(50)/GR2/R13(50)/GR3/R14(50)/GR4/R15(50)
1/IPIP1/IP1(50)/HPIP2/IHP2(50)/RPIP1/RVAL(50)/LPIP1/LVAL(50)
1/IFPL/IPL0(50)/RFPL1/ORPRIN(50)/RFPL2/ORMAX(50)
1/RFPL3/ORMIN(50)
LOGICAL L1,L2,L3,L4,L5,DBGFIL,LVAL
CHARACTER*4 IH1,IH2,IHP2,NSDA
C
COMMON/F01/I9(200)
COMMON/DISC/DBGFIL
COMMON/LUNITS/LUNIT(60)
EXTERNAL WAYOUT
C
C 2 Set dimensions of data-for-GROUND arrays here. WARNING: the
C corresponding arrays in the MAIN program of the satellite
C (see SATLIT) must have the same dimensions.
COMMON/LGRND/LG(20)/IGRND/IG(20)/RGRND/RG(100)/CGRND/CG(10)
LOGICAL LG
CHARACTER*4 CG
C
C 3 Set dimensions of data-for-GREX2 arrays here. WARNING: the
C corresponding arrays in the MAIN program of the satellite
C (see SATLIT) must have the same dimensions.
COMMON/LSGD/LSGD(20)/ISG/ISGD(20)/RSG/RSGD(100)/CSG/CSGD(10)
LOGICAL LSGD
CHARACTER*4 CSGD
C
C 4 Set dimension of patch-name array here. WARNING: the array
C NAMPAT in the MAIN program of the satellite must have the
C dimension.
COMMON/NPAT/NAMPAT(100)
CHARACTER*8 NAMPAT
C
C

```

```

C   CONFIG FILE name declaration.
COMMON/CNFG/CNFIG
CHARACTER CNFIG*48

C
C 5   The numbers in the next two statements (which must be ident-
C     ical) indicate how much computer memory is to be set aside
C     for storing the main and auxiliary variables. The user may
C     alter them if he wishes, to accord with the number of
C     grid nodes and dependent variables he is concerned with.
C*****F-ARRAY MODIFICATION
COMMON F(400000)
NFDIM=400000

C
C 6   Logical-unit numbers and file names, not to be changed.
CALL CNFGZZ(2)
CALL EARSET(1)
CALL OPENFL(6)

C
C     User may here change message transmitted to logical unit
C     LUPR3
C*****
CALL WRIT40('GROUND STATION DEVELOPED BY: AMER A AMER')
CALL MAIN1(NFDIM)
CALL WAYOUT(0)
STOP
END
C*****
C$DIR**GROSTA
SUBROUTINE GROSTA
INCLUDE 'SATEAR'
INCLUDE 'GRDLOC'
INCLUDE 'GRDEAR'
C.... This subroutine directs control to the GROUNDS selected by
C     the satellite settings of USEGRX, NAMGRD & USEGRD.
C
C     Subroutine GREX2 contains options for fluid properties,
C     turbulence models, wall functions, chemical reaction etc. It
C     was introduced in version 2.0 of PHOENICS.
C
C     IF(USEGRX) CALL GREX2

C
C.... BTSTGR contains the sequences used in conjunction with
C     the BFC test battery.
C
C     IF(NAMGRD.EQ.'BTST') CALL BTSTGR

C
C.... TESTGR contains test battery sequences used in conjunction
C     with the test-battery SATLIT subroutine, TESTST.
C
C     IF(NAMGRD.EQ.'TEST') CALL TESTGR

C
C.... SPECGR is a generic "special" GROUND the name of which can
C     be used by anyone for their own purposes. SPC1GR, SPC2GR and
C     SPC3GR permit the user to attach his own library of special
C     GROUNDS selected according to the prescription of NAMGRD.
C
C     IF(NAMGRD.EQ.'SPEC') CALL SPECGR
C     IF(NAMGRD.EQ.'SPC1') CALL SPC1GR
C     IF(NAMGRD.EQ.'SPC2') CALL SPC2GR

```



```

          IF(IGR.EQ.19) GO TO 19
          GO TO (1,2,3,4,5,6,24,8,9,10,11,12,13,14,24,24,24,24,19,20,24,
124,23,24),IGR
C*****
C
C--- GROUP 1. Run title and other preliminaries
C
      1 GO TO (1001,1002),ISC
      1001 CONTINUE
C*****Special earth arrays to be used.
      CALL MAKE(XU2D)
      CALL MAKE(YV2D)
      CALL MAKE(YG2D)
      CALL MAKE(DYG2D)
      CALL MAKE(DYV2D)
      CALL MAKE(DZWNZ)
      CALL MAKE(EASP2)
      CALL MAKE(EASP3)
      CALL MAKE(EASP4)
      CALL MAKE(EASP5)
      CALL MAKE(EASP6)
      CALL MAKE(EASP8)
      CALL MAKE(EASP9)
      CALL MAKE(EASP10)
      IVFSQ=INAME('VFSQ')
      RETURN
      1002 CONTINUE
      RETURN
C*****
C
C--- GROUP 2. Transience; time-step specification
C
      2 CONTINUE
      RETURN
C*****
C
C--- GROUP 3. X-direction grid specification
C
      3 CONTINUE
      RETURN
C*****
C
C--- GROUP 4. Y-direction grid specification
C
      4 CONTINUE
      RETURN
C*****
C
C--- GROUP 5. Z-direction grid specification
C
      5 CONTINUE
      RETURN
C*****
C
C--- GROUP 6. Body-fitted coordinates or grid distortion
C
      6 CONTINUE
      RETURN
C*****
C * Make changes for this group only in group 19.

```

```

C--- GROUP 7. Variables stored, solved & named
C*****
C
C--- GROUP 8. Terms (in differential equations) & devices
C
  8 GO TO (81,82,83,84,85,86,87,88,89,810,811,812,813,814,815)
  1,ISC
81 CONTINUE
C * ----- SECTION 1 -----
C For U1AD.LE.GRND--- phase 1 additional velocity (VELAD).
  RETURN
82 CONTINUE
C * ----- SECTION 2 -----
C For U2AD.LE.GRND--- phase 2 additional velocity (VELAD).
  RETURN
83 CONTINUE
C * ----- SECTION 3 -----
C For V1AD.LE.GRND--- phase 1 additional velocity (VELAD).
  RETURN
84 CONTINUE
C * ----- SECTION 4 -----
C For V2AD.LE.GRND--- phase 2 additional velocity (VELAD).
  RETURN
85 CONTINUE
C * ----- SECTION 5 -----
C For W1AD.LE.GRND--- phase 1 additional velocity (VELAD).
  RETURN
86 CONTINUE
C * ----- SECTION 6 -----
C For W2AD.LE.GRND--- phase 2 additional velocity (VELAD).
  RETURN
87 CONTINUE
C * ----- SECTION 7 ---- VOLUMETRIC SOURCE FOR GALA
  RETURN
88 CONTINUE
C * ----- SECTION 8 --- CONVECTION FLUXES
  RETURN
89 CONTINUE
C * ----- SECTION 9 --- DIFFUSION COEFFICIENTS
  RETURN
810 CONTINUE
C * ----- SECTION 10 --- CONVECTION NEIGHBOURS
  RETURN
811 CONTINUE
C * ----- SECTION 11 --- DIFFUSION NEIGHBOURS
  RETURN
812 CONTINUE
C * ----- SECTION 12 --- LINEARISED SOURCES
  RETURN
813 CONTINUE
C * ----- SECTION 13 --- CORRECTION COEFFICIENTS
  RETURN
814 CONTINUE
C * ----- SECTION 14 --- USER'S SOLVER
  RETURN
815 CONTINUE
C * ----- SECTION 15 --- CHANGE SOLUTION
  RETURN
C * Make all other group-8 changes in
C*****

```

```

C
C--- GROUP 9. Properties of the medium (or media)
C
C The sections in this group are arranged sequentially in their
C order of calling from EARTH. Thus, as can be seen from below,
C the temperature sections (10 and 11) precede the density
C sections (1 and 3); so, density formulae can refer to
C temperature stores already set.
C 9 GO TO (91,92,93,94,95,96,97,98,99,900,901,902,903),ISC
C*****
900 CONTINUE
C * ----- SECTION 10 -----
C For TMP1.LE.GRND----- phase-1 temperature Index AUX(TEMP1)
RETURN
901 CONTINUE
C * ----- SECTION 11 -----
C For TMP2.LE.GRND----- phase-2 temperature Index AUX(TEMP2)
RETURN
902 CONTINUE
C * ----- SECTION 12 -----
C For EL1.LE.GRND----- phase-1 length scale Index AUX(LEN1)
C LENGTH SCALE CALCULATION
C IF(IGR.EQ.9.AND.ISC.EQ.12) THEN
CALL FN22(IVFSQ,1.0E-10)
C SET EPSILON
IF(STORE(EP)) THEN
CALL FNEPS(EP,KE,IVFSQ,RG(2))
ENDIF
C DETERMINE MACRO LENGTH SCALE
CALL FN1(EASP5,0.0)
CALL FNLEN(EASP5,KE,IVFSQ)
C SET MIXING LENGTH, Lm=Cmu**0.75*L/Cd**0.25
CALL FN2(AUX(LEN1),EASP5,0.0,RG(3)**0.75/RG(4))
C COMPUTE DISSIPATION FACTOR f1=1.+C2WP*(DLDY)**2
C MAINLY WE ARE CALCULATING GRADL AS DL/DY ONLY IN THIS SECTION
CALL GETYX(EASP5,GLENG,15,24)
CALL GETYX(YG2D,GYG,15,24)
DO 1006 IY=1,NY
DO 1006 IX=1,NX
IF(IY.EQ.1)THEN
ELSE
GO TO 1005
IF (IY.EQ.NY) GOTO 1003
ENDIF
GRADLH=(GLENG(IY+1,IX)-GLENG(IY,IX))/(GYG(IY+1,IX)-GYG(IY,IX))
GRADLL=(GLENG(IY,IX)-GLENG(IY-1,IX))/(GYG(IY,IX)-GYG(IY-1,IX))
GRADLSQ(IY,IX)=0.5*(GRADLH*GRADLH+GRADLL*GRADLL)
GOTO 1006
1005 GRADL=(GLENG(IY+1,IX)-GLENG(IY,IX))/(GYG(IY+1,IX)-GYG(IY,IX))
GRADLSQ(IY,IX)=0.5*GRADL*GRADL
GOTO 1006
1003 GRADL=(GLENG(IY,IX)-GLENG(IY-1,IX))/(GYG(IY,IX)-GYG(IY-1,IX))
GRADLSQ(IY,IX)=0.5*GRADL*GRADL
1006 CONTINUE
CALL FN1(EASP6,0.0)
CALL FN1(EASP6,GRADLSQ)
CALL FN2(EASP5,EASP6,1.0,RG(8))
ENDIF
RETURN
903 CONTINUE

```



```

C * ----- SECTION 13 -----
C For EL2.LE.GRND----- phase-2 length scale Index AUX(LEN2)
  RETURN
91 CONTINUE
C * ----- SECTION 1 -----
C For RHO1.LE.GRND--- density for phase 1 Index AUX(DEN1).
  RETURN
92 CONTINUE
C * ----- SECTION 2 -----
C For DRH1DP.LE.GRND--- D(LN(DEN))/DP for phase 1 (D1DP).
  RETURN
93 CONTINUE
C * ----- SECTION 3 -----
C For RHO2.LE.GRND--- density for phase 2 Index AUX(DEN2).
  RETURN
94 CONTINUE
C * ----- SECTION 4 -----
C For DRH2DP.LE.GRND--- D(LN(DEN))/DP for phase 2 (D2DP).
  RETURN
95 CONTINUE
C * ----- SECTION 5 -----
C For ENUT.LE.GRND--- reference turbulent kinematic viscosity.
C TURBULENT VISCOSITY CALCULATION
C IF(IGR.EQ.9.AND.ISC.EQ.5) THEN
C   GKWCON=RG(1)**0.25
C   CALL FN31(AUX(VIST),KE,AUX(LEN1),GKWCON,0.5,1.0)
C   ENDIF
  RETURN
96 CONTINUE
C * ----- SECTION 6 -----
C For ENUL.LE.GRND--- reference laminar kinematic viscosity.
  RETURN
97 CONTINUE
C * ----- SECTION 7 -----
C For PRNDTL( ).LE.GRND--- laminar PRANDTL nos., or diffusivity.
  RETURN
98 CONTINUE
C * ----- SECTION 8 -----
C For PHINT( ).LE.GRND--- interface value of first phase(FII1).
  RETURN
99 CONTINUE
C * ----- SECTION 9 -----
C For PHINT( ).LE.GRND--- interface value of second phase(FII2)
  RETURN
C*****
C
C--- GROUP 10. Inter-phase-transfer processes and properties
C
  10 GO TO (101,102,103,104),ISC
101 CONTINUE
C * ----- SECTION 1 -----
C For CFIPS.LE.GRND--- inter-phase friction coeff. AUX(INTFRC).
  RETURN
102 CONTINUE
C * ----- SECTION 2 -----
C For CMDOT.EQ.GRND- inter-phase mass transfer Index AUX(INTMDT)
  RETURN
103 CONTINUE
C * ----- SECTION 3 -----
C For CINT( ).EQ.GRND--- phasel-to-interface transfer

```

```

C                                          coefficients (COI1)
C      RETURN
104 CONTINUE
C      * ----- SECTION 4 -----
C      For CINT( ).EQ.GRND--- phase2-to-interface transfer
C                                          coefficients (COI2)
C      RETURN
C*****
C--- GROUP 11. Initialization of variable or porosity fields
C
C      11 CONTINUE
C      RETURN
C*****
C--- GROUP 12. Convection and diffusion adjustments
C
C      12 CONTINUE
C      RETURN
C*****
C--- GROUP 13. Boundary conditions and special sources
C
C      13 CONTINUE
C      GO TO (130,131,132,133,134,135,136,137,138,139,1310,
C      11311,1312,1313,1314,1315,1316,1317,1318,1319,1320,1321),ISC
130 CONTINUE
C----- SECTION 1 ----- coefficient = GRND
C      COEFFICIENTS FOR SOURCE TERMS
C      IF(IGR.EQ.13.AND.ISC.EQ.1) THEN
C          IF(NPATCH.NE.'KWSOR1') RETURN
C          IF(INDVAR.EQ.KE) CALL FN31(CO,AUX(VIST),AUX(LEN1),
C      &SQRT(RG(1)),1.0,-2.0)
C          IF(INDVAR.EQ.IVFSQ) THEN
C      CALL FN31(CO,AUX(VIST),AUX(LEN1),SQRT(RG(3))*RG(6)/RG(9),
C      &1.0,-2.0)
C      CALL FN26(CO,EASP5)
C          ENDIF
C      ENDIF
C      RETURN
131 CONTINUE
C----- SECTION 2 ----- coefficient = GRND1
C      RETURN
132 CONTINUE
C----- SECTION 3 ----- coefficient = GRND2
C      RETURN
133 CONTINUE
C----- SECTION 4 ----- coefficient = GRND3
C      RETURN
134 CONTINUE
C----- SECTION 5 ----- coefficient = GRND4
C      RETURN
135 CONTINUE
C----- SECTION 6 ----- coefficient = GRND5
C      RETURN
136 CONTINUE
C----- SECTION 7 ----- coefficient = GRND6
C      RETURN
137 CONTINUE
C----- SECTION 8 ----- coefficient = GRND7

```

```

      RETURN
138 CONTINUE
C----- SECTION 9 ----- coefficient = GRND8
      RETURN
139 CONTINUE
C----- SECTION 10 ----- coefficient = GRND9
      RETURN
1310 CONTINUE
C----- SECTION 11 ----- coefficient = GRND10
      RETURN
1311 CONTINUE
C----- SECTION 12 ----- value = GRND
C BOUNDARY CONDITIONS OVER THE HOLES
C THE (1/7)th POWER LAW IS CONSIDERED FOR VELOCITIES
      IF (IZ.LE.3) RETURN
      IF (IZ.LE.9) GO TO 112
      GO TO 118
112 IF (IZ.EQ.4) KNZ=1
      IF (IZ.EQ.5) KNZ=2
      IF (IZ.EQ.6) KNZ=3
      IF (IZ.EQ.7) KNZ=2
      IF (IZ.EQ.8) KNZ=1
      IF (IZ.EQ.9) KNZ=1
      DO 106 NHOLE=1,2
      IF (NHOLE.EQ.1) GO TO 105
      GO TO 110
105 IF (IZ.EQ.4) NP1=5
      IF (IZ.EQ.4) NP2=5
      IF (IZ.EQ.5) NP1=4
      IF (IZ.EQ.5) NP2=6
      IF (IZ.EQ.6) NP1=3
      IF (IZ.EQ.6) NP2=7
      IF (IZ.EQ.7) NP1=4
      IF (IZ.EQ.7) NP2=6
      IF (IZ.EQ.8) NP1=5
      IF (IZ.EQ.8) NP2=5
      IF (IZ.EQ.9) NP1=5
      IF (IZ.EQ.9) NP2=5
      GO TO 111
110 IF (IZ.EQ.4) NP1=20
      IF (IZ.EQ.4) NP2=20
      IF (IZ.EQ.5) NP1=20
      IF (IZ.EQ.5) NP2=21
      IF (IZ.EQ.6) NP1=19
      IF (IZ.EQ.6) NP2=22
      IF (IZ.EQ.7) NP1=20
      IF (IZ.EQ.7) NP2=21
      IF (IZ.EQ.8) NP1=20
      IF (IZ.EQ.8) NP2=20
      IF (IZ.EQ.9) NP1=20
      IF (IZ.EQ.9) NP2=20
111 CALL GETZ(DZWNZ,GZG,NZ)
      DO 114 IX=NP1,NP2
      DO 114 IY=1,1
      GW1V(IY,IX)=GUC*(((GZG(IZ)*KNZ)/0.0194)**(1/7))
      GWV(IY,IX)=GW1V(IY,IX)*1.194
      GW1(IY,IX)=GW1V(IY,IX)*(COS(THETA))
      GV1(IY,IX)=GW1V(IY,IX)*(SIN(THETA))
      GLE=0.4*GZG(IZ)*KNZ
      GNKE(IY,IX)=3.33*(GLE**2)*((GW1V(IY,IX)/0.00647)**2)

```

```

      GNEP(IY,IX)=0.1643*(GNKE(IY,IX)**1.5)/GLE
C     W-FIELD IS CALCULATED FROM EPS=RG(2)*KE*W**0.5
      GNW(IY,IX)=(GNEP(IY,IX)/(RG(2)*GNKE(IY,IX)))**2
114  CONTINUE
106  CONTINUE
      GO TO 158
118  IF (IZ.LE.14) GO TO 158
      IF (IZ.EQ.15) KNZ=1
      IF (IZ.EQ.16) KNZ=2
      IF (IZ.EQ.17) KNZ=3
      IF (IZ.EQ.18) KNZ=2
      IF (IZ.EQ.19) KNZ=1
      IF (IZ.EQ.20) KNZ=1
      IF (IZ.EQ.15) NP1=14
      IF (IZ.EQ.15) NP2=14
      IF (IZ.EQ.16) NP1=13
      IF (IZ.EQ.16) NP2=15
      IF (IZ.EQ.17) NP1=12
      IF (IZ.EQ.17) NP2=16
      IF (IZ.EQ.18) NP1=13
      IF (IZ.EQ.18) NP2=15
      IF (IZ.EQ.19) NP1=14
      IF (IZ.EQ.19) NP2=14
      IF (IZ.EQ.20) NP1=14
      IF (IZ.EQ.20) NP2=14
      IF (IZ.LE.20) GO TO 120
      GO TO 146
120  CALL GETZ(DZWNZ,GZG,NZ)
      DO 140 IX=NP1,NP2
      DO 140 IY=1,1
      GW1V(IY,IX)=GUC*(((GZG(IZ)*KNZ)/0.0194)**(1/7))
      GWV(IY,IX)=GW1V(IY,IX)*1.194
      GW1(IY,IX)=GW1V(IY,IX)*(COS(THETA))
      GV1(IY,IX)=GW1V(IY,IX)*(SIN(THETA))
      GLE=0.4*GZG(IZ)*KNZ
      GNKE(IY,IX)=3.33*(GLE**2)*((GW1V(IY,IX)/0.00647)**2)
      GNEP(IY,IX)=0.1643*(GNKE(IY,IX)**1.5)/GLE
C     W-FIELD IS CALCULATED FROM EPS=CD*KE*W**0.5
      GNW(IY,IX)=(GNEP(IY,IX)/(RG(2)*GNKE(IY,IX)))**2
140  CONTINUE
      GO TO 158
146  IF (IZ.GT.20) GO TO 158
158  CONTINUE
      IF (INDVAR.EQ.P1) THEN
      CALL SETYX(VAL,GWV,15,24)
      ELSEIF(INDVAR.EQ.V1) THEN
      CALL SETYX(VAL,GV1,15,24)
      ELSEIF(INDVAR.EQ.W1) THEN
      CALL SETYX(VAL,GW1,15,24)
      ELSEIF(INDVAR.EQ.KE) THEN
      CALL SETYX(VAL,GNKE,15,24)
      ELSEIF(INDVAR.EQ.IVFSQ) THEN
      CALL SETYX(VAL,GNW,15,24)
      ENDIF
      RETURN
1312 CONTINUE
C----- SECTION 13 ----- value = GRND1
C     VALUES FOR SOURCE TERMS RELATED TO K-W MODEL
      IF(IGR.NE.13.AND.ISC.NE.13) RETURN
      IF(NPATCH.EQ.'KWSOR1') THEN

```

```

        IF(INDVAR.EQ.KE) THEN
        CALL FN31(VAL,LGEN1,AUX(LEN1),1.0/SQRT(RG(1)),1.0,2.0)
        ELSE IF(INDVAR.EQ.IVFSQ) THEN
        CALL FN31(VAL,LGEN1,EASP5, RG(3)*RG(7)/RG(6),1.0,-1.0)
        ENDIF
        ELSE IF(NPATCH.EQ.'KWSOR2'.AND.INDVAR.EQ.IVFSQ) THEN
        CALL FN21(VAL,EASP4,AUX(VIST),0.0, RG(5))
        ENDIF
        RETURN
1313 CONTINUE
C----- SECTION 14 ----- value = GRND2
        CALL SUB2(IGR,13,ISC,14)
        IF(NPATCH.EQ.'WFUN'.AND.INDVAR.EQ.IVFSQ) THEN
        IF(WALDIS.EQ.0) THEN
        CALL FN1(EASP8,DZ/2.)
        ELSE
        CALL FN2(EASP8,WALDIS,0.0,0.5)
        ENDIF
        CALL FN31(VAL,12,EASP8,17.62,1.0,-2.0)
        ENDIF
        RETURN
1314 CONTINUE
C----- SECTION 15 ----- value = GRND3
        RETURN
1315 CONTINUE
C----- SECTION 16 ----- value = GRND4
        RETURN
1316 CONTINUE
C----- SECTION 17 ----- value = GRND5
        RETURN
1317 CONTINUE
C----- SECTION 18 ----- value = GRND6
        RETURN
1318 CONTINUE
C----- SECTION 19 ----- value = GRND7
        RETURN
1319 CONTINUE
C----- SECTION 20 ----- value = GRND8
        RETURN
1320 CONTINUE
C----- SECTION 21 ----- value = GRND9
        RETURN
1321 CONTINUE
C----- SECTION 22 ----- value = GRND10
        RETURN
C*****
C
C--- GROUP 14. Downstream pressure for PARAB=.TRUE.
C
        14 CONTINUE
        RETURN
C*****
C * Make changes for this group only in group 19.
C--- GROUP 15. Termination of sweeps
C--- GROUP 16. Termination of iterations
C--- GROUP 17. Under-relaxation devices
C--- GROUP 18. Limits on variables or increments to them
C*****
C
C--- GROUP 19. Special calls to GROUND from EARTH

```

```

C      19 GO TO (191,192,193,194,195,196,197,198),ISC
191 CONTINUE
C      * ----- SECTION 1 ---- START OF TIME STEP.
      RETURN
192 CONTINUE
C      * ----- SECTION 2 ---- START OF SWEEP.
      RETURN
193 CONTINUE
C      * ----- SECTION 3 ---- START OF IZ SLAB.
      RETURN
194 CONTINUE
C      * ----- SECTION 4 ---- START OF ITERATION.
C*****THE METHOD OF CALCULATING EBAR
C*****TRAPEZOIDAL RULE WAS APPLIED
      IBAR=INAME('EBAR')
      IETA=INAME('ETA')
      CALL GETYX(IETA,GETA,15,24)
      DO 2222 IY=1,1
      DO 2222 IIX=5,14
      IIX1=IIX-4
      A=0.049*(GETA(1,5)+GETA(1,6))+0.0833*(GETA(1,6)+GETA(1,7))
      B=0.0441*(GETA(1,7)+2*GETA(1,8)+2*GETA(1,9)+GETA(1,10))
      C=0.034*(GETA(1,10)+GETA(1,11))+0.0833*(GETA(1,11)+2*GETA(1,12)
&+GETA(1,13))+0.0345*(GETA(1,13)+GETA(1,14))
      GBAR(IY,IIX1)=A+B+C
2222 CONTINUE
      CALL SETYX(IBAR,GBAR,15,24)
C
      IF(IGR.EQ.19.AND.ISC.EQ.4) THEN
C      STRAIN TERM
C      DWDY NEEDED
C      VORTICITY TERM
      CALL GVORTSQ
      ENDIF
      RETURN
195 CONTINUE
C      * ----- SECTION 5 ---- FINISH OF ITERATION.
      RETURN
196 CONTINUE
C      * ----- SECTION 6 ---- FINISH OF IZ SLAB.
C*****ADDITIONS TO ACCOUNT FOR X/D
      CALL GETYX(XU2D,GXOD,15,24)
      DO 777 IY=1,NY
      DO 777 IX=1,NX
      GXOD(IY,IX)=GXOD(IY,IX)/DIA
777 CONTINUE
      CALL SETYX(INAME('XOD'),GXOD,15,24)
C*****ADDITIONS TO ACCOUNT FOR Y/D
      CALL GETYX(YV2D,GYOD,15,24)
      DO 7777 IY=1,NY
      DO 7777 IX=1,NX
      GYOD(IY,IX)=GYOD(IY,IX)/DIA
7777 CONTINUE
      CALL SETYX(INAME('YOD'),GYOD,15,24)
C
C*****THE METHOD OF CALCULATING ETA.
      IF(STORE(INAME('ETA'))) THEN
      IOE=LOF(INAME('ETA'))
      IOT=LOF(H1)

```

```

DO 222 IY=1,NY
DO 222 IX=1,NX
I=(IX-1)*NY+IY
222 F(I0E+I)=(328.0-F(I0T+I))/30.0
ENDIF
C
RETURN
197 CONTINUE
C * ----- SECTION 7 ----- FINISH OF SWEEP.
RETURN
198 CONTINUE
C * ----- SECTION 8 ----- FINISH OF TIME STEP.
RETURN
C*****
C
C--- GROUP 20. Preliminary print-out
C
20 CONTINUE
RETURN
C*****
C * Make changes for this group only in group 19.
C--- GROUP 21. Print-out of variables
C--- GROUP 22. Spot-value print-out
C*****
C
C--- GROUP 23. Field print-out and plot control
23 CONTINUE
RETURN
C*****
C
C--- GROUP 24. Dumps for restarts
C
24 CONTINUE
RETURN
END
C*****
SUBROUTINE GVORTSQ
INCLUDE 'SATEAR'
INCLUDE 'GRDLOC'
INCLUDE 'GRDEAR'
EQUIVALENCE (IZ,IZSTEP)
C
CALL FN1(EASP2,0.0)
CALL FN1(EASP3,0.0)
CALL FN1(EASP4,0.0)
C-----
C Z-COMPONENT OF VORTICITY : (DW/DY-DV/DZ)**2
C-----
C CALCULATION INCLUDES MAIN Z-COMPONENT, PARAB ONLY
C COMPUTE DW/DY AT SOUTH FACES
CALL FN67(EASP3,W1,SOUTH(W1),SOUTH(DYG2D),1.0,-1.0)
C SET DW/DY AT IY=1
CALL SUB2(L0E9,L0F(EASP3),L0E10,L0F(EASP2))
CALL SUB2(I1,L0E9+1,I2,I0E9+(NX-1)*NY+1)
DO 2 I=I1,I2,NY
2 F(I)=F(I+1)
C COMPUTE DW/DY AT NORTH FACES
CALL FN0(EASP2,NORTH(EASP3))
C SET DW/DY AT IY=NY
CALL SUB2(I1,L0E10+NY,I2,L0E10+NX*NY)

```

```

      DO 4 I=I1,I2,NY
4 F(I)=F(I-1)
C   COMPUTE dvortZ/DY
      CALL FN67(EASP4,EASP2,EASP3,DYV2D,1.0,-1.0)
C   SQUIRE dvortX/DY
      CALL FN21(EASP4,EASP4,EASP4,0.0,1.0)
      RETURN
      END
C*****
      SUBROUTINE SPECGR
      CALL WRIT40('DUMMY SUBROUTINE SPECGR CALLED.      ')
      CALL WRIT40('PLEASE ATTACH SPECGR OBJECT AT LINK.  ')
      CALL WAYOUT(2)
      RETURN
      END
C*****
      SUBROUTINE SPC1GR
      CALL WRIT40('DUMMY SUBROUTINE SPC1GR CALLED.      ')
      CALL WRIT40('PLEASE ATTACH SPC1GR OBJECT AT LINK.  ')
      CALL WAYOUT(2)
      RETURN
      END
C*****
      SUBROUTINE SPC2GR
      CALL WRIT40('DUMMY SUBROUTINE SPC2GR CALLED.      ')
      CALL WRIT40('PLEASE ATTACH SPC2GR OBJECT AT LINK.  ')
      CALL WAYOUT(2)
      RETURN
      END
C*****
      SUBROUTINE SPC3GR
      CALL WRIT40('DUMMY SUBROUTINE SPC3GR CALLED.      ')
      CALL WRIT40('PLEASE ATTACH SPC3GR OBJECT AT LINK.  ')
      CALL WAYOUT(2)
      RETURN
      END
C*****
      SUBROUTINE QUIZ
      RETURN
      END
C*****
C*****A user defined subroutine
      SUBROUTINE FNLEN(K1,K2,K3)
      COMMON F(1)
      COMMON/IGE/IXF,IXL,IYF,IYL,IGFILL(21)
      COMMON/NAMFN/NAMFUN
      CHARACTER*6 NAMFUN
      IF(IXL.LT.0) RETURN
      NAMFUN='FNLEN '
      CALL L0F3(K1,K2,K3,I,I2M1,I3M1,IADD)
      DO 1 IX=IXF,IXL
      I=I+IADD
      DO 1 IY=IYF,IYL
      I=I+1
1      F(I)=SQRT(F(I2M1+I)/F(I3M1+I))
      RETURN
      END
C*****
C*****A user defined subroutine
      SUBROUTINE FNEPS(K1,K2,K3,A)

```



```

COMMON F(1)
COMMON/IGE/IXF,IXL,IYF,IYL,IGFILL(21)
COMMON/NAMFN/NAMFUN
CHARACTER*6 NAMFUN
IF(IXL.LT.0) RETURN
NAMFUN='FNEPS '
CALL L0F3(K1,K2,K3,I,I2M1,I3M1,IADD)
  DO 2 IX=IXF,IXL
    I=I+IADD
    DO 2 IY=IYF,IYL
      I=I+1
2      F(I)=A*F(I2M1+I)*SQRT(F(I3M1+I))
RETURN
END

```

# APPENDIX II

## Listing of figures.

The followings are adopted in all figures to refer each turbulence model to its relevant prediction for both velocity and temperature profiles.

Isotropic $k - \epsilon$ model prediction	—————
Non isotropic $k - \epsilon$ model prediction	— — — —
$k - \omega$ model prediction	— · — · —
Modified $k - \omega$ model prediction	- - - - -

# METHODS FOR TURBINE COOLING

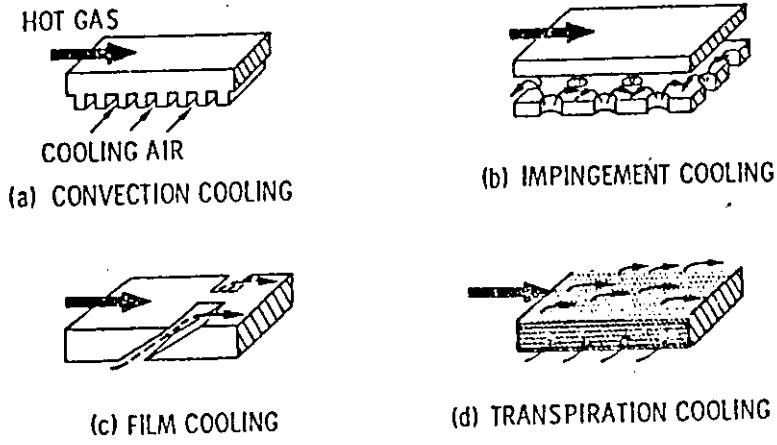


fig.(1-1)

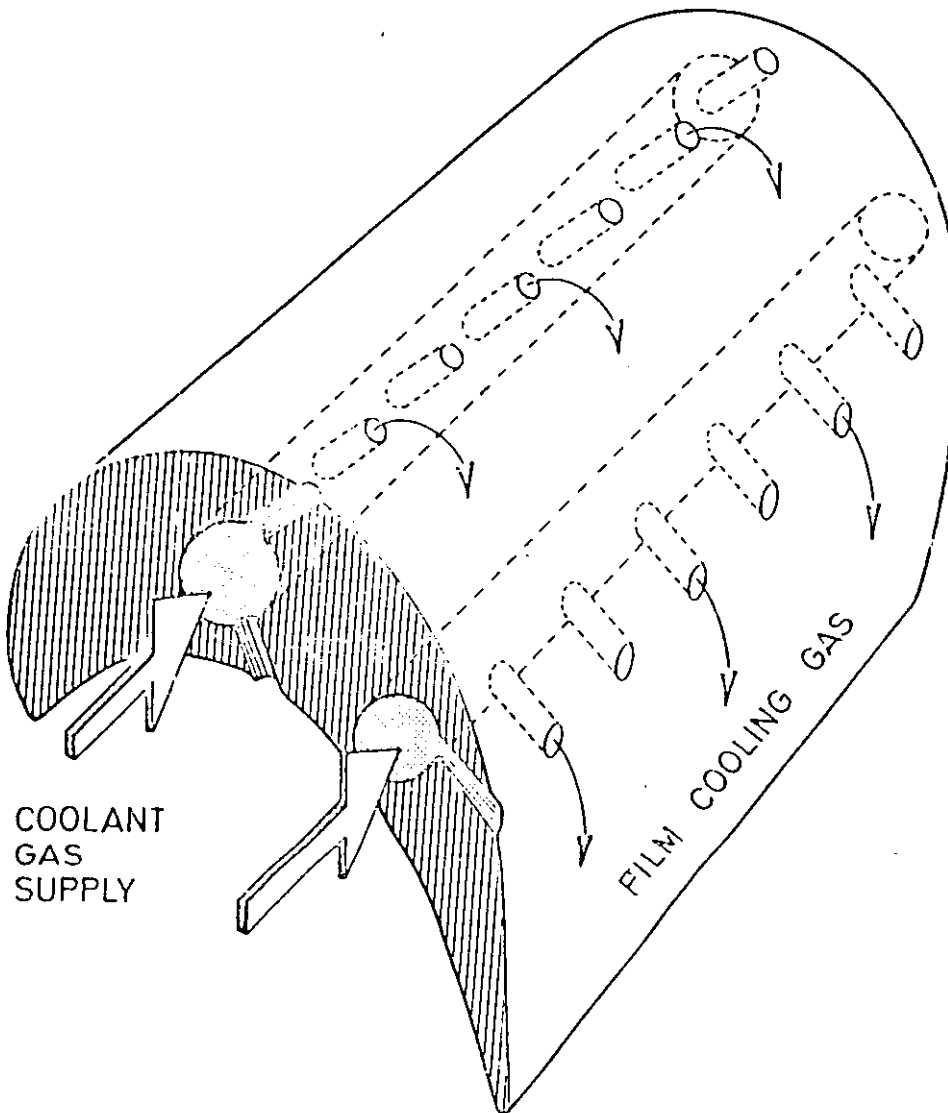
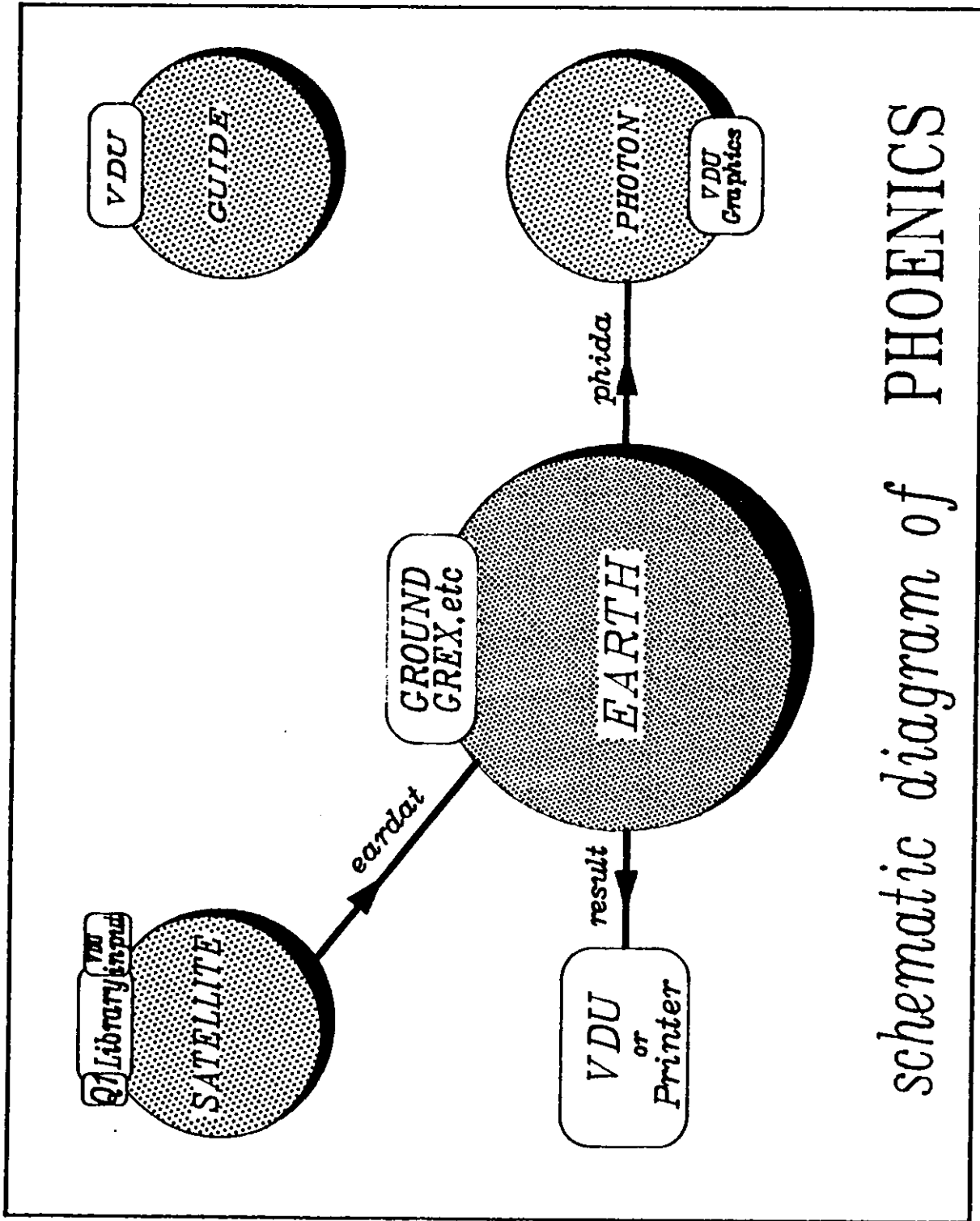
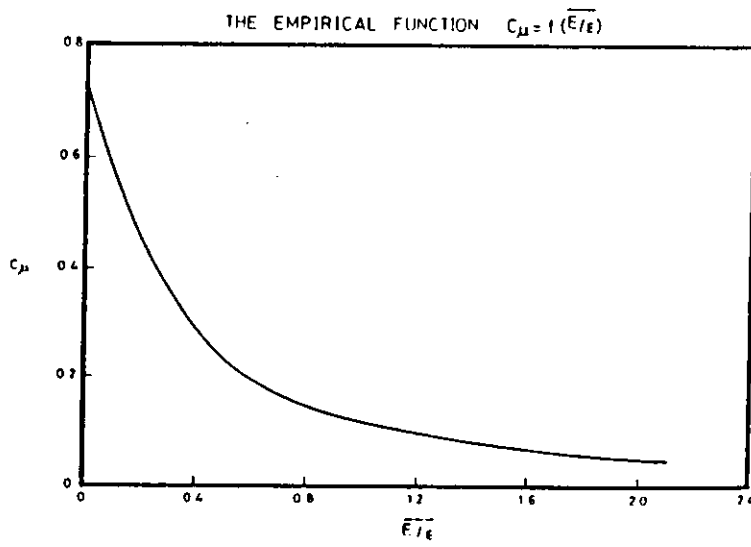


fig.(2-1)



schematic diagram of PHOENICS

Fig ( 3 - 1 )



The empirical function  $C_{\mu} = f(\overline{E}/\epsilon)$

fig.(4-1)

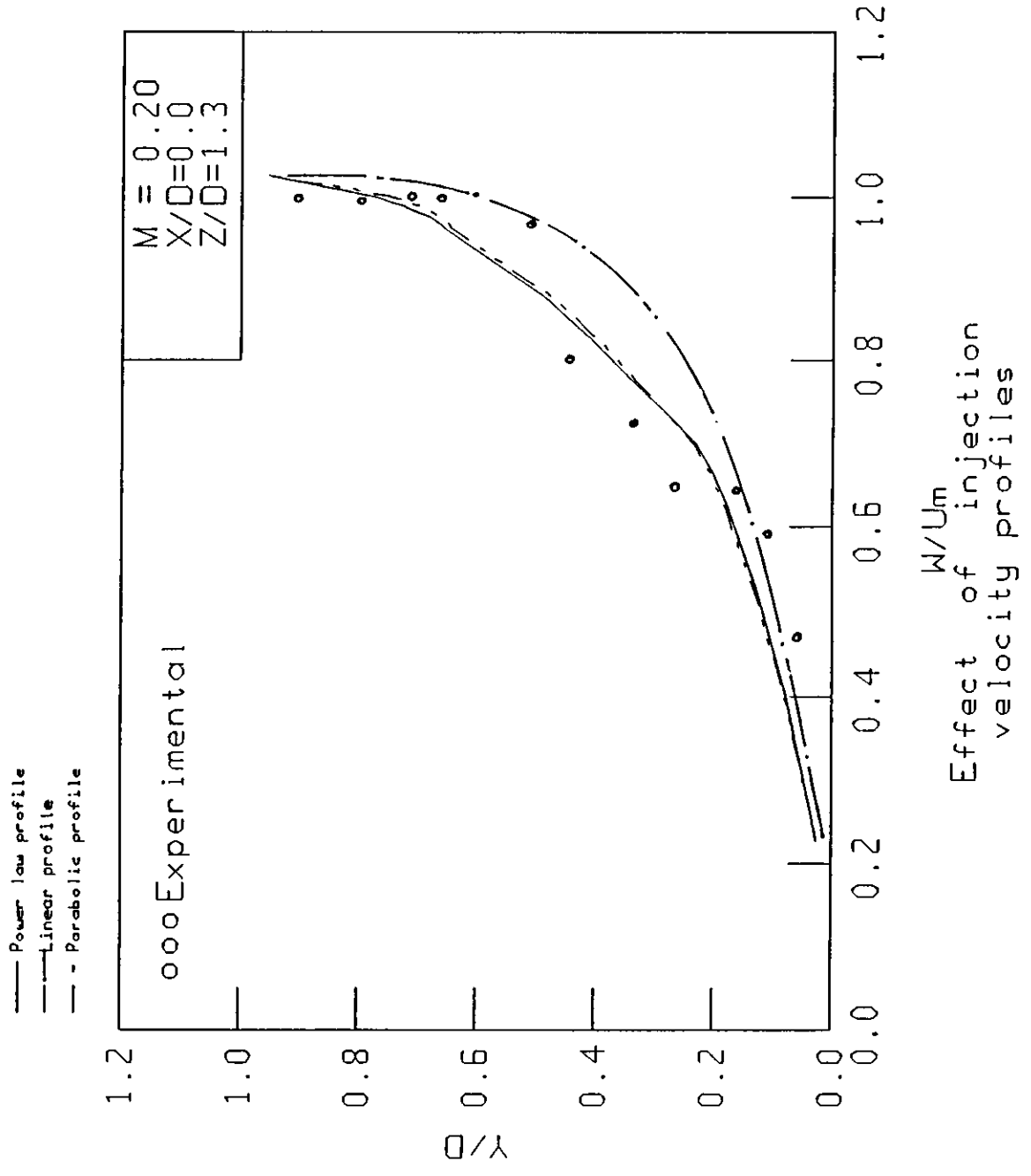


fig.(5-1a)  
 All Rights Reserved - Library of University of Jordan - Center of Thesis Deposit

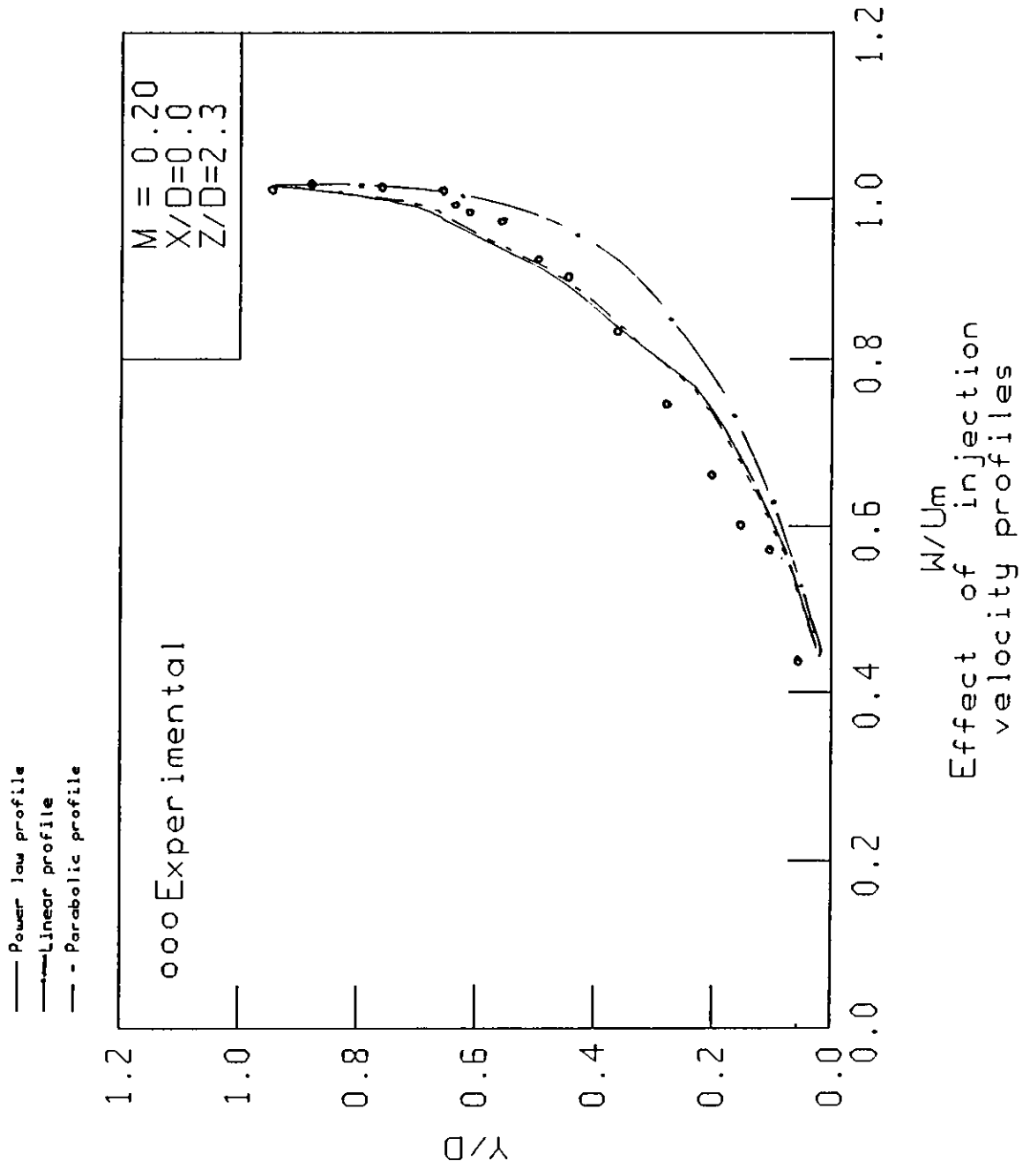


fig.(5-1b)

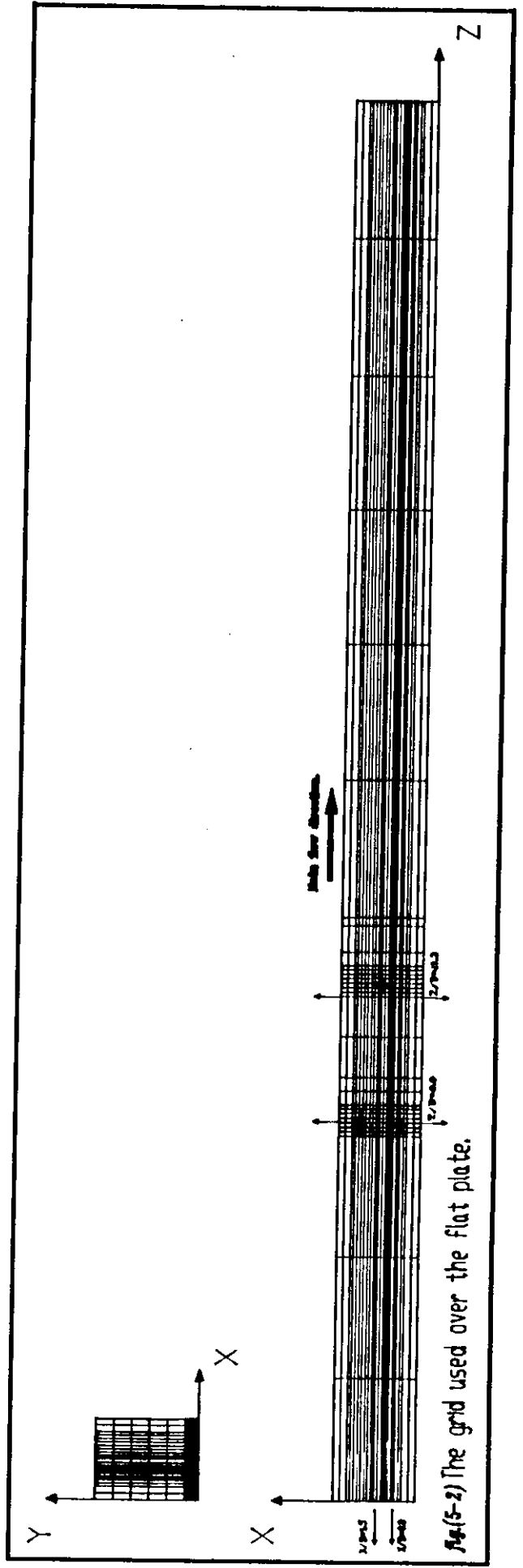
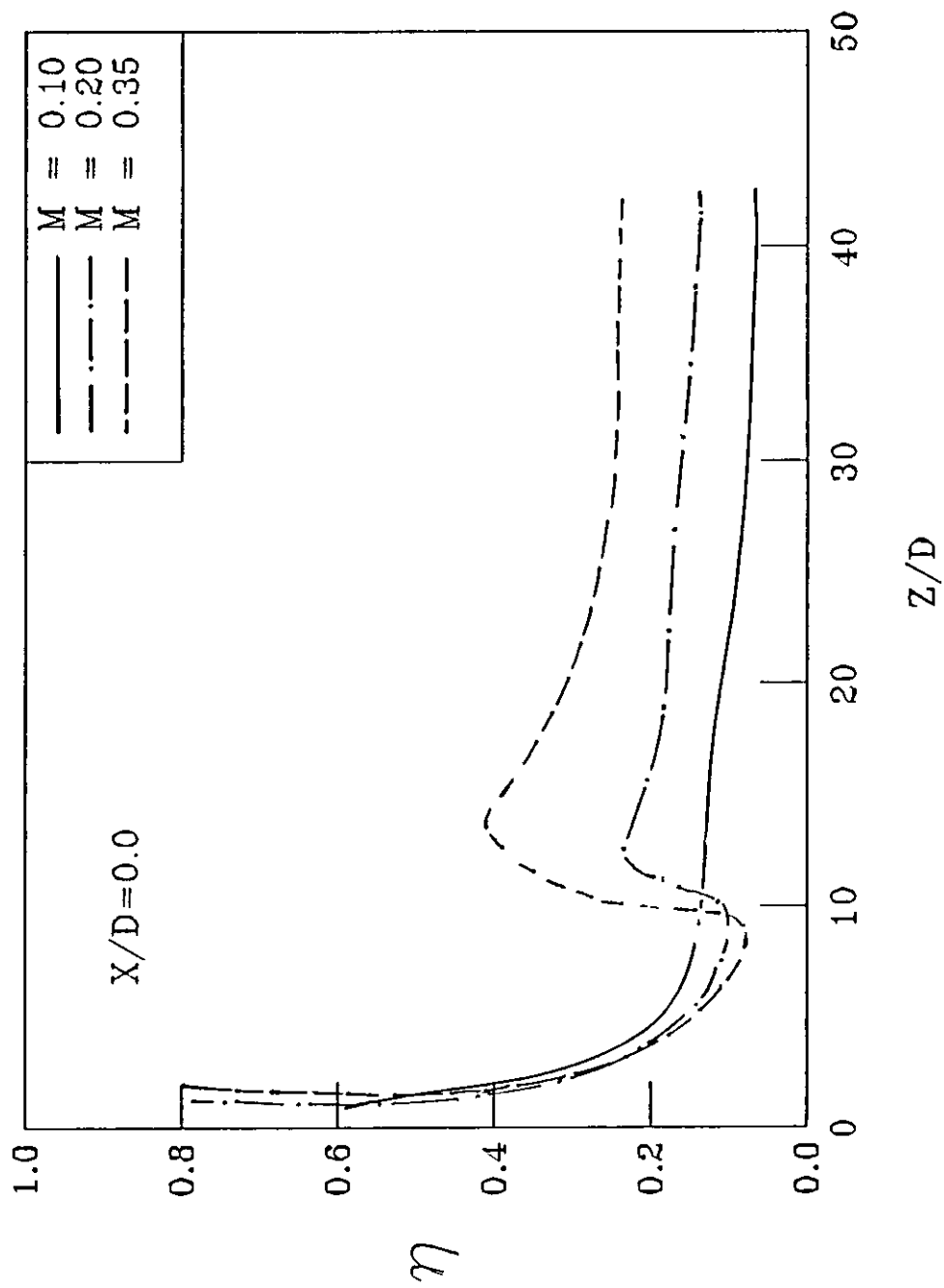


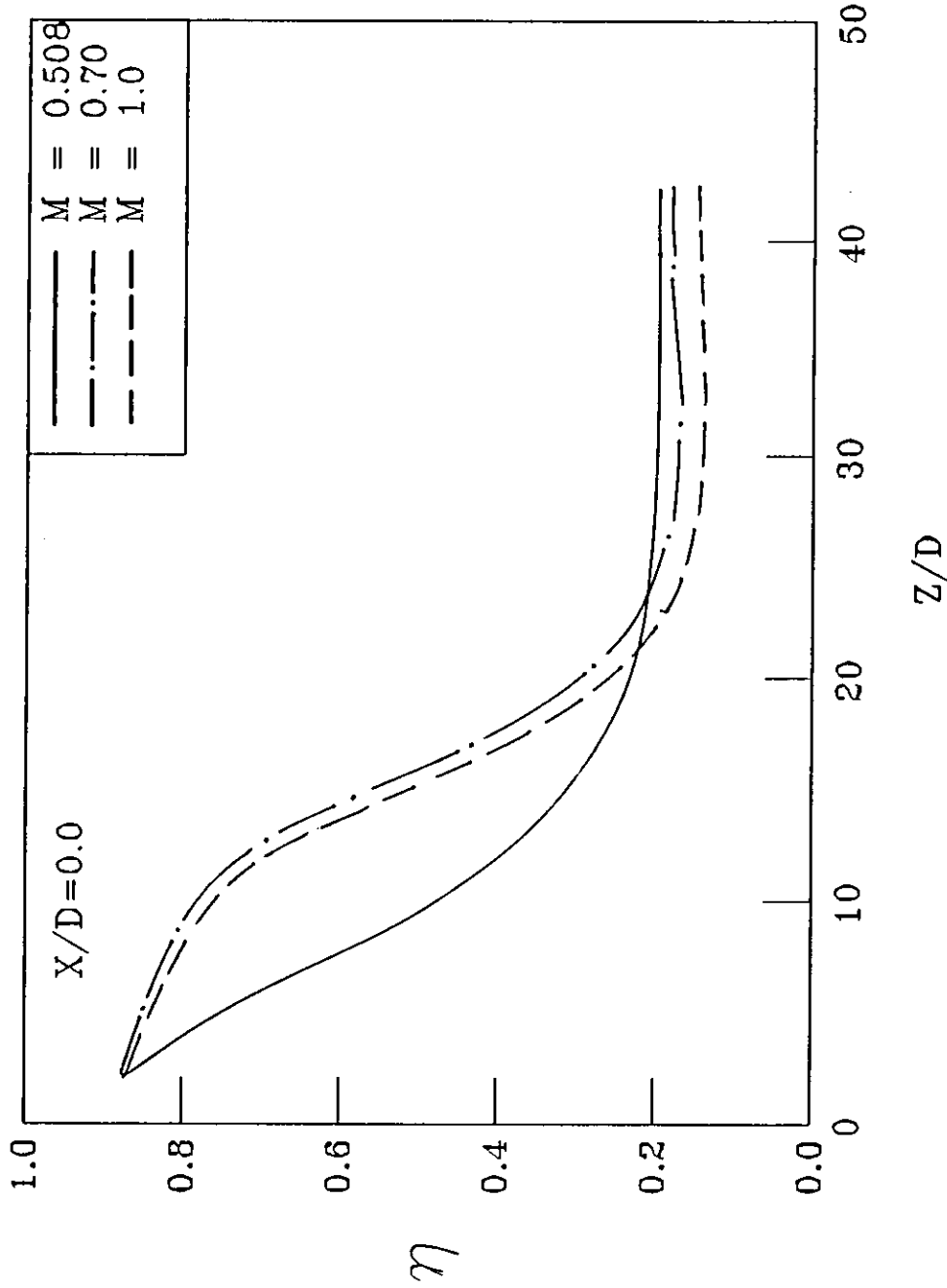
Fig. (5-2) The grid used over the flat plate.





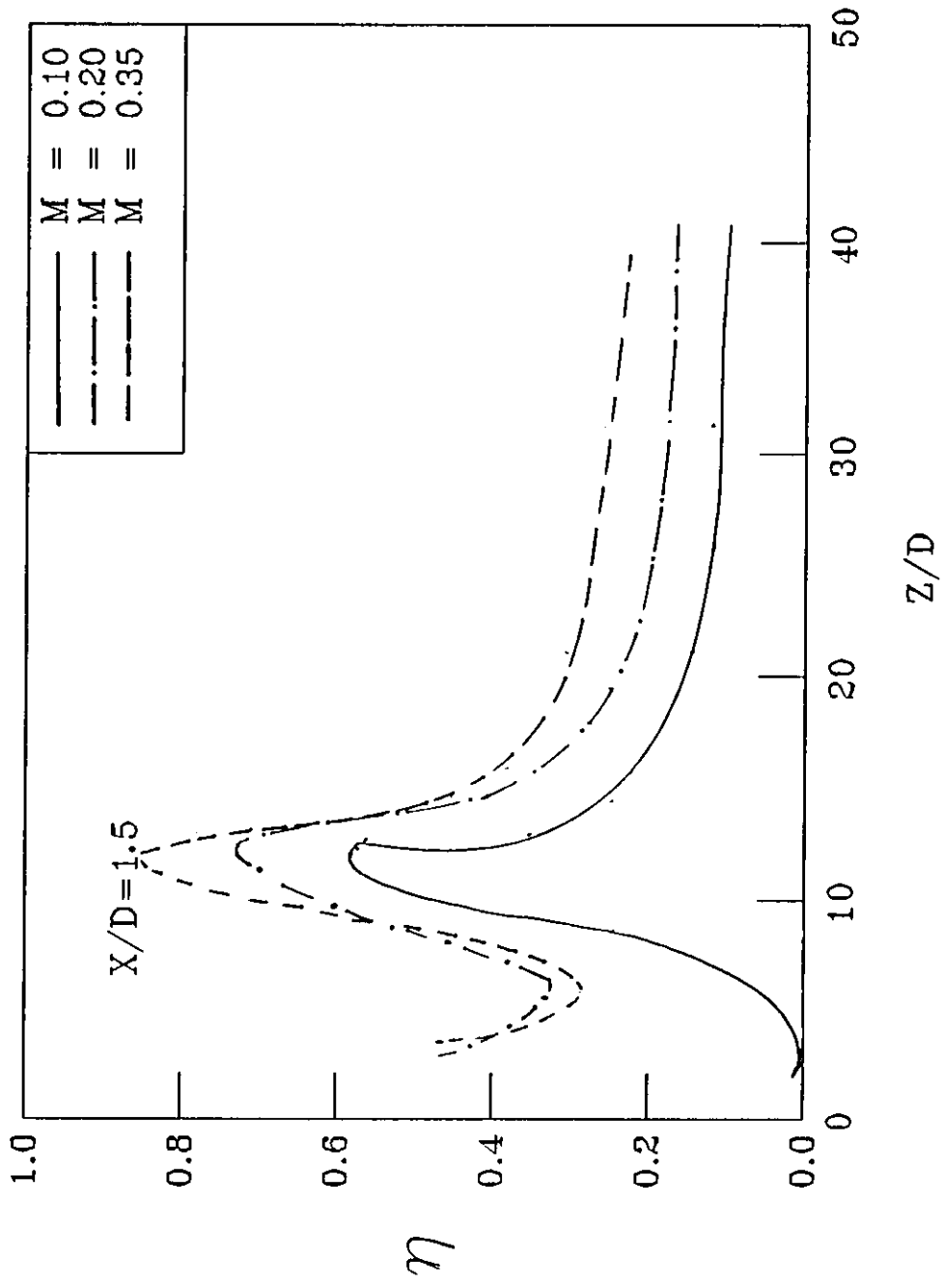
Film cooling effectiveness  
at low blowing rates

fig.(5-3a)



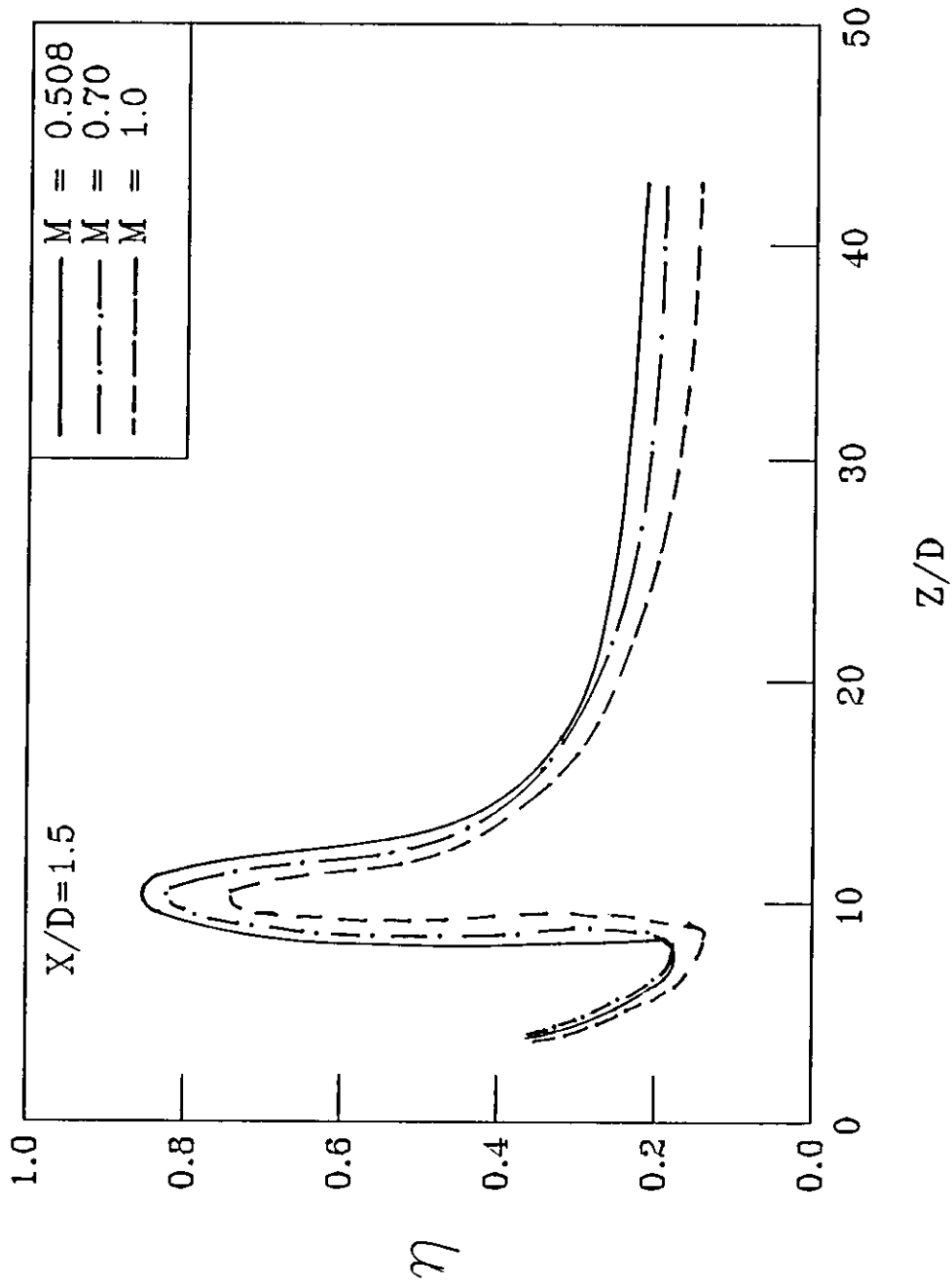
Film cooling effectiveness  
at high blowing rates

fig.(5-3b)



Film cooling effectiveness  
at low blowing rates

fig.(5-3c)



Film cooling effectiveness  
at high blowing rates

fig.(5-3d)

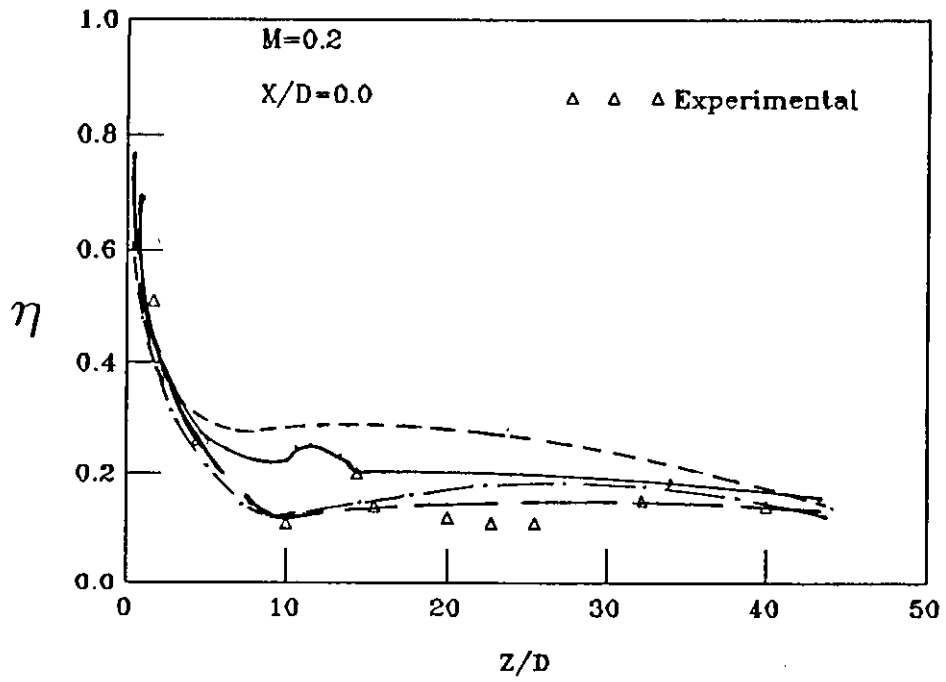


fig.(5-4a)

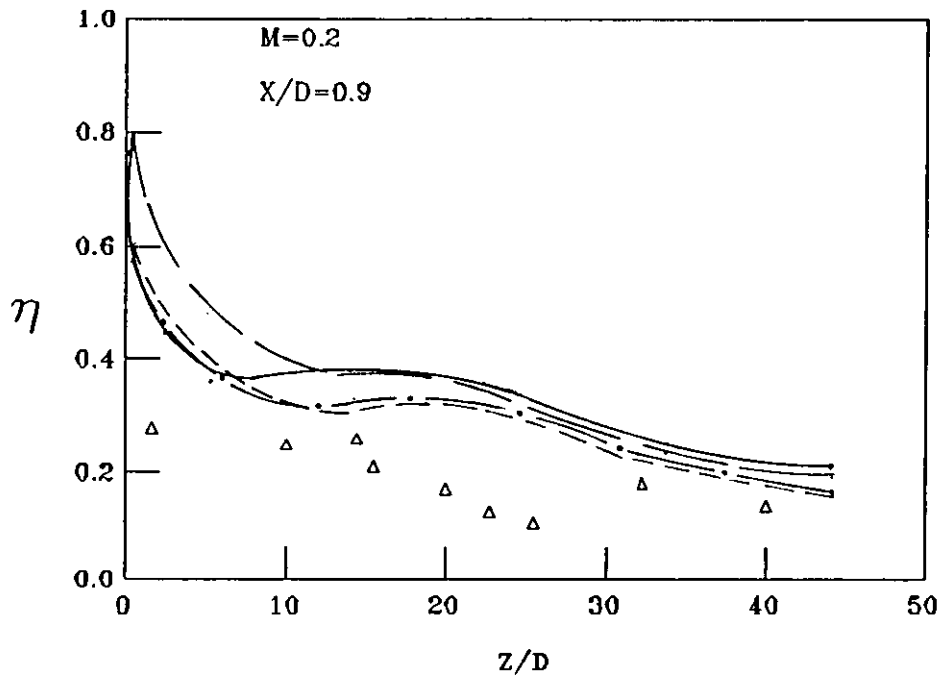


fig.(5-4b)

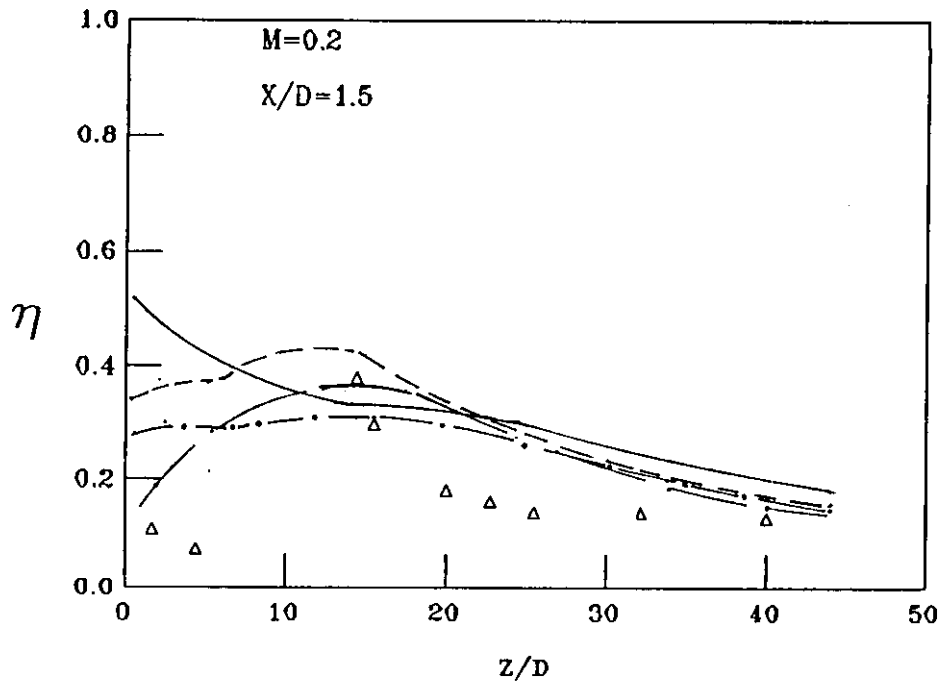


fig.(5-4c)

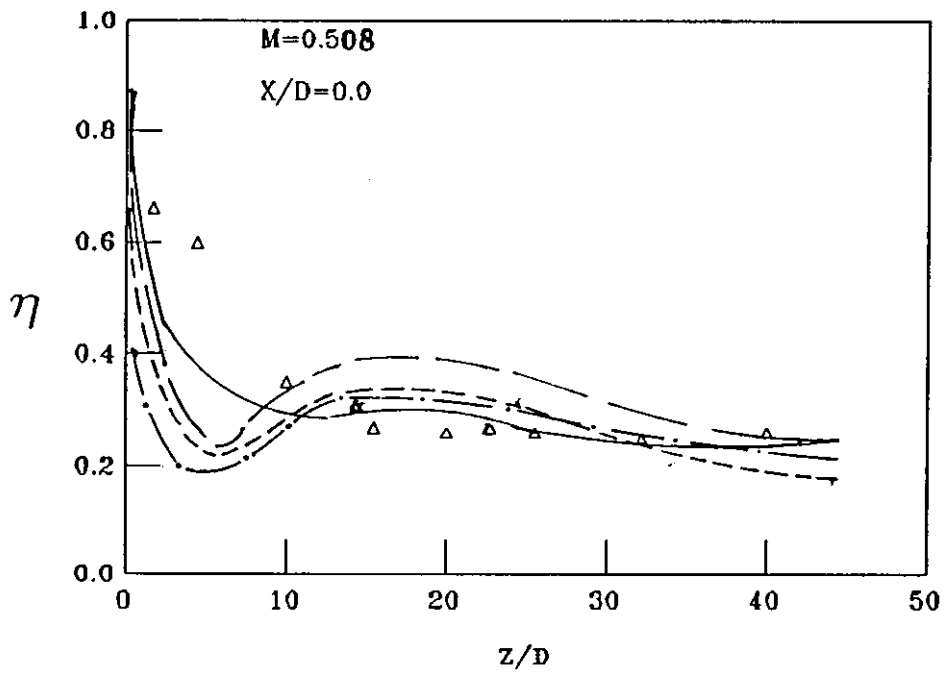


fig.(5-5a)

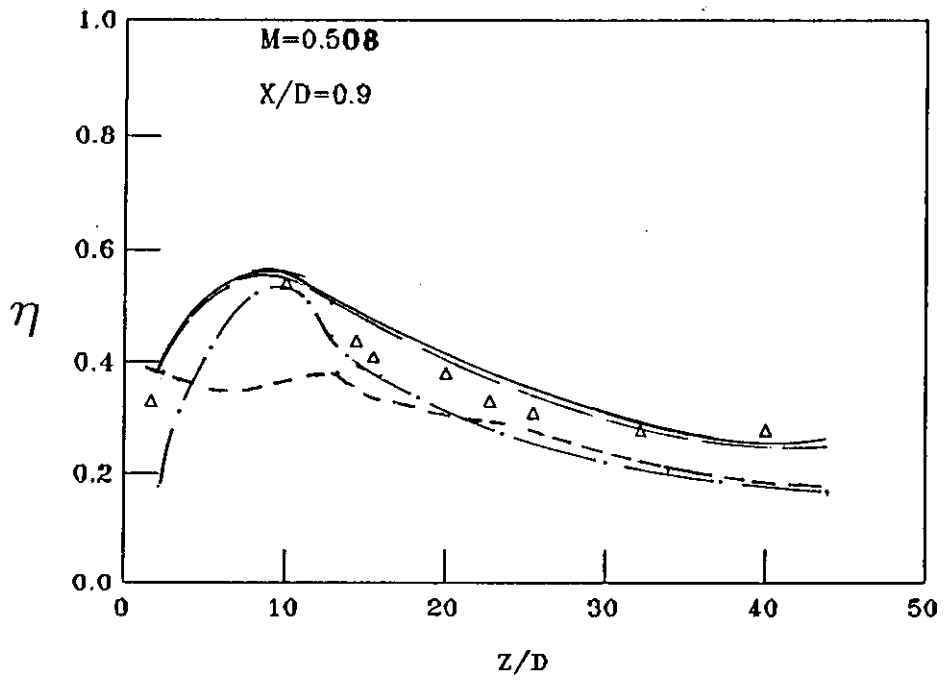


fig.(5-5b)

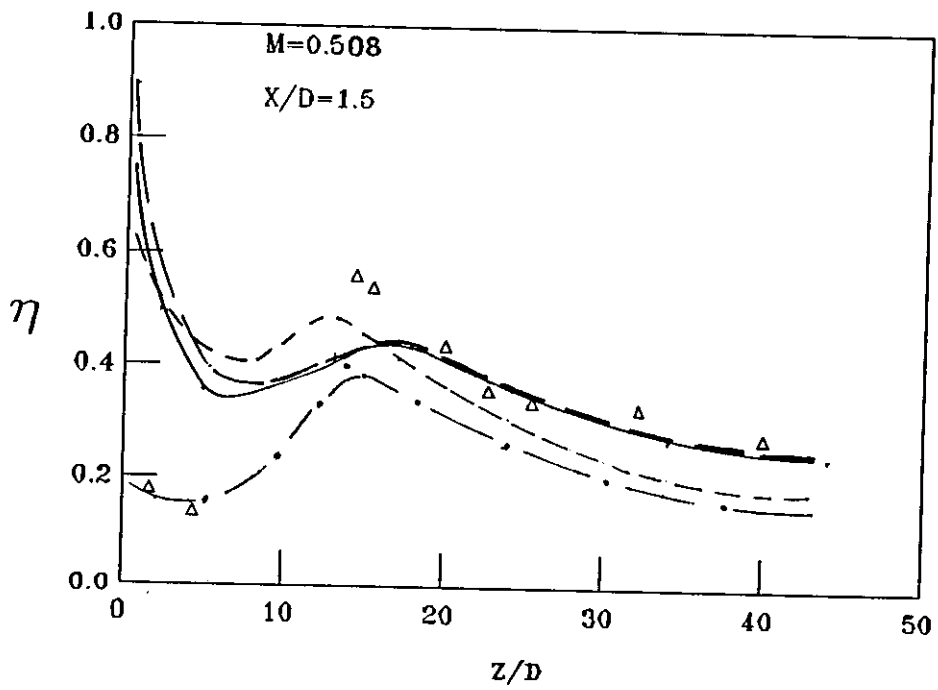


fig.(5-5c)

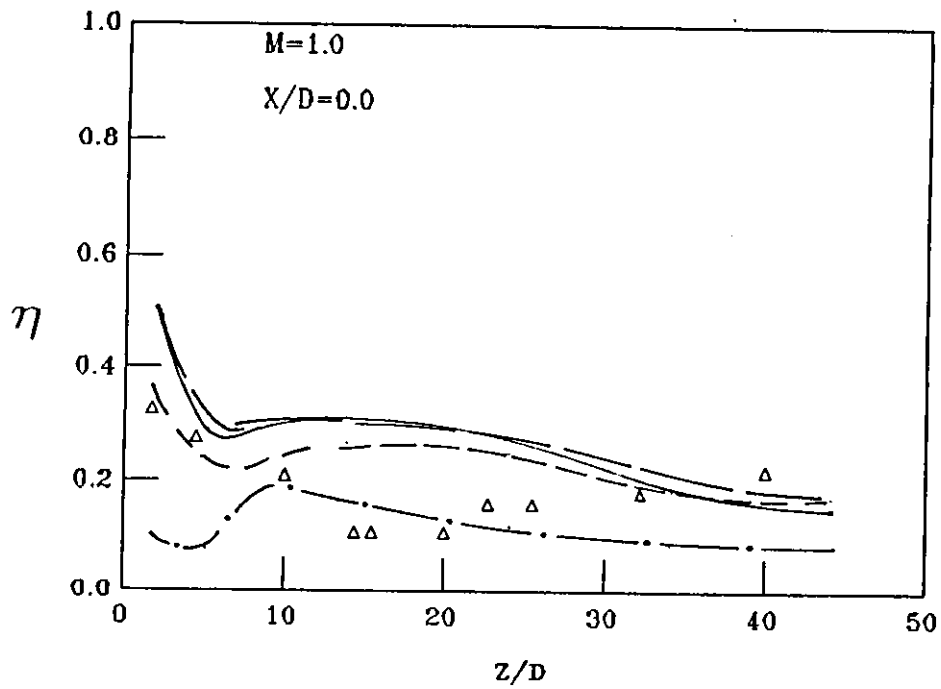


fig.(5-6a)

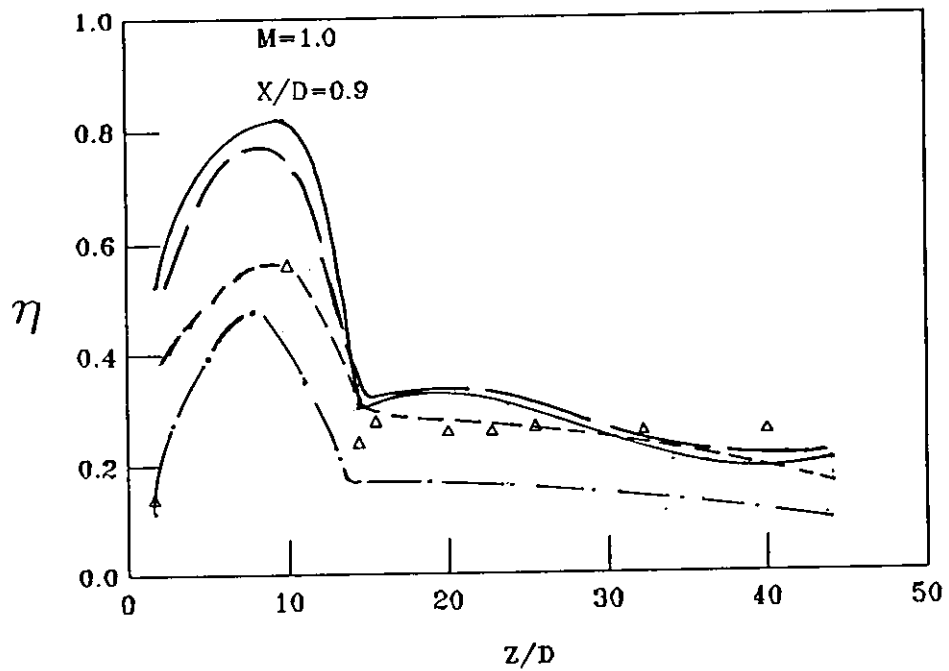


fig.(5-6b)



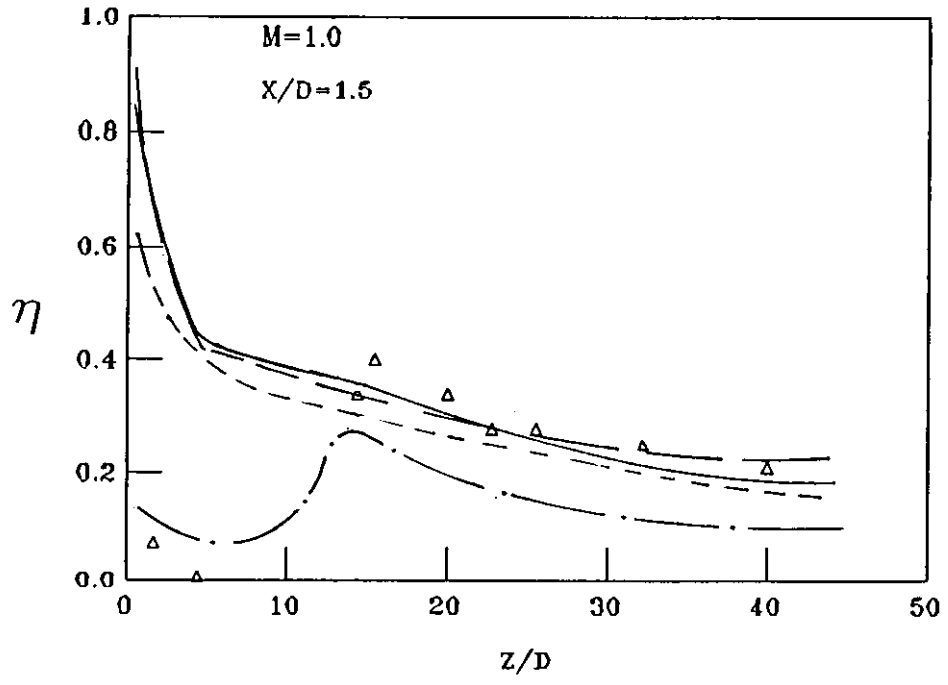


fig.(5-6c)

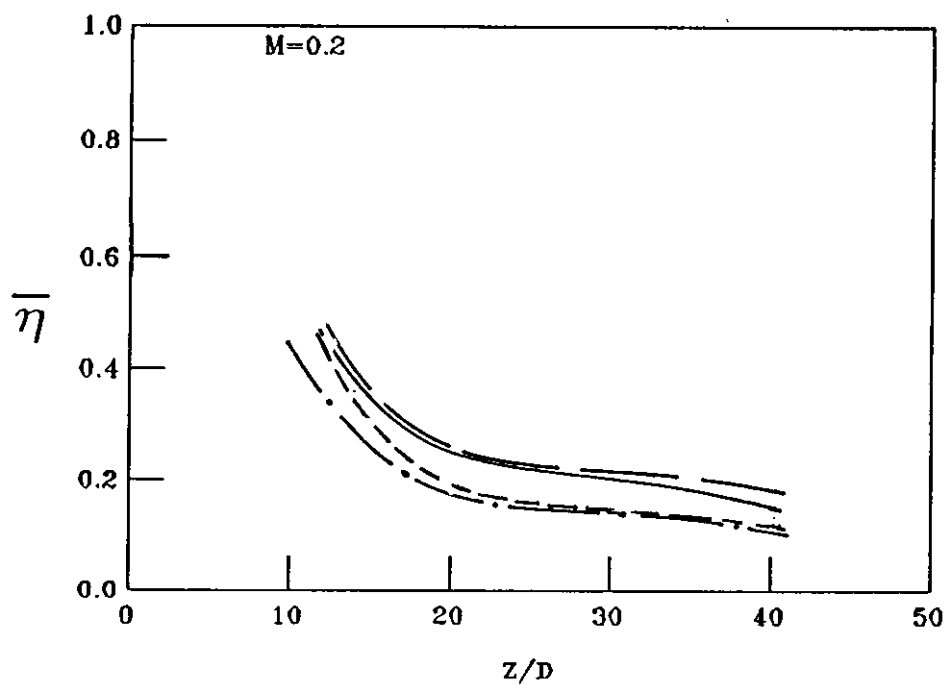


fig.(5-7a)

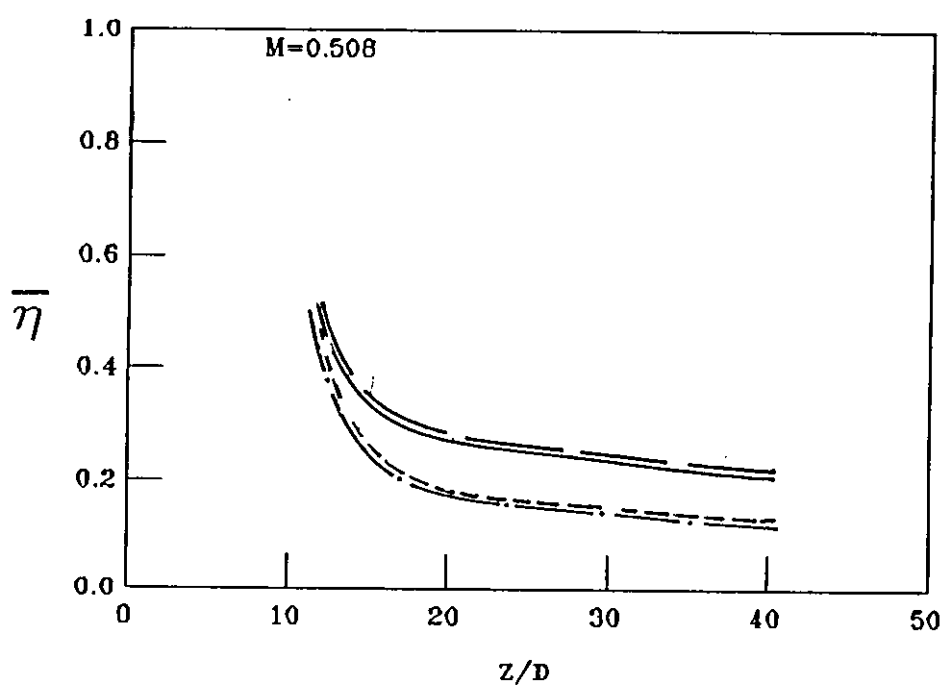


fig.(5-7b)

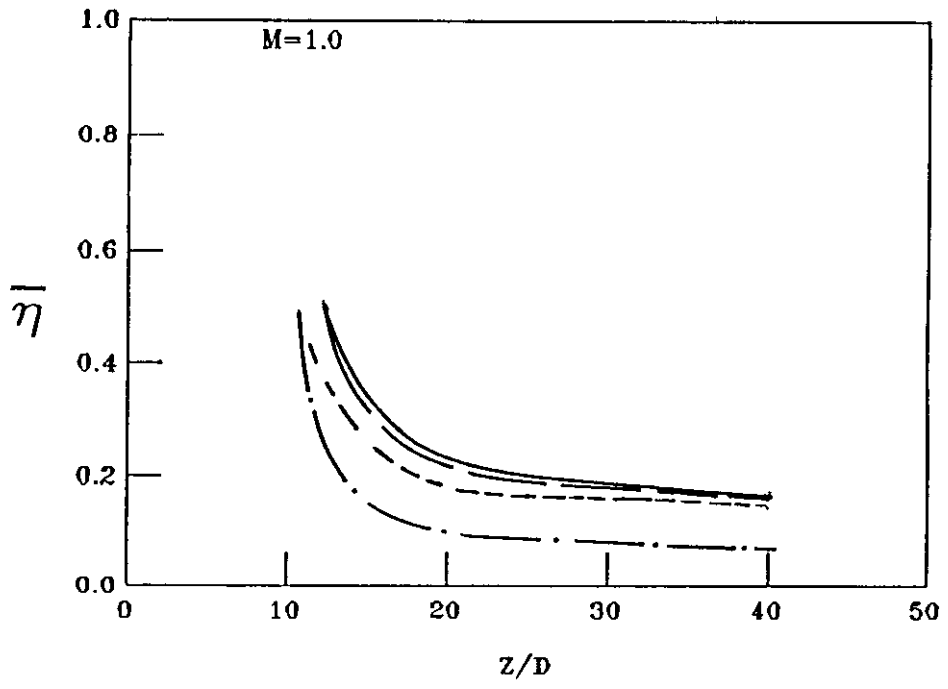


fig.(5-7c)

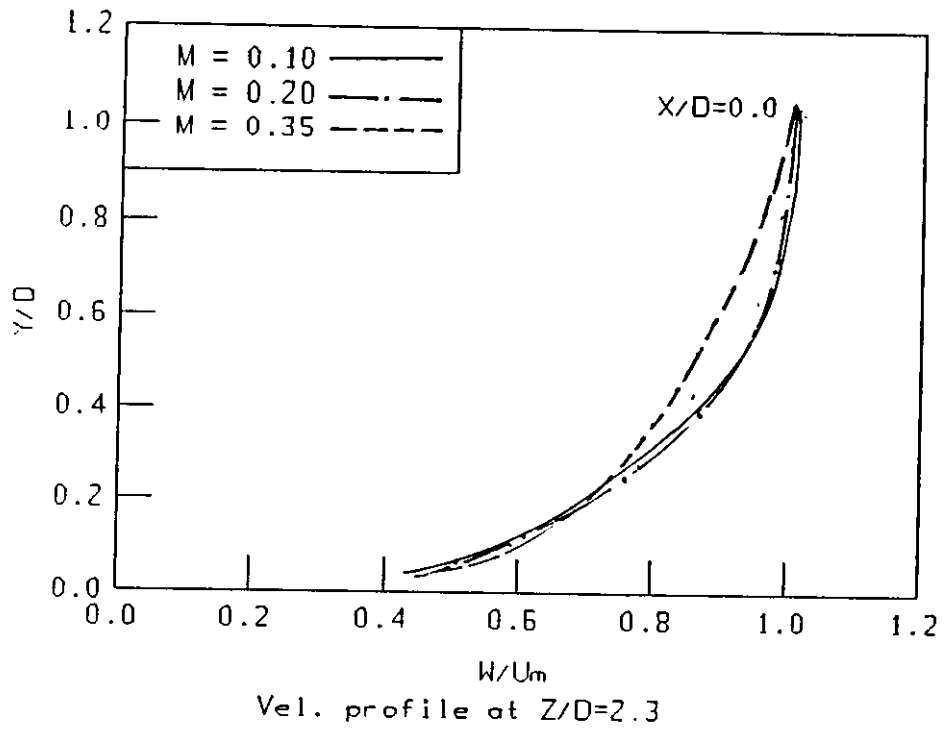


fig.(5-8a)

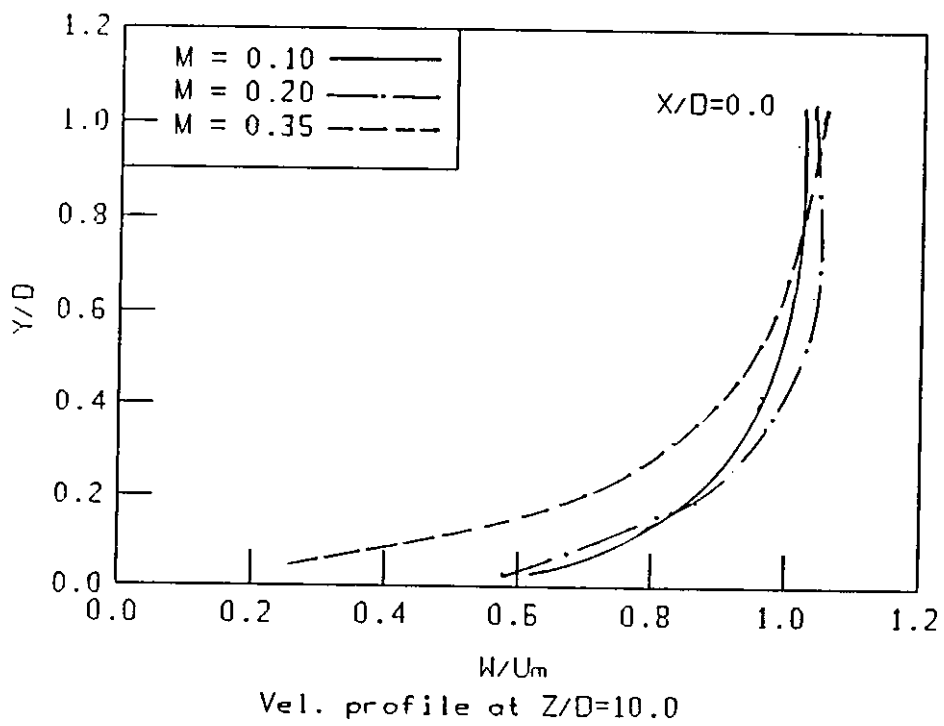


fig.(5-8b)

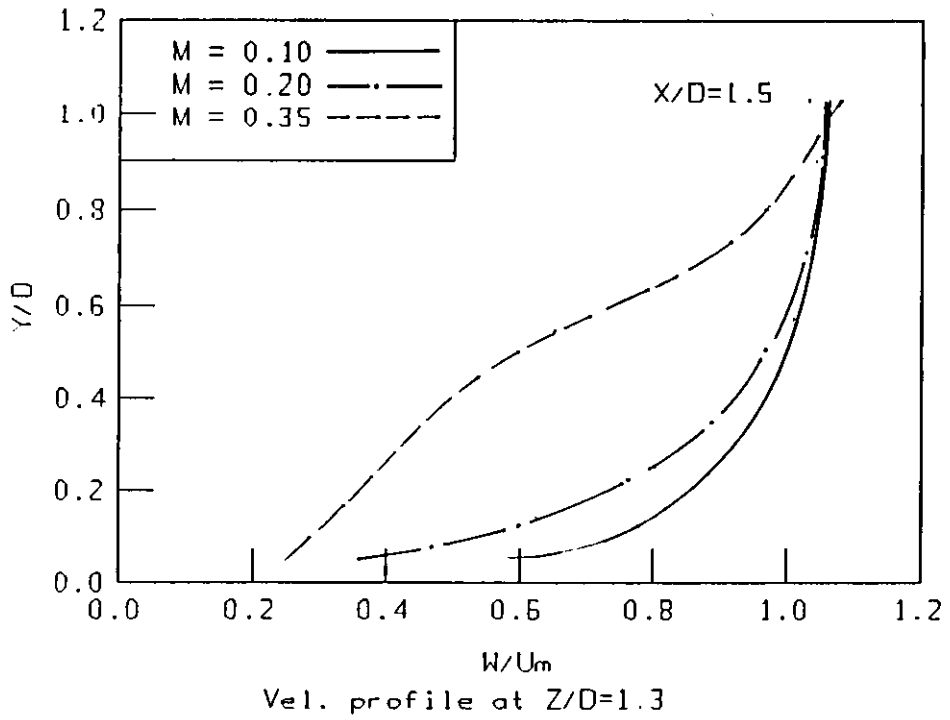


fig.(5-8c)

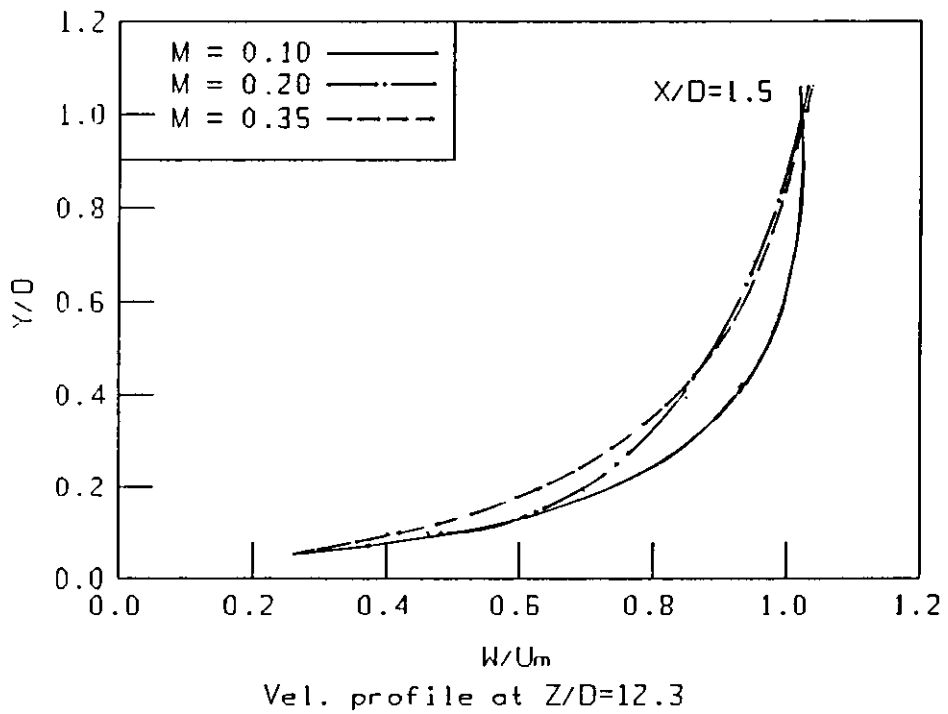


fig.(5-8d)

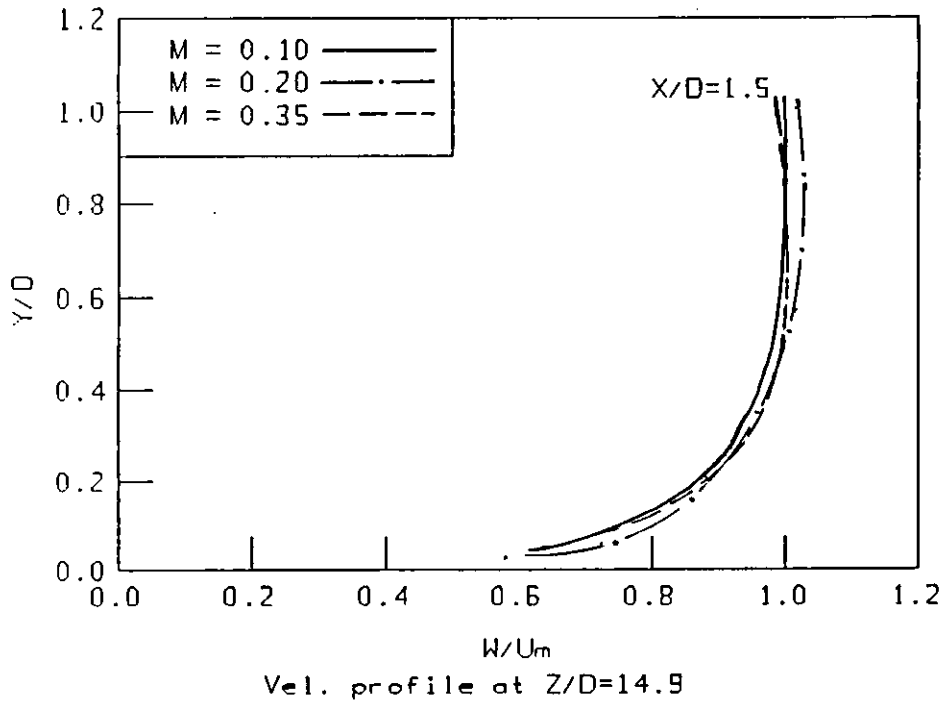


fig.(5-8e)

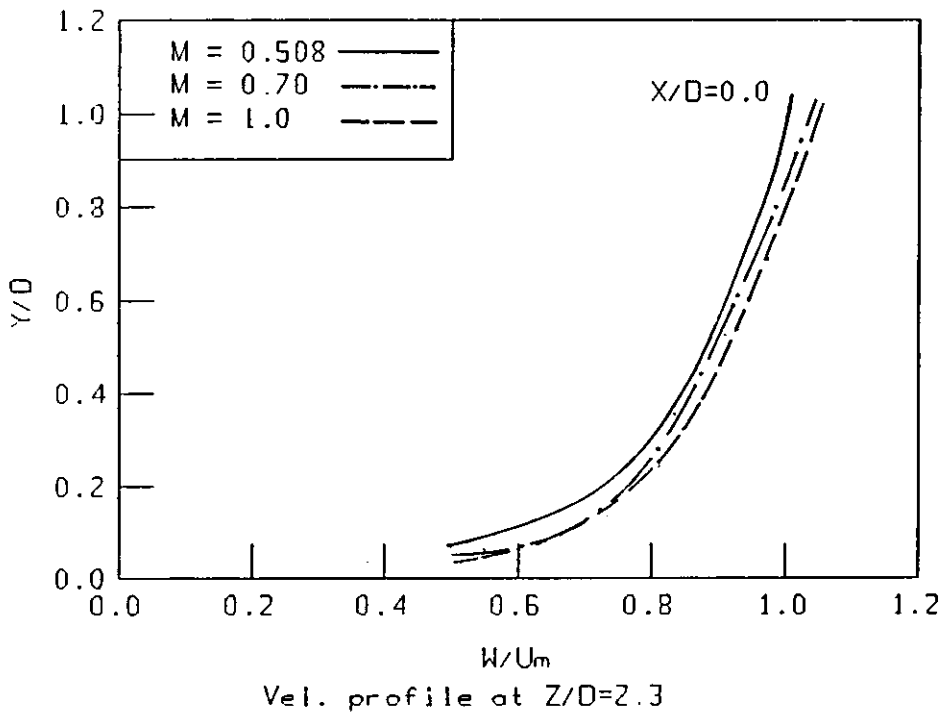


fig.(5-9a)

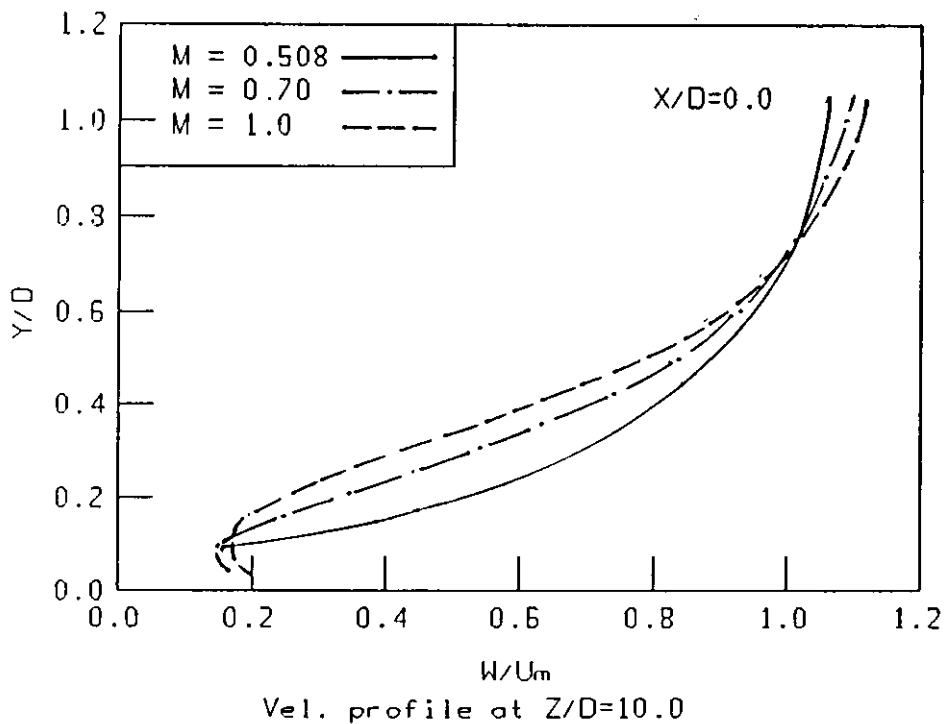


fig.(5-9b)

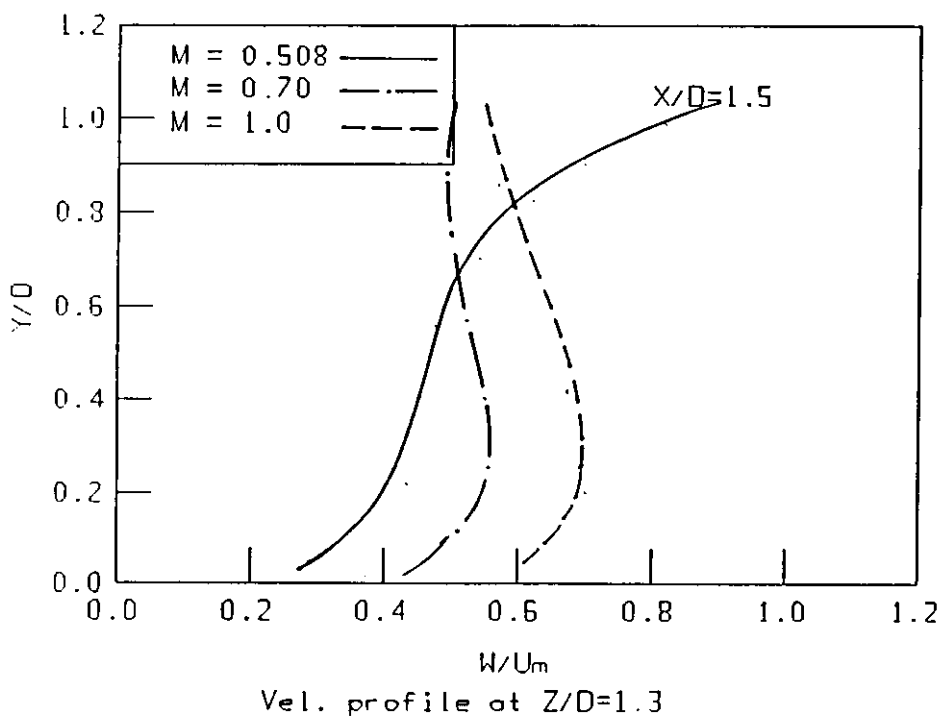


fig.(5-9c)

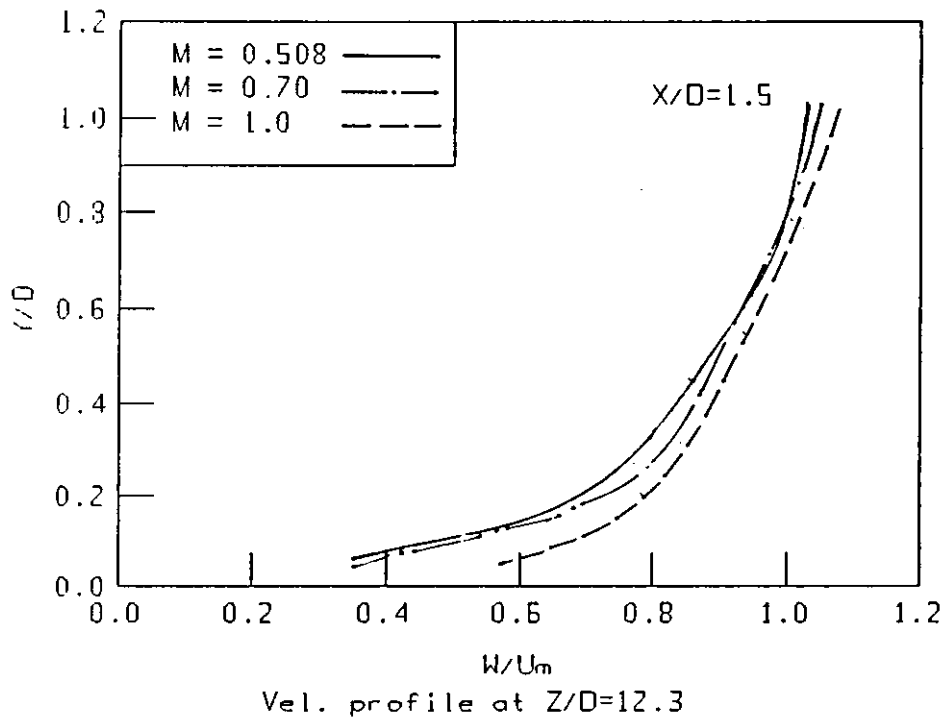


fig.(5-9d)

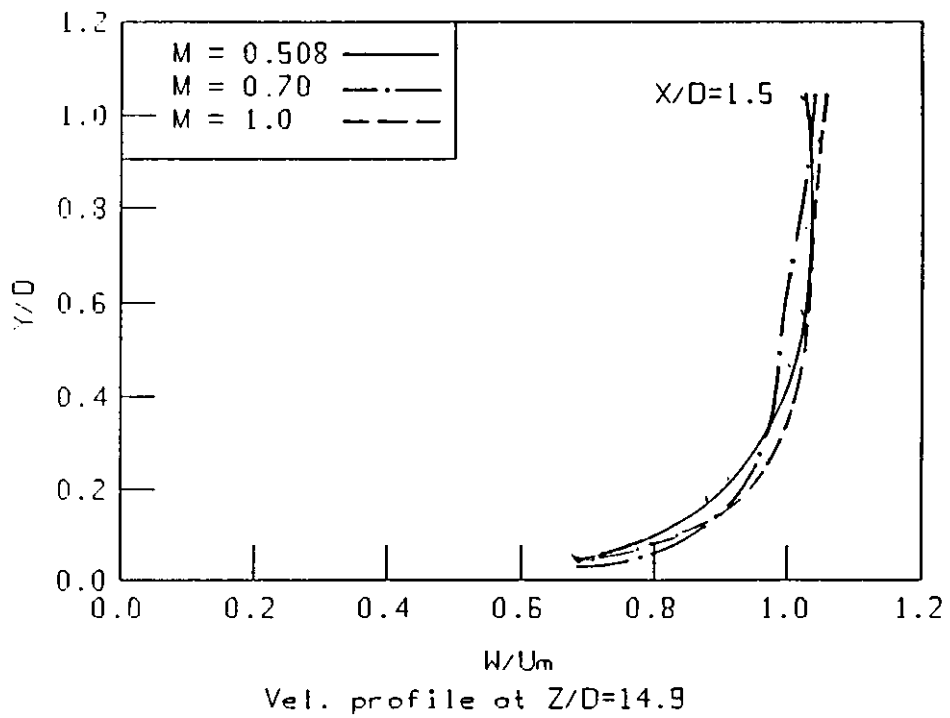


fig.(5-9e)



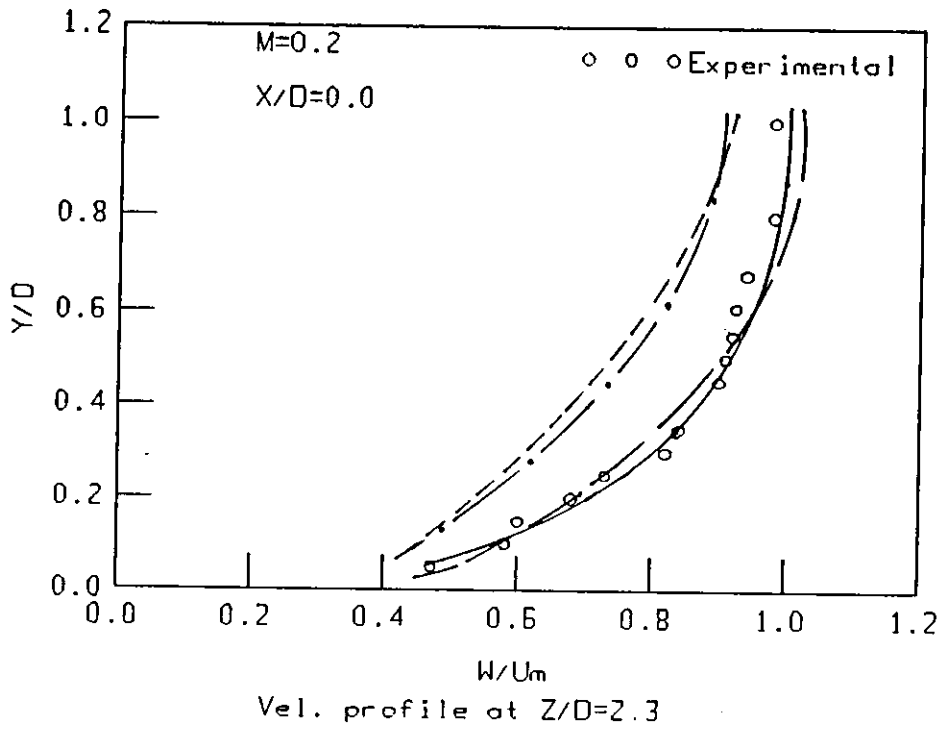


fig.(5-10a)

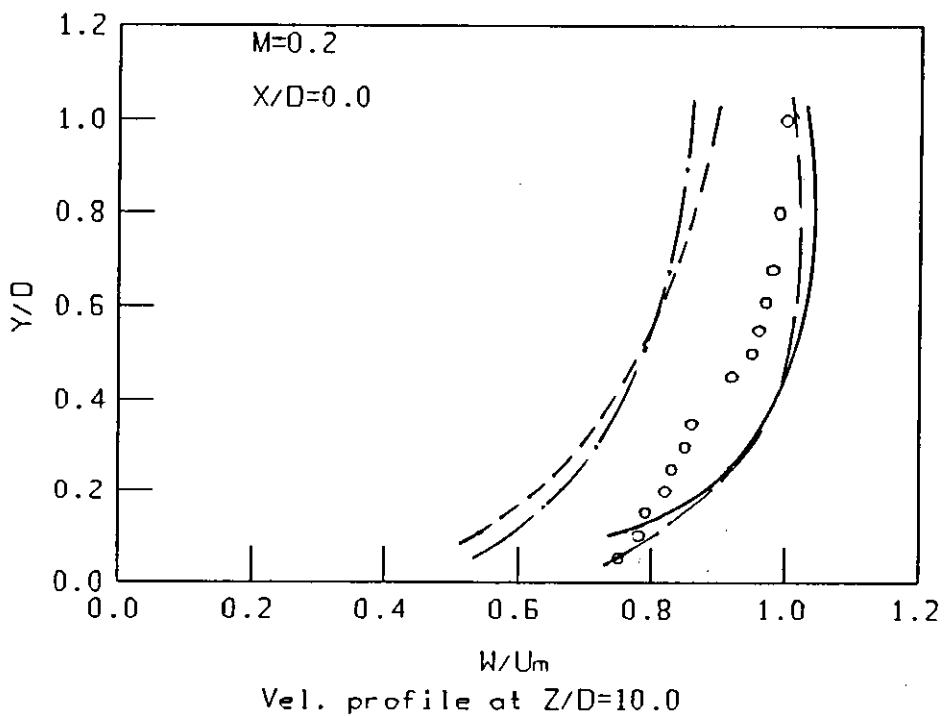


fig.(5-10b)

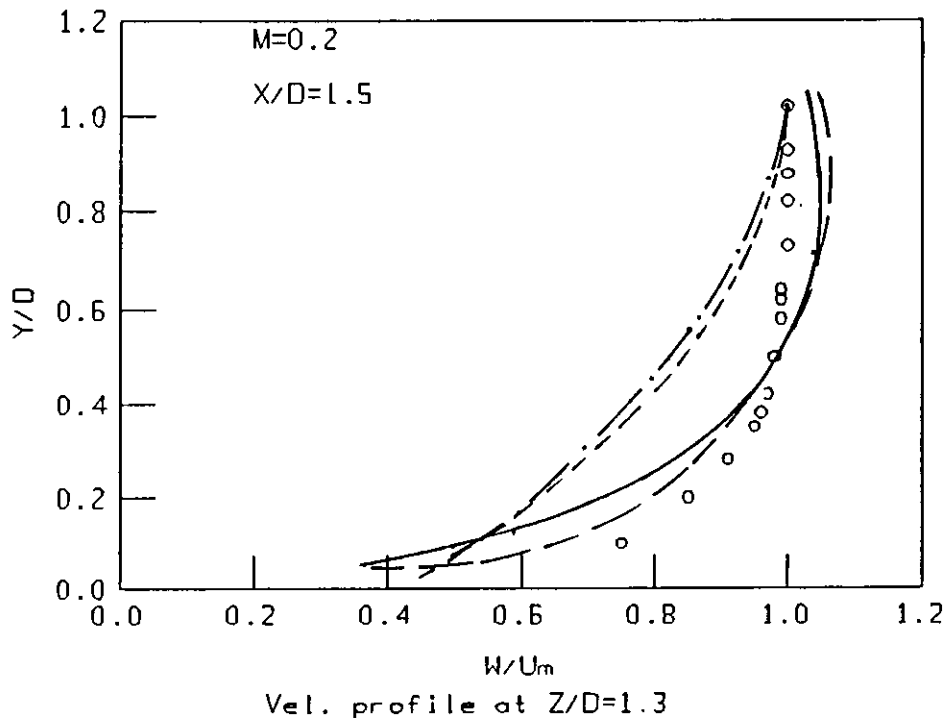


fig.(5-10c)

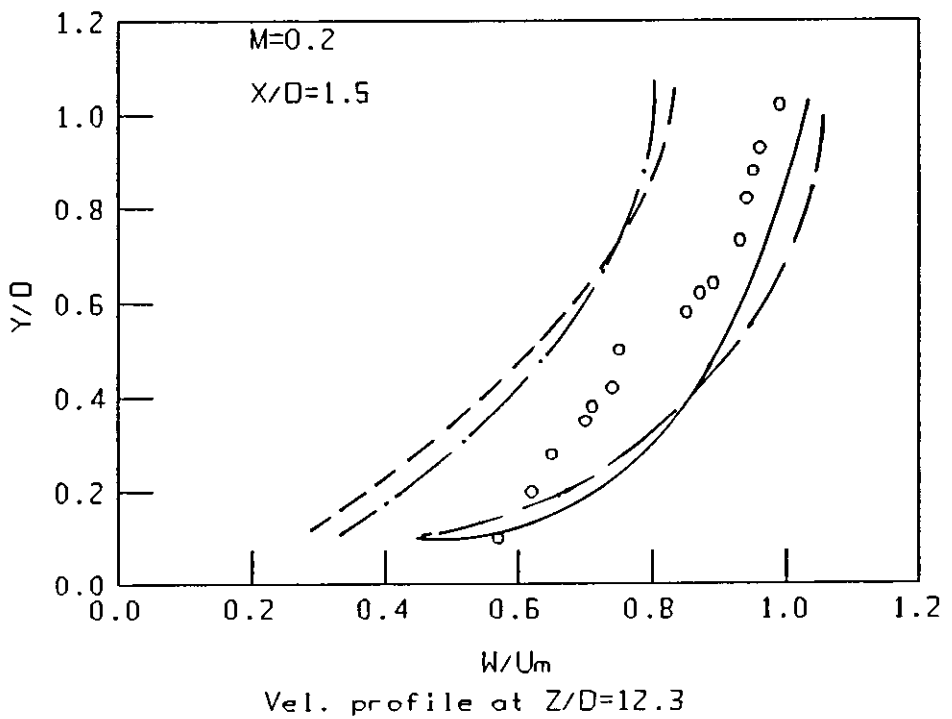


fig.(5-10d)

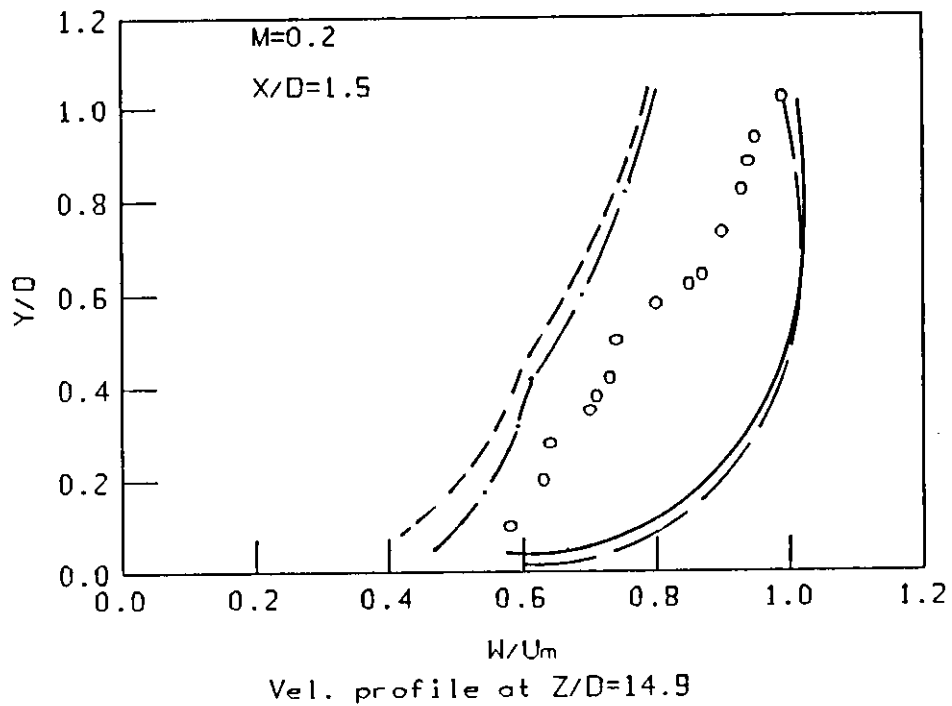


fig.(5-10e)

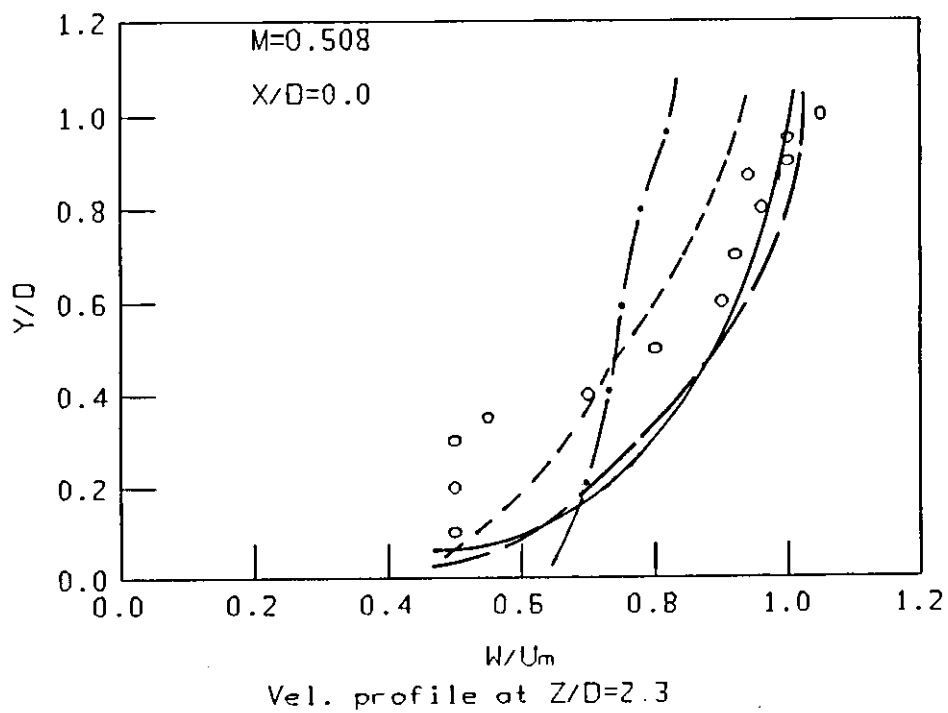


fig.(5-11a)

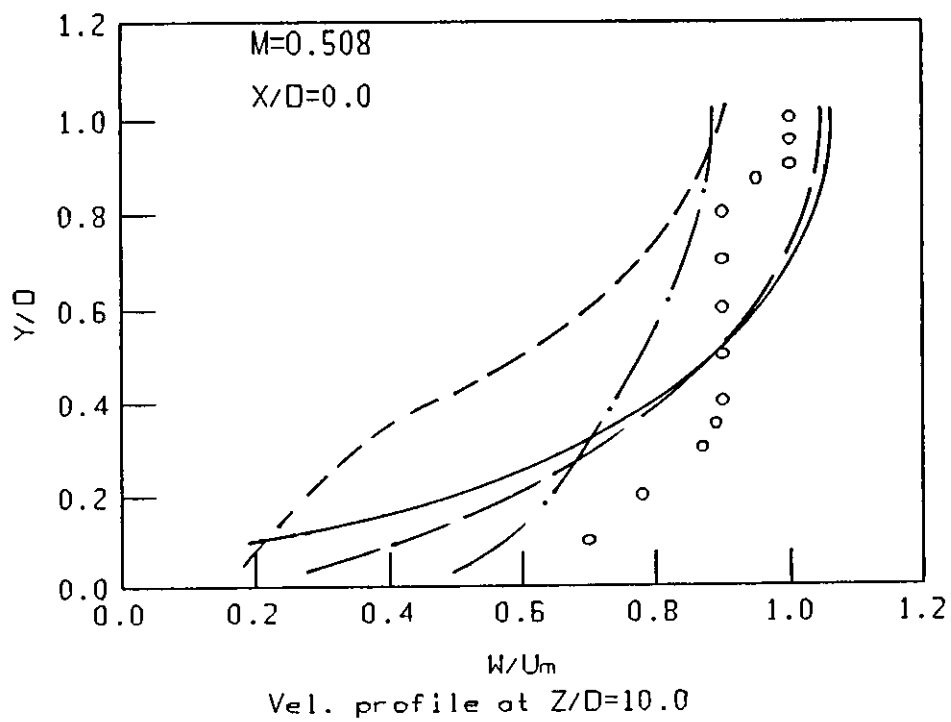


fig.(5-11b)

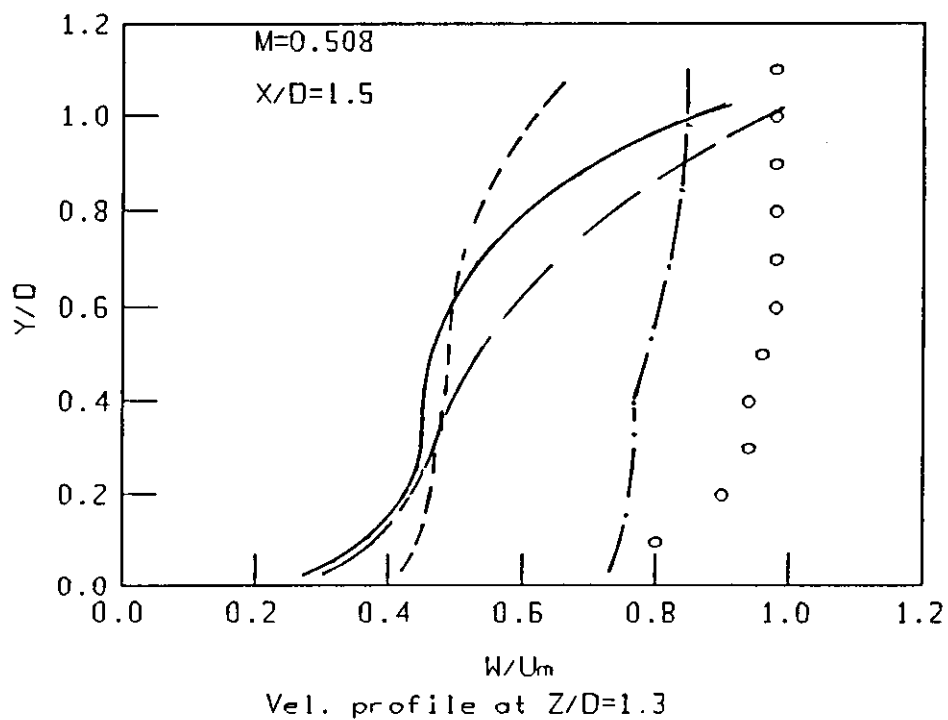


fig.(5-11c)

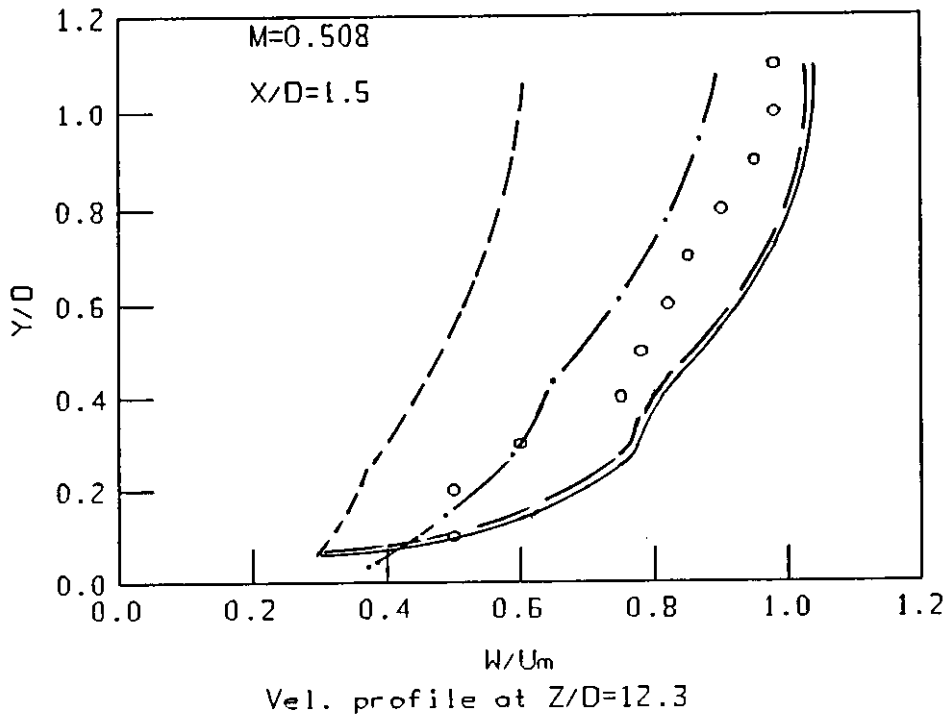


fig.(5-11d)

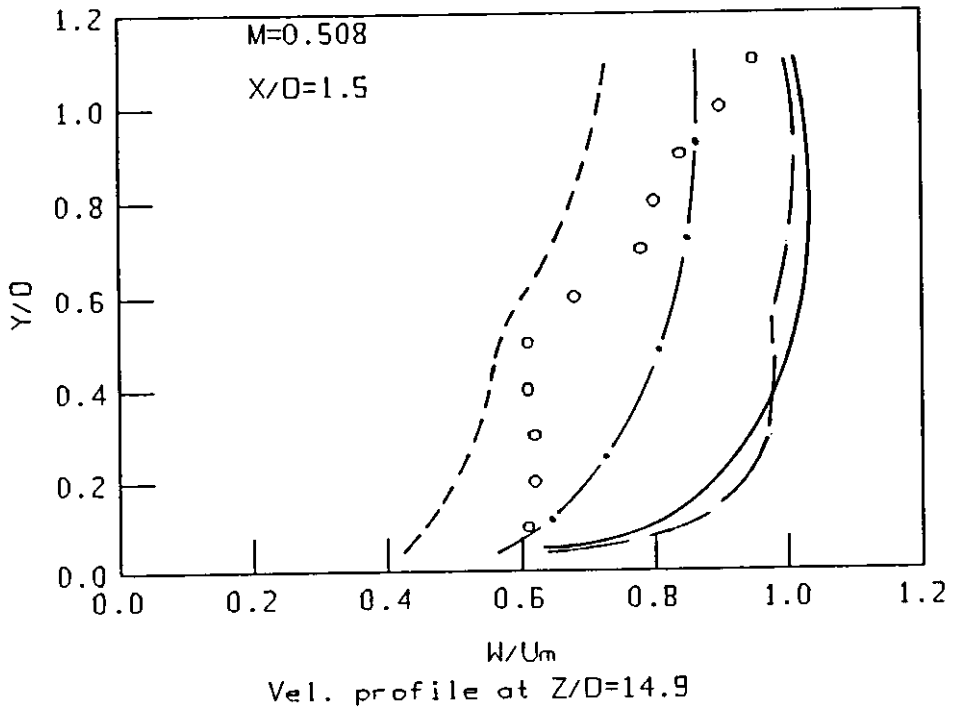


fig.(5-11e)

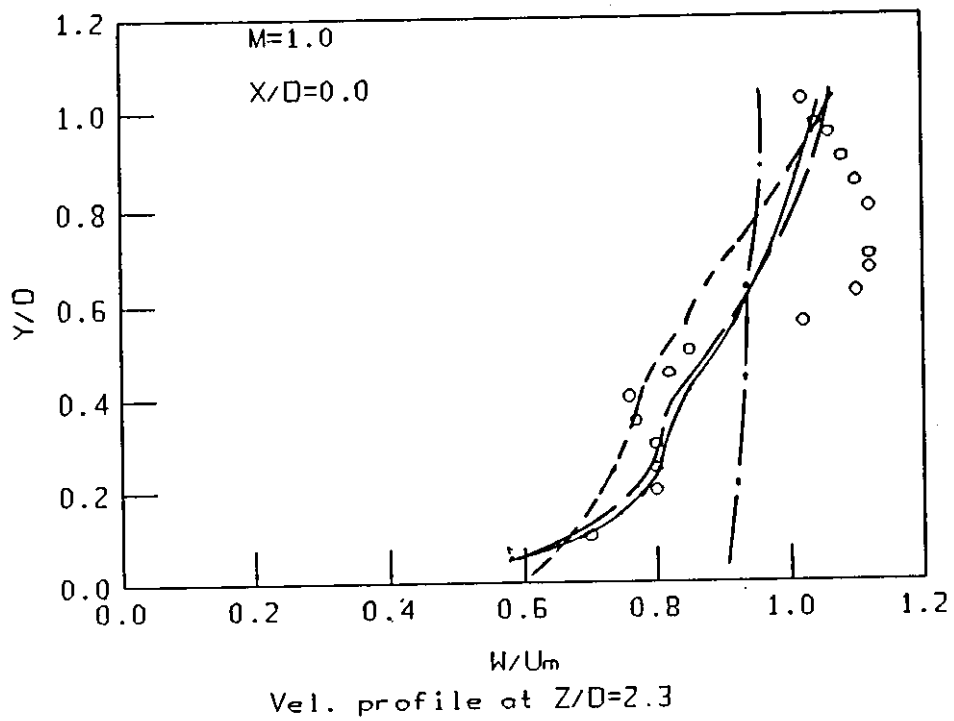


fig.(5-12a)

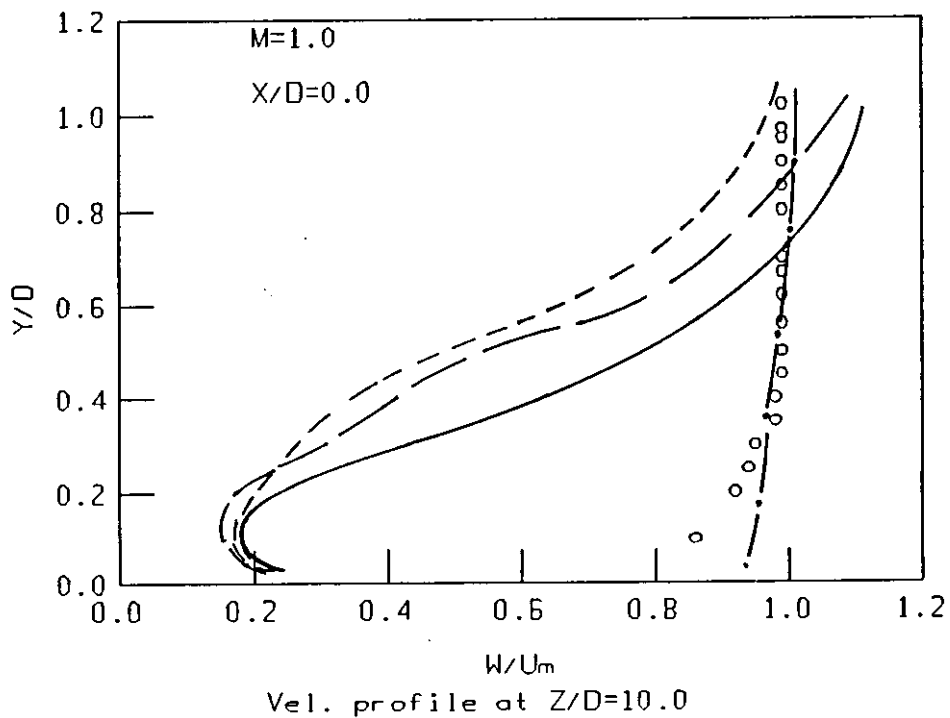


fig.(5-12b)

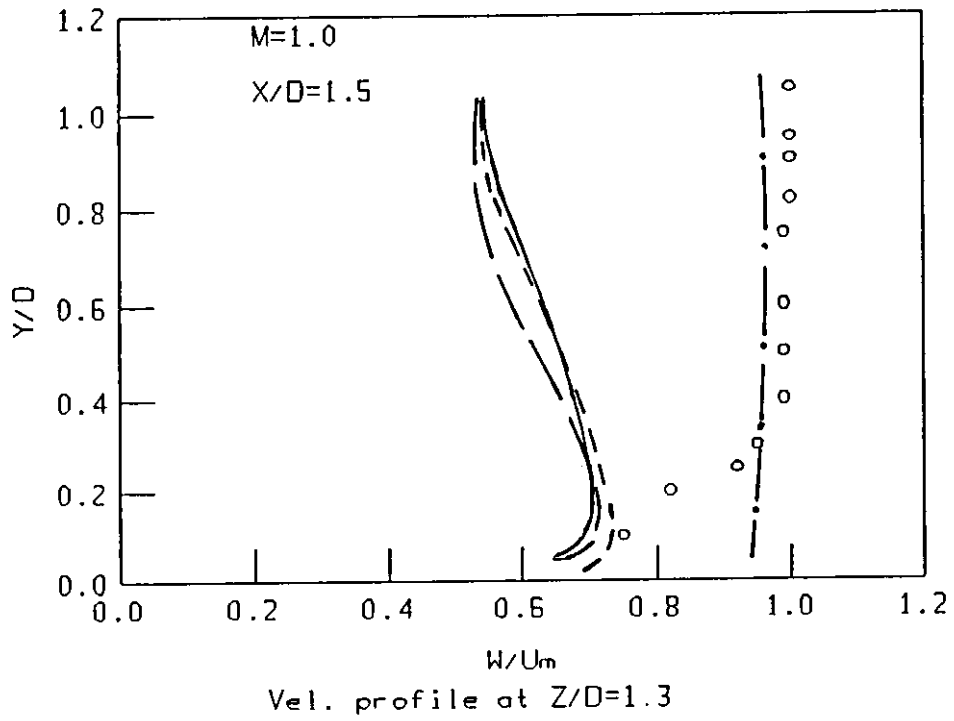


fig.(5-12c)

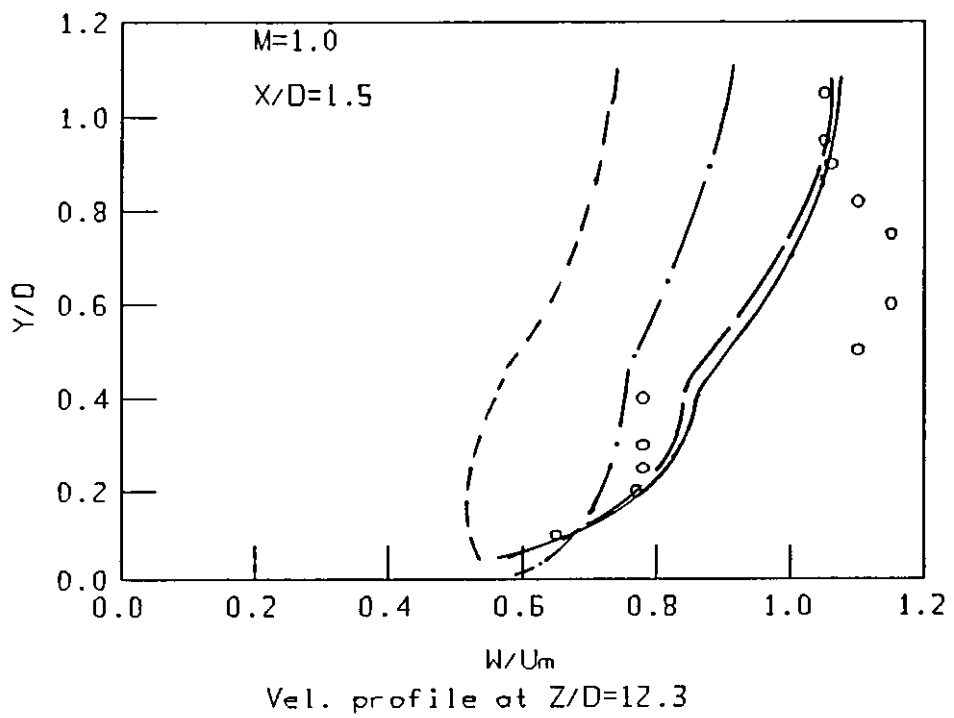


fig.(5-12d)

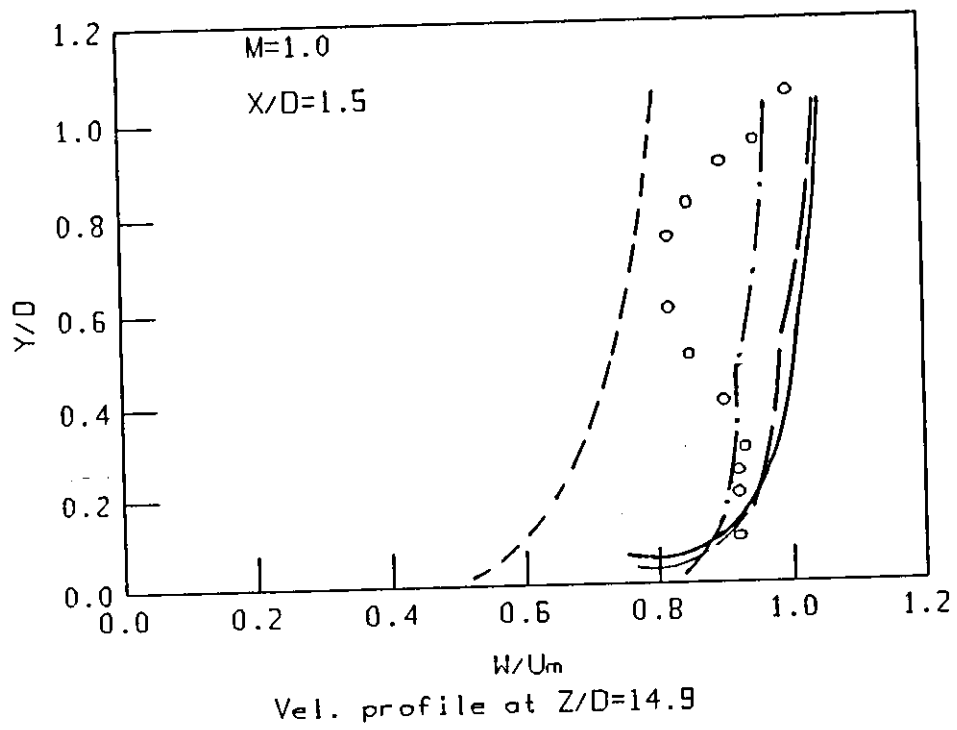
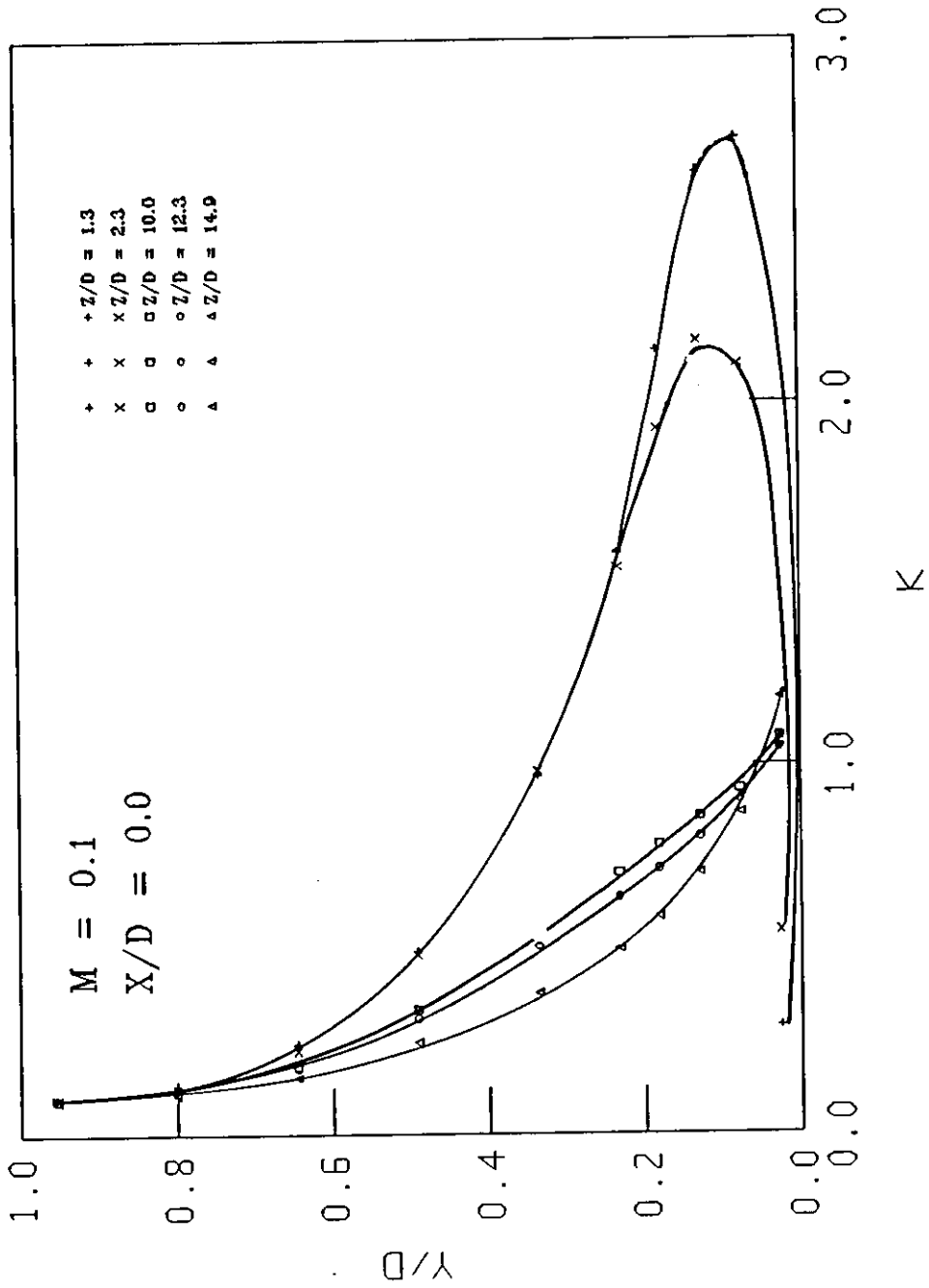


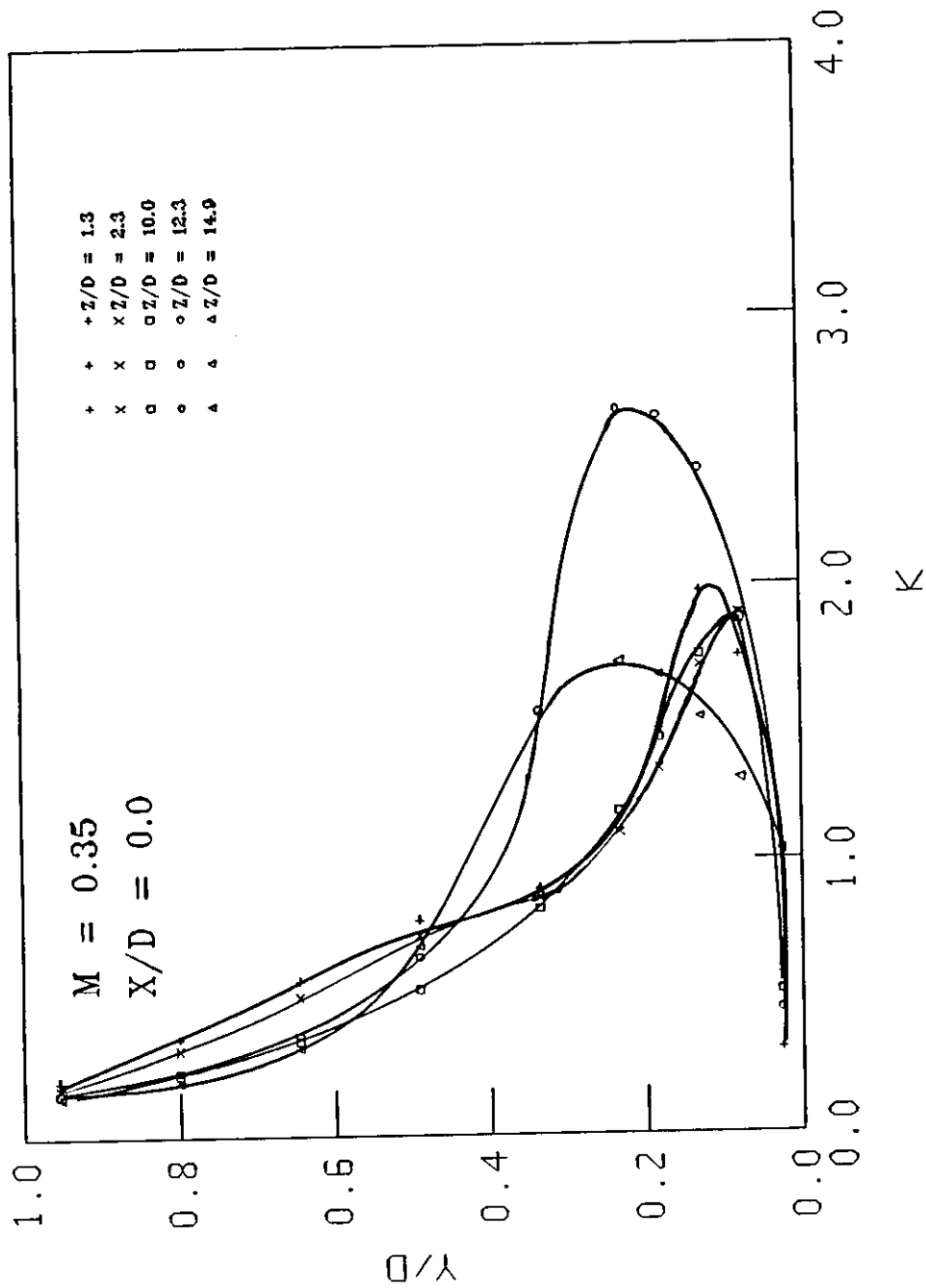
fig.(5-12e)





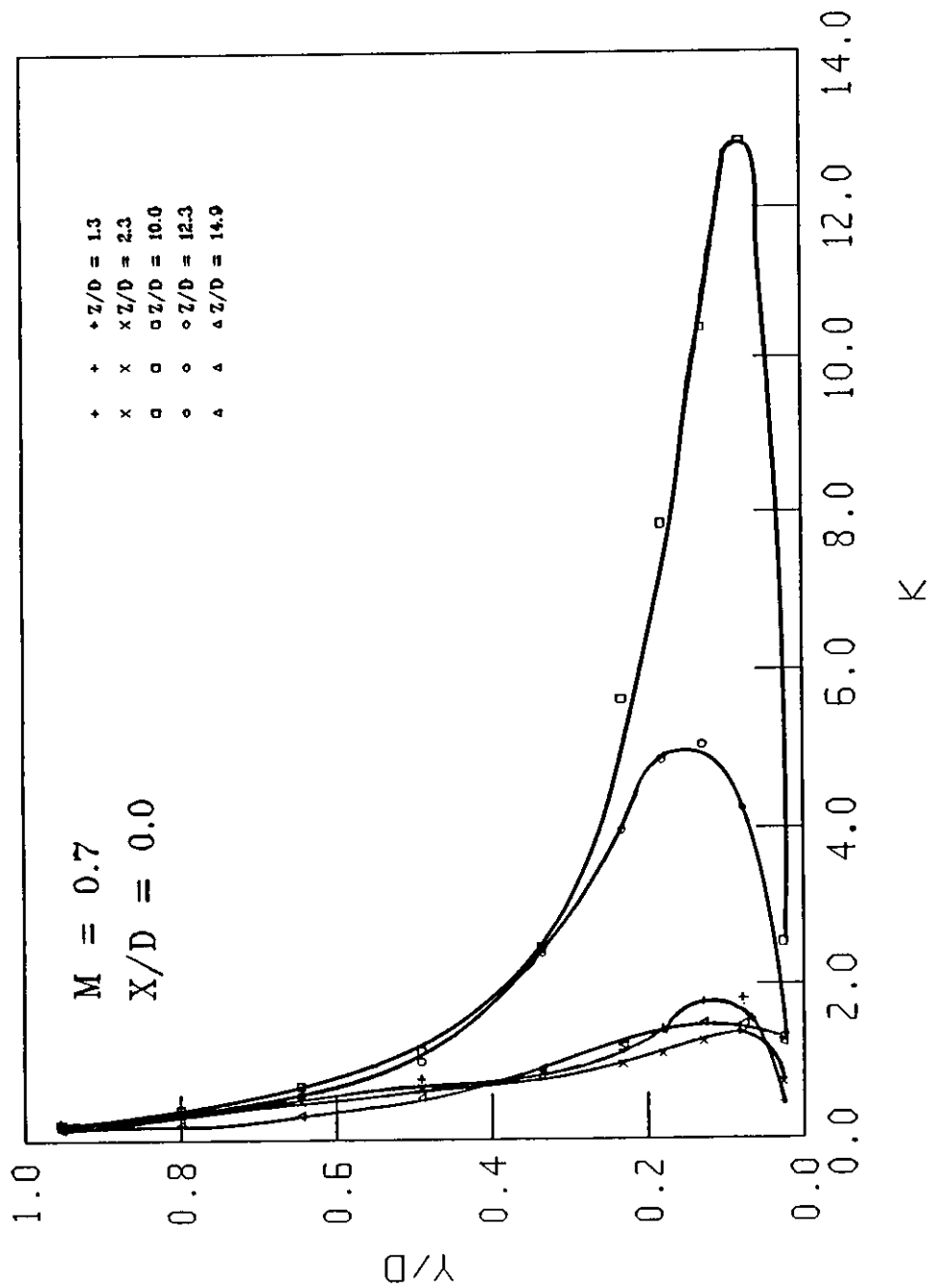
Turbulent kinetic energy variation with  $Y/D$

fig.(5-13a)



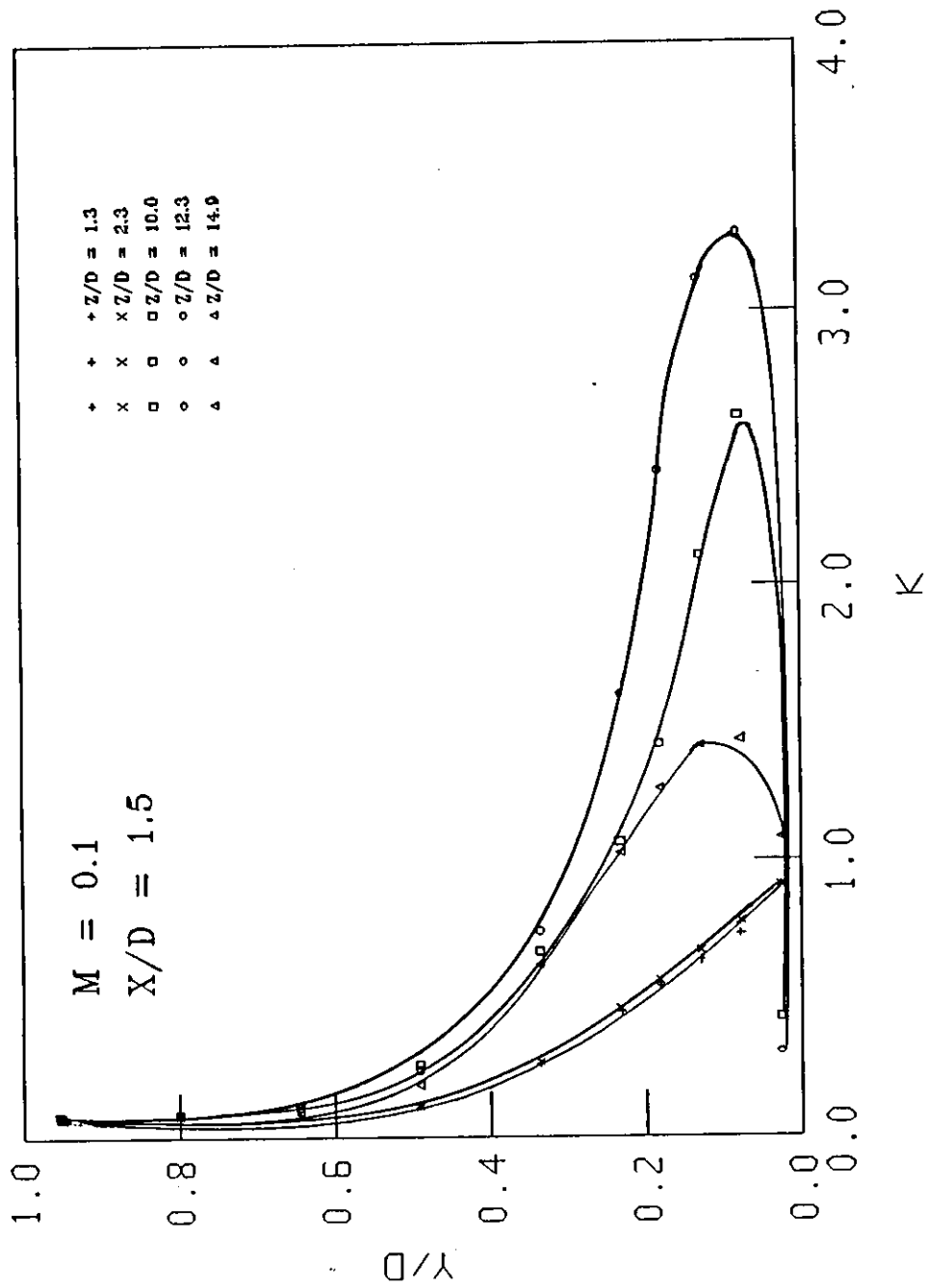
Turbulent kinetic energy variation with Y/D

fig.(5-13b)



Turbulent kinetic energy variation with Y/D

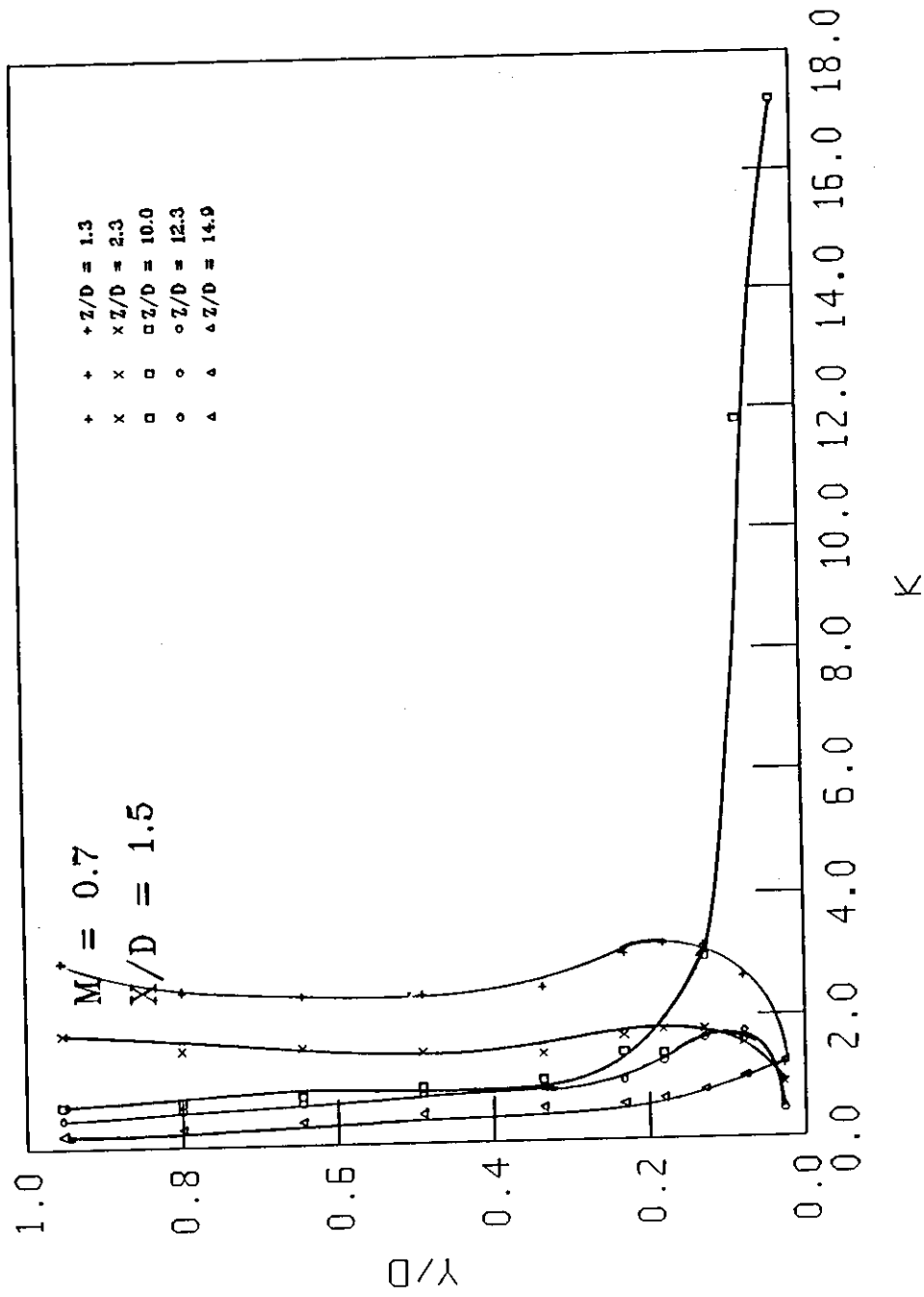
fig.(5-13c)



Turbulent kinetic energy variation with  $Y/D$

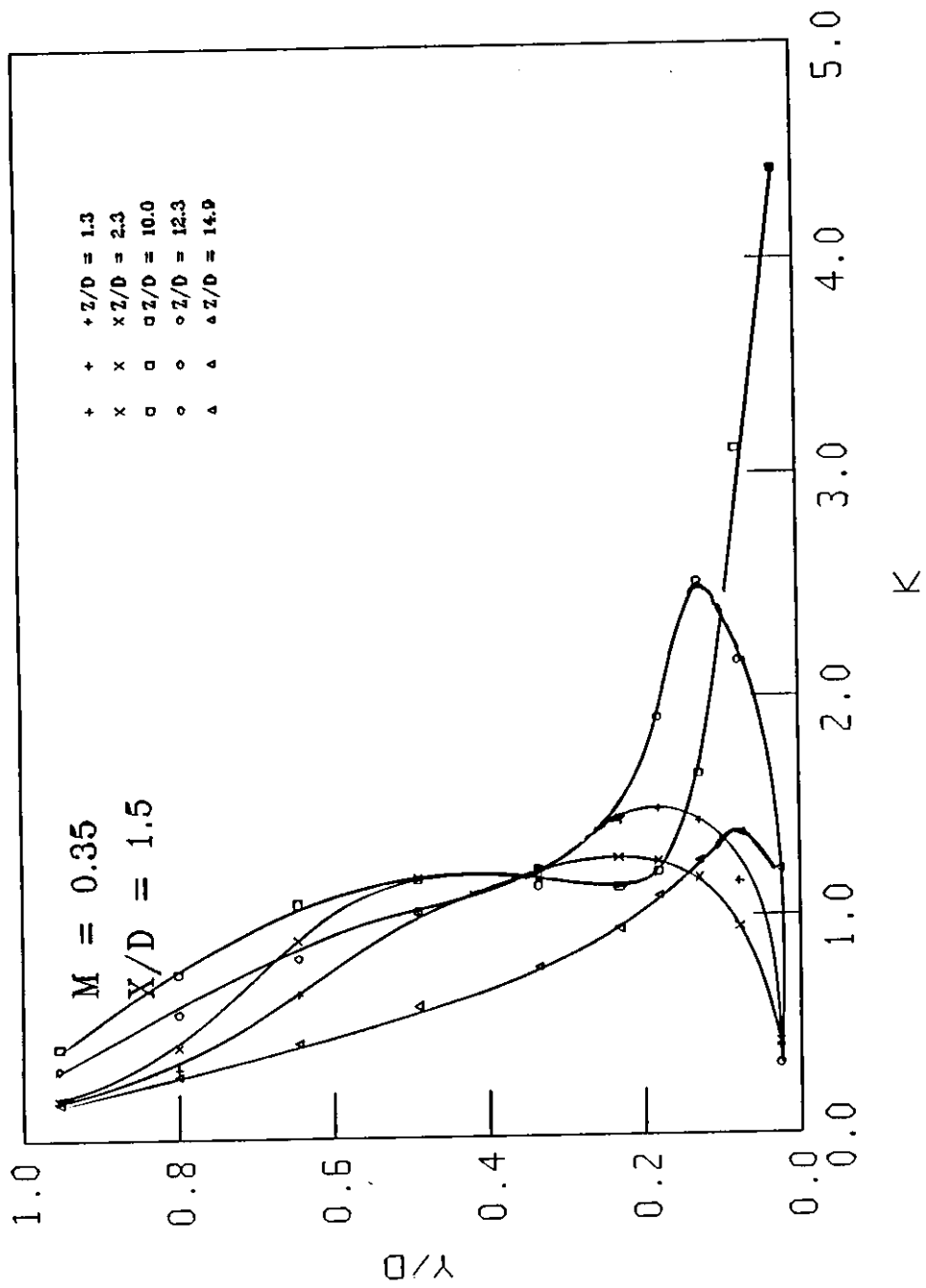
fig.(5-13d)

385793



Turbulent kinetic energy variation with  $Y/D$

fig.(5-13e)



Turbulent kinetic energy variation with  $Y/D$

fig.(5-13f)

## التوقع الرياضي للتبريد الطبقي

البحث المستعرض هو بحث له سمه نظريه ويتعلق بالتوقع الرياضي للتبريد الطبقي من خلال صفيين من الثقوب . لقد استعرضت خلال هذا البحث التوقعات الرياضية للفتالية وحقل السرعة على السواء ، باستخدام الأنماط الرياضية ذات المعادلتين .

لقد تم تطوير عدة أنماط رياضية تنتمي لهذه الفئة ، أي فئة الانماط الرياضية ذات المعادلتين ومن هذه الأنماط ، النمط الرياضي (  $K-W$  ) والمقترح من قبل *Spalding* عام ١٩٧١م وصيغة معدّلة لنفس النمط مقترحة من قبل *Spalding* و *Ilgubsi* عام ١٩٨٢ وكذلك تم تطوير النمط الرياضي (  $K-E$  ) مترافقا مع صيغة معدلة غير سوّية الخواص في جميع الاتجاهات والمقترحة من قبل *Bergeles* عام ١٩٧٦م .

لقد استخدمت حزمة المحاكاه بواسطة الحاسوب المسماه *PHOENICS* والمبرمجة بواسطة شركة *CHAM* المحدوده بانجلترا في البحث المذكور .

ان النمط الرياضي (  $K-E$  ) سوّى الخواص في جميع الاتجاهات هو النمط الوحيد المبيّت في الحزمة سابقة الذكر ، في حين قام الدارس بصياغة الانماط الرياضية الثلاثة الاخرى وهي : النمط الرياضي (  $K-W$  ) ، والنمط الرياضي (  $K-E$  ) غير سوّى الخواص في جميع الاتجاهات .

ان صياغة الأنماط الرياضية والتي قام بها الدّارس تمت بشكل رئيسي من خلال ملف أَل ( *GROUND* ) وبلاستفادة من البرامج الجزئية المزوّدة بها الحزمة المذكورة *PHOENICS* .

ان المقارنات التي عقدت بين النتائج المتوقعة رياضيا باستخدام الأنماط الرياضية الدّوامية المذكورة وبين نتائج تجريبية سابقة دلّلت على أن امكانية أي نمط رياضي دوّامي لتوقع نتائج تجريبية تعتمد وبشكل كبير على معدل النفخ من خلال الثقوب المذكورة وكذلك على البعد عن ثقوب الحقن .

في النهاية استعرض الدّارس وناقش بشكل مستفيض الاستنباطات وبعض التوصيات لأعمال مستقبلية .